

PHOTOCONDUCTIVITY AND SURFACE EFFECTS IN Zn-
DOPED POLYCRYSTALLINE STANNIC OXIDE

By

HERMAN EXCELL MATTHEWS, JR.


Bachelor of Science
Lamar State College of Technology
Beaumont, Texas
1962

Master of Science
Oklahoma State University
Stillwater, Oklahoma
1965

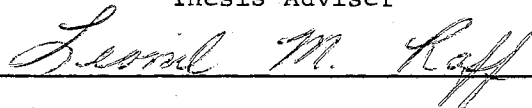
Submitted to the faculty of the Graduate College
of the Oklahoma State University
in partial fulfillment of the requirements
for the degree of
DOCTOR OF PHILOSOPHY
July, 1967

PHOTOCONDUCTIVITY AND SURFACE EFFECTS IN Zn-
DOPED POLYCRYSTALLINE STANNIC OXIDE

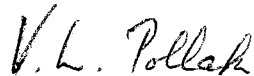
Thesis Approved:



Thesis Adviser











Dean of the Graduate College

JAN 16 1968

ACKNOWLEDGMENTS

The author wishes to express his deepest gratitude to Dr. E. E. Kohnke for his patience and guidance throughout the execution of this work and to the National Aeronautics and Space Administration for support in the form of a student traineeship. He is also indebted to H. Hall and W. Adkins for their help with the design and construction of experimental equipment and to Dr. J. Houston for help and suggestions during the earlier stages of this work. And finally the author wishes to express his appreciation to J. Rutledge for valuable suggestions and stimulating discussion throughout the course of the work and to recognize his wife, Sybil, for her help in reducing data, typing, and proofreading.

TABLE OF CONTENTS

Chapter	Page
I. INTRODUCTION.	1
Metal Oxides	1
Polycrystalline Bodies	2
Scope of Present Study and General Model	4
II. SEMICONDUCTOR STATISTICS AND SURFACE BARRIERS	8
Compensated Semiconductor Statistics	8
Effect of a Chemisorbed Surface Species.	11
Calculation of the Surface Potential	13
III. CURRENT DECAY TRANSIENTS AND PHOTOCONDUCTIVITY.	19
Dark Current Transients.	19
Effect of Light on Electrical Conductivity	23
Photocurrent Transients.	24
Photoelectronic Measurements	26
IV. SAMPLES, APPARATUS AND EXPERIMENTAL PROCEDURES.	29
Samples.	29
Apparatus.	31
Measuring Techniques	44
V. RESULTS	46
Introductory Remarks	46
Equilibrium Dark Conductivity.	46
Dark Current Decays.	52
Photocurrent Decays.	52
Photoelectronic Measurements	56
VI. DISCUSSION AND CONCLUSIONS.	76
Summary of Results	76
Surface Adsorption Process	77
Equilibrium Dark Conductivity.	82
Current Decays	88
Photoelectronic Measurements	91
Summary.	95
Suggestions for Further Study.	96

TABLE OF CONTENTS (Continued)

Chapter	Page
BIBLIOGRAPHY	99

LIST OF TABLES

Table	Page
I. Results of Photomeasurements in Different Ambients.	80
II. Activation Energies and Compensation Factors Calculated From Curves of Figure 12,	85
III. Activation Energies and Calculated Fermi Levels From Curves in Figure 13	87
IV. Comparison of Initial Current Values.	89

LIST OF FIGURES

Figure	Page
1. Simple Band Model of an n-Type Semiconductor.	9
2. Simple Band Model of an n-Type Semiconductor Modified by Surface Acceptor States	11
3. Relative Density as a Function of Firing Temperature at a Fixed Firing Time	30
4. Dark Current as a Function of Sample Voltage.	32
5. Gas Handling System	34
6. Electrical Measurements - Heater System	35
7. Simple Optical System	37
8. Output Dispersion Curve for the Deuterium Lamp.	38
9. Cryostat Sample Holder System	39
10. Guard Tube.	41
11. Sample holder	42
12. Dark Conductivity as a Function of Temperature for a Dense Sample After Various Fixing Procedures.	48
13. Dark Conductivity as a Function of Temperature for a Porous Sample After Various Fixing Procedures.	50
14. Dark Conductivity as a Function of Temperature for a Porous Sample.	51
15. Dark Current Decay of a Dense Sample.	53
16. Dark Current Decay of a Dense Sample.	54
17. Dark Current Decay of a Porous Sample	55
18. Photocurrent Decay of a Dense Sample in Different Ambients (3131Å).	57

LIST OF FIGURES (Continued)

Figure	Page
19. Photocurrent Decay of a Dense Sample in Air at 24°C (2536Å)	58
20. Photocurrent Decay of a Dense Sample in Air at 60°C (2536Å)	59
21. Photocurrent Decay of a Dense Sample in Vacuum (2536Å)	60
22. Photocurrent Decay of a Dense Sample in Vacuum (3131Å)	61
23. Photocurrent Rise and Decay of a Dense Sample in Air (2536Å)	62
24. Photocurrent Decay of a Dense Sample in Air From Two Different Current Values (2536Å)	63
25. Spectral Response of a Dense Sample in Different Ambients.	65
26. Continuous Thermal Quenching for a Dense Sample in Differ- ent Ambients (3131Å)	66
27. Continuous Thermal Quenching for a Dense Sample in Differ- ent Ambients (2536Å)	67
28. Continuous Thermal Quenching for a Porous Sample in Differ- ent Ambients (3131Å)	68
29. Thermally Stimulated Currents of a Dense Sample in Differ- ent Ambients (3131Å)	69
30. Thermally Stimulated Currents of a Dense Sample in Differ- ent Ambients (2536Å)	70
31. Thermally Stimulated Currents of a Porous Sample in Differ- ent Ambients (3131Å)	71
32. Comparison of Thermally Stimulated Currents of a Dense Sample in Air Following Different Pre-Measurement Treat- ment (3131Å)	73
33. Comparison of Thermally Stimulated Currents of a Dense Sample in Vacuum Following Different Pre-Measurement Treatment (2536Å)	74
34. Comparison of Thermally Stimulated Currents of a Porous Sample in Vacuum Following Different Pre-Measurement Treatment (3131Å)	75
35. Pictorial Representation of SnO ₂ Surface	77

CHAPTER I

INTRODUCTION

Metal Oxides

Although metal oxides have been used in various electronic devices for years, this application has largely resulted from experimental trial and only recently has there come about any detailed understanding of the fundamental electronic processes responsible for their technologically useful properties. Quantitative descriptions of fundamental electronic behavior such as those available for silicon and germanium have been less than successful, although some qualitative understanding of particular effects is possible. One reason for this lack of quantitative understanding is inherent in the questionable applicability of simple semiconducting ideas to these more complicated systems.

An obvious difference between the two types of systems arises from the compound nature of the metal oxides, which contain both positive and negative ions whereas silicon and germanium are monatomic. Ideas involving impurity doping of samples must be drastically altered in the case of metal oxides since the approach used in silicon and germanium is not applicable. Consider a metal oxide which has the metal ion in its highest valence state in the crystal lattice. Doping with a lower valence cation leads to self-compensation, i.e., to an almost intrinsic or n-type semiconductor. An example is found in the $\text{ThO}_2 - \text{Y}_2\text{O}_3$ system in which Y^{3+} replaces Th^{4+} substitutionally¹ resulting in an n-type

material, not a p-type one as would result in silicon or germanium. P-type behavior in a metal oxide is only observed when the metal ion has a higher valence state available and this result can be obtained without doping, i.e., the samples are intrinsically p-type². The above mechanism will be discussed in more detail later in this chapter since it is pertinent to the physical system investigated.

Another problem which impedes detailed study of some metal oxides is the technological difficulty of obtaining large, high-quality single crystals. Oxide crystal growth techniques are limited because of the high melting points--usually in excess of 1000°C --and the fact that many of these oxides decompose before they melt. Therefore the actual growth of a particular compound takes special materials and equipment and the optimum techniques and condition of growth may not be well established. A case of interest is the crystal growth of SnO_2 . This has been done in three ways: flux growth³, hydrothermal growth⁴, and vapor transport growth⁵. These all require extensive equipment, but the resultant samples are still smaller than desired and their properties vary widely depending upon the technique used.

Polycrystalline Bodies

Because the growth of SnO_2 single crystals is extremely complicated with the result often being unsatisfactory, a program was undertaken to produce ceramics (polycrystalline bodies) of SnO_2 in hopes of obtaining better samples for investigation purposes. There are several reasons for and against using polycrystalline bodies and these plus specific reasons they were produced and studied in this laboratory will be discussed.

The first obvious reason for producing polycrystalline samples is size. Single crystal samples grown locally are typically 1mm x 1mm x 3mm which limits the possible scope of investigation. Polycrystalline samples, on the other hand, can be produced in almost any size or cut to practically any desired shape. The second reason is that the powder can be easily doped with known amounts and kinds of dopants previous to firing, thus giving a reasonable control of impurity concentration. Controlled doping of single crystals has not been accomplished in this laboratory and any impurities are unintentionally introduced during the growth process.

The first obvious reason against using polycrystalline samples is that they are not single crystals and therefore do not have the advantageous properties of single crystals. In addition one must worry about the dopant-material chemical reaction during the sintering process. Will the end product be a solid solution or will it have a secondary phase? What will be the final amount of dopant and its position (substitutional lattice site, interstitial lattice site, grain boundary)? Of course, these questions also exist in part for crystal growth, especially when flux growth methods are used.

The particular reasons for using polycrystalline bodies in this laboratory were to obtain larger samples with variable surface-to-bulk ratios and to correlate experimental data already obtained on single crystals with that on polycrystalline specimens. Relationships between surface and bulk properties are of continuing interest in this laboratory and the possibility of correlation of certain electrical properties with surface area looked advantageous. This is especially true since instrumentation is available for measurements of the surface area and

type of surface structure⁶. Another region of correlation was in the area of photo-measurements. Houston⁷ had performed an extensive photo-electronic analysis of single crystal SnO_2 and Hurt⁸ had performed a study of surface effects using photoconductivity. Both of these studies had uncovered interesting effects which were not fully explained but suggested the importance of the surface in determining specimen electrical properties.

Therefore it was decided that these types of measurements might form a good basis for investigation of the polycrystalline samples. A general discussion of photoconductivity will be given in Chapter III. There will now be a brief discussion of the specific measurements which were carried out on polycrystalline SnO_2 during the course of this work and of the general model developed to explain the results.

Scope of the Present Study and General Model

There are three primary areas which will be covered: dark conductivity versus temperature under various "fixing" procedures, kinetic measurements of both phototransients and dark conductivity transients following rapid ambient changes, and selected photoelectronic measurements. In the terminology of this report, a "fixing" procedure is a combination temperature-ambient gas pressure-time treatment in which the sample has been taken to some standard state and then "fixed" under a particular set of conditions. A typical "pressure-fix" procedure would be to maintain the sample at 1×10^{-3} torr and 100°C for 24 hours to achieve a standard state and then fix it at one atmosphere for 70 hours after the temperature had been reduced to 50°C . A typical "vacuum-fix" would be to maintain the sample at one atmosphere and

100°C for 24 hours to achieve a standard state and then fix it at 3×10^1 torr for 80 hours after the temperature was increased to 110°C. Following this fixing procedure, data was taken for dark conductivity versus temperature and correlated with data taken for other fixing procedures.

Kinetic measurements were used to observe either phototransients or dark current transients. The phototransients were measured at fixed temperatures in various ambients using different times and types of illumination. A typical decay would follow a 16 sec illumination with 2536Å light of a particular intensity in air at room temperature. This data might then be correlated with the same light, same illumination time, same ambient, same temperature but different intensity or with same light, same ambient, same temperature, same intensity but different illumination time. The dark conductivity decays were taken after a rapid ambient change from a "vacuum-fixed" initial condition to one atmosphere. In other words the sample might be fixed in two initial conductivity states (e.g., one fixed at 1×10^{-2} torr at 100°C for 40 hours and one fixed at 1×10^{-1} torr at 50°C for 10 hours) and the decays from these two states correlated if possible.

The photoelectronic measurements made were of thermally stimulated currents, continuous thermal quenching and spectral response. Since these will be discussed more fully in Chapter III they are only listed here. It should also be mentioned before leaving the types of measurements that all were made on samples of various porosities, providing another variable the surface-to-bulk ratio.

Before going to the general model, the regions in which the above measurements were made should be mentioned. The temperatures that

these samples were subjected to ranged from $+125^{\circ}\text{C}$ to -180°C . The pressure extremes were one atmosphere and 10^{-5} torr. Because of the very moderate conditions under which the samples were fixed and the measurements were made, one would expect no bulk changes to occur. Therefore any proposed model must take this into account.

The general model to be used in explaining the experimental data assumes that the samples are compensated n-type insulators with surface acceptor states arising from the presence of chemisorbed oxygen. Variations of dark conductivity and photoconductivity with various parameters will be later explained in terms of this general model. Before going on, though, a brief justification for formulating a model based on the above two assumptions will be given.

Since the unfired samples contain 0.7% ZnO and the ionic sizes of Zn^{2+} and Sn^{4+} are nearly identical (Pauling ionic radius of $\text{Zn}^{4+} = 0.71\text{\AA}$ and $\text{Zn}^{2+} = 0.74\text{\AA}$), one expects substitution of Zn^{2+} ions in Sn^{4+} sites during the sintering process. This gives rise to a charge unbalance which might be relieved in one of several ways:

- (1) Increasing the valence state of two Sn^{4+} ions to Sn^{5+} ,
- (2) Creation of two bound holes,
- (3) Creation of an oxygen vacancy in the anion sub-lattice,
- (4) Introduction in interstitial cations near the Zn^{2+} site.

The first possibility can be reasonably eliminated since Sn^{5+} is not known to exist in any compound. The second possibility is highly improbable, since this type of charge compensation by holes is usually found only in one-constituent semiconductors, e.g., silicon or germanium, and then only to a very limited extent⁹. Therefore, the zinc substitutional must be compensated for by either the third or fourth

possibility.

Although both of these charge neutralization methods are probably represented to some degree or another in the specimens, the main point of interest is not to separate the two but to realize that both these conditions are "self-compensating" in the semiconductor terminology of the conduction process. In other words, they provide no excess of donor levels over acceptor levels in the forbidden gap. Such excesses do exist since the specimens exhibit n-type conductivity, but in general they arise from the presence of other defects in the regular lattice including interstitial ions not involved in the charge neutralization scheme.

The above system of a compensated n-type insulator is now perturbed by the presence of surface acceptor states arising from chemisorbed oxygen. The oxygen immobilizes an electron from the bulk at the surface thus creating a surface space charge layer and adding to the degree of compensation of the sample. A discussion of this effect on the bulk properties and the revision of certain bulk equations due to the presence of the chemisorbed oxygen will be presented in Chapter II.

CHAPTER II

SEMICONDUCTOR STATISTICS AND SURFACE BARRIERS

In the present chapter equations involved in compensated semiconductor statistics will be reviewed and discussed. Then the modification of the simple band picture due to the presence of surface acceptor states and their effects on the above equations will be analyzed. A general calculation of the surface potential of an n-type insulator with surface acceptors will then be made and the results discussed. Finally a general equation for the density of carriers which will be used in all calculations is presented from the previous arguments.

Compensated Semiconductor Statistics

Semiconductor statistics have been presented in a number of papers and texts, an excellent example being Semiconductor Statistics by J. S. Blakemore.¹⁰ The discussion presented here, however, will only include ideas pertinent to the particular case of compensated semiconductor statistics. An explanatory figure, definition of terms, and a brief derivation of the fundamental equation will be included.

Assume first the simple band model of an n-type semiconductor shown in Figure 1. In this model N_d is the density of donor states whose activation energy is E_d , N_a is the density of acceptor states whose energy is E_a , E_f represents the position of the Fermi level, and E_c and E_v are the energies of the conduction and valence bands

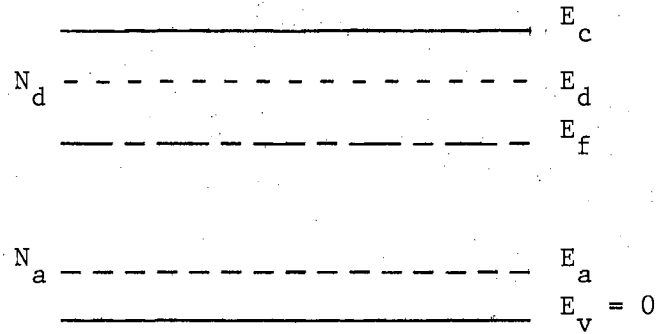


Figure 1. Simple Band Model of an n-Type Semiconductor

respectively (note that the arbitrary zero of energy has been chosen at E_v). The occupation density of the i^{th} level by electrons will be denoted by n_i and the occupation density of the conduction band by electrons by n .

Since there must be no excess charge in the sample a simple analysis leads to the following equation for conservation of charge.

$$n + n_a = N_d - n_d \quad (1)$$

Equation (1) can be rewritten using the fact that electrons obey Fermi statistics and that the occupation of any level can be written as

$$n_i = \frac{N_i}{1 + \beta \exp [(E_i - E_f)/KT]} \quad (2)$$

to give the form

$$n + N_a = \frac{N_d}{1 + \beta^{-1} \exp [(E_f - E_d)/KT]} \quad (3)$$

where β is a statistical weighting factor of the order of one. Solving equation (3) for $\exp(E_f/KT)$ and putting this into the equation for the occupation density of electrons in the conduction band if $E_c - E_f > 3KT$,

$$n = N_c \exp [(E_f - E_c)/KT] , \quad (4)$$

gives an expression for n which can be simplified using the approximation $n \ll N_a < N_d$ to the well known equation* for the density of conduction electrons in a compensated semiconductor.

$$n = \beta N_c \frac{N_d - N_a}{N_a} \exp [(E_d - E_c)/KT] \quad (5)$$

Equation (5) now gives an explicit relationship between n and T in terms of the sample parameters. It should be pointed out that since all the work to be reported in the following sections was done on compensated insulators, i.e., wide band gap n-type semiconductors, then the assumption $n \ll N_a < N_d$ used in obtaining equation (5) appears appropriate to the physical system and all calculations were made assuming equation (5) to correctly determine the equilibrium number of carriers. The actual physical quantity measured in these experiments was the current through the sample under an applied voltage and it is related to the number of carriers through the conductivity as shown,

$$\sigma = il/VA = ne\mu \quad (6)$$

where σ is the conductivity, i is the current, v is the applied voltage, l and A are gross sample parameters length and area, e is the electronic charge and μ is the mobility. If there is no temperature dependence in equation (6) except that appearing in the exponential of equation (5)--the temperature dependence of $N_c\mu$ is zero or very slight

* For a more rigorous derivation of this equation see Chapter 3 of reference 9.

compared to the exponential temperature dependence--then values of $E_c - E_d$ can be obtained from plots of $\ln \sigma$ versus T^{-1} . Also if appropriate values of μ and m^* are known, values of the quantity $\beta[(N_d - N_a)/N_a]$ can be calculated at a specific temperature. These types of plots and calculations will be shown later.

Effect of a Chemisorbed Surface Species

The discussion and derivation of equation (5) has thus far only considered the case of flat bands as shown in Figure 2. This discussion will now be extended to include the possibility of surface acceptors in the form of chemisorbed oxygens immobilizing electrons in states at the surface thus creating a space charge layer at the surface and to describe the effect of their presence on equation (5).

If surface acceptor states are introduced on the sample then this changes the energy band picture from flat bands as shown in Figure 1 to a configuration shown in Figure 2 due to the negative space charge layer at the surface.

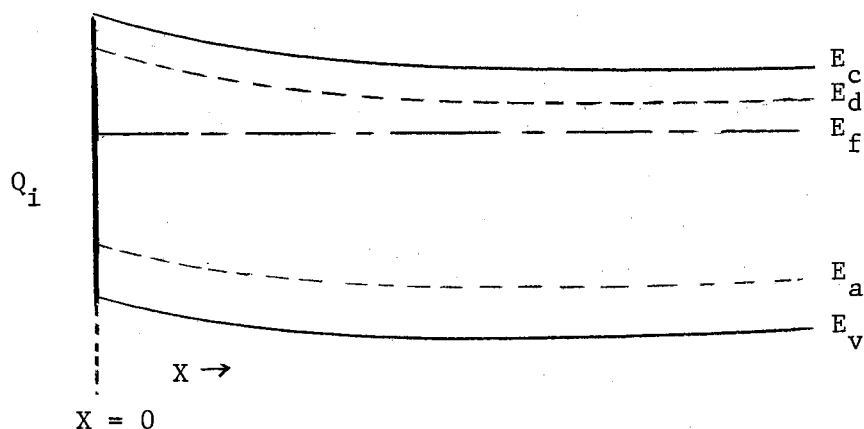


Figure 2. Simple Band Model of n-Type Semiconductor Modified by Surface Acceptor States.

Here Q_i is the density of the i^{th} surface state whose occupation will be noted by q_i and the other symbols have the same meaning as in Figure 1. The locations of the surface states are not shown because their positions are not completely understood, but since the equilibrium Fermi level at the surface which determines the occupation of surface states is the same as that in the bulk^{*}, it establishes the relationship between surface and bulk properties of the semiconductor. Therefore if equation (5) is to correctly represent the equilibrium number of carriers then it must be modified to take into consideration the equilibrium between the surface and bulk states established through the Fermi level.

This will be attempted in very simple fashion by defining an effective acceptor density

$$N_a^* = N_a + x_0 q_0 \quad (7)$$

where N_a is the acceptor density represented in Figure 2, x_0 is the surface-to-bulk ratio, and q_0 is the equilibrium surface density of the chemisorbed species. Such a modification is a direct outgrowth of the previously stated assumption that the effect of the surface acceptors is to immobilize electrons at the surface and thus to increase the degree of compensation in the sample. From an experimental point of view one cannot directly use conductivity magnitude measurements to differentiate between a compensation due only to an N_a and compensation due to an N_a^* . It should be possible, however, to take advantage of the

* A good discussion of this point is found in Chapter 7 of The Electronic Theory of Catalysis on Semiconductors by F. F. Vol'kenshtein, Macmillan Company, New York (1963).

fact that q_0 is a function of pressure and temperature which allows different equilibrium values of q_0 to be obtained under different treatment conditions. This can cause variations in n through equation (5) under conditions for which the value of N_a itself would not be expected to change. Furthermore, kinetic behavior when q changes from one equilibrium value to another should be observable for analysis using equation (5). Discussion and experimental data relating to the above points will be presented later.

Calculation of the Surface Potential

A general calculation of the potential in the space charge layer of an n-type insulator with surface acceptor density q_1 will be done under simplifying conditions. This is done to complete the discussion of surface barriers, to identify important parameters, and to appraise the effect of the free electron density in perturbing the normal fixed-charge electrostatic potential. This latter point has recently been considered by Lee and Mason¹¹ but applied specifically to the smaller bandgap monatomic semiconductors, silicon and germanium. The case to be discussed here will be a sample with completely ionized acceptors and donor levels which are either completely ionized or completely un-ionized.

The pictorial representation for electron energy versus distance into the sample is shown in Figure 2 where $x = 0$ at the surface and $x = \infty$ in the bulk. One defines the following electron potential in terms of Figure 2,

$$\Phi(x) = e^{-1} [E_c(x) - E_c(\infty)] \quad (8)$$

which gives rise to following boundary conditions

$$\begin{aligned} \text{at } x = 0 & \quad \Phi = \Phi_s \\ \text{at } x = \infty & \quad \Phi = 0 \quad (d\Phi/dx)_{\infty} = 0 \end{aligned} \quad (9)$$

In order to find the functional relationship between Φ and x one needs to use the one dimensional Poisson's equation in the form

$$\frac{d^2 \Phi(x)}{dx^2} = \frac{\rho(x)}{\epsilon} \quad (10)$$

where $\rho(x)$ is the charge density at any point x and ϵ is the permittivity of the material. The charge density at any point $x > 0$ is expressible as

$$\rho(x) = e[N_d^+ - N_a^- - n(x)] \quad (11)$$

where N_d^+ is the density of ionized donors, N_a^- is the density of ionized acceptors, and $n(x)$ is gradient of conduction electrons. (Note since $E_f \gg E_c/2$ there is no concentration gradient of holes because $p = 0$ for all x). The final assumption is that Boltzmann statistics are applicable when determining the number of conduction electrons, i.e. $E_c - E_f > 3KT$.

Since the sample must be electrically neutral one can write conservation of charge as

$$\int_0^{\infty} \rho(x) dx = e \sum q_i \quad (12)$$

where q_i is the occupation of the i^{th} surface state by electrons (Note this is really an application of Gauss' law). If one now integrates equation (10) using boundary conditions (9) and conservation of charge,

one gets the following result

$$\int_0^{\infty} d\left(\frac{d\phi}{dx}\right) = \int_0^{\infty} \frac{\rho(x)}{\epsilon} dx$$

$$\left(\frac{d\phi}{dx}\right)_{\infty} - \left(\frac{d\phi}{dx}\right)_0 = \frac{e\sum q_i}{\epsilon}$$

$$\left(\frac{d\phi}{dx}\right)_0 = \frac{-e\sum q_i}{\epsilon} \quad (13)$$

which is an expression for the electric field at the surface. Since Boltzmann statistics are applicable one can write the number of electrons in the bulk as $n_B = N_C \exp\{[E_f - E_C(\infty)/KT]\}$ and the number of electrons near the surface as $n = N_C \exp\{[E_f - E_C(\infty) - e\phi]/KT\}$. Combining these two one gets the general expression

$$n = n_B \exp(-e\phi/KT). \quad (14)$$

Using the identity

$$\frac{d^2\phi}{dx^2} = \frac{1}{2} \frac{d}{d\phi} \left(\frac{d\phi}{dx}\right)^2 \quad (15)$$

one can now rewrite equation (10) using equation (11) and equation (14) in the form

$$\frac{d^2\phi}{dx^2} = \frac{\rho(x)}{\epsilon} = \frac{e}{\epsilon} [Nd^+ - N_a^- - n(x)]$$

$$\frac{d}{d\phi} \left(\frac{d\phi}{dx}\right)^2 = \frac{2e}{\epsilon} [Nd^+ - N_a^- - n_B \exp(-e\phi/KT)]. \quad (16)$$

One can now integrate equation (16) and use condition (9) to get an expression for $d\phi/dx$.

$$\int_{\frac{d\phi}{dx} = \infty}^{\phi} \left(\frac{d\phi}{dx}\right)^2 = \frac{2e}{\epsilon} \int_0^{\phi} [N_d^+ - N_a^- - n_B \exp(-e\phi/KT)] d\phi$$

$$\left(\frac{d\phi}{dx}\right)^2 = \frac{2e}{\epsilon} \left\{ [N_d^+ - N_a^-] \phi + \frac{n_B KT}{e} [\exp(-e\phi/KT) - 1] \right\} \quad (17)$$

If one looks at equation (17) at the surface $\phi = \phi_s$ and assumes $e\phi_s > 3KT$ or $1 > \exp(-e\phi_s/KT)$ then one can get, using equation (13) a general expression for ϕ_s

$$\left(\frac{e\Sigma q_i}{\epsilon}\right)^2 = \frac{2e}{\epsilon} \left[(N_d^+ - N_a^-) \phi_s - \frac{n_B KT}{e} \right]$$

$$\phi_s = \frac{e(\Sigma q_i)^2}{2e(N_d^+ - N_a^-)} + \frac{n_B KT}{e(N_d^+ - N_a^-)} \quad (18)$$

One can also now get an approximation for the potential as a function of x near the surface from equation (17) by assuming $e\phi > 3KT$. (Note, one chooses the negative sign in step two because one knows the electric field is negative near the surface)

$$\left(\frac{d\phi}{dx}\right)^2 = \frac{2e}{\epsilon} \left[(N_d^+ - N_a^-) \phi - \frac{n_B KT}{e} \right]$$

$$\frac{d\phi}{dx} = - \left(\frac{2e}{\epsilon}\right)^{\frac{1}{2}} \left[(N_d^+ - N_a^-) \phi - \frac{n_B KT}{e} \right]^{\frac{1}{2}}$$

$$\int_{\phi_s}^{\phi} \frac{d\phi}{[(N_d^+ - N_a^-) \phi - n_B KT/e]^{\frac{1}{2}}} = \left(\frac{2e}{\epsilon}\right)^{\frac{1}{2}} \int_0^x dx$$

$$\phi = \frac{e(N_d^+ - N_a^-)}{2\epsilon} x^2 - \frac{1}{2} \left(\frac{2e}{\epsilon}\right)^{\frac{1}{2}} \left[(N_d^+ - N_a^-) \phi_s - \frac{n_B KT}{e} \right]^{\frac{1}{2}} x + \phi_s \quad (19)$$

ϕ can now be expressed only in terms of the physical parameters of the sample by using equation (19) and equation (18) which gives

$$\phi = \frac{e(N_d^+ - N_a^-)}{2\epsilon} x^2 - \frac{e\Sigma q_i}{\epsilon} x + \frac{e(\Sigma q_i)^2}{2\epsilon(N_d^+ - N_a^-)} + \frac{\ln_B KT}{\epsilon} \quad (20)$$

Equation (20) is the functional dependence of ϕ on x near the surface ($e\phi > 3KT$) and correctly predicts two previous results, equation (18) and equation (13), when these boundary conditions are applied.

Although this calculation was limited to the case of completely ionized donors and acceptors, it is not as restricted as it may seem. This is due both to the nature of compensated semi-conductors--the Fermi level must lie in or below a donor level thus causing it to be partially ionized throughout the bulk--and to the fact that the region of interest is near the surface. In this region the donor levels will have their maximum ionization due to the bending of the levels away from the Fermi level.

This calculation as mentioned before is mainly for completeness and has no direct experimental verification. Other authors^{12,13} have used a calculation of this type to get an analytical relationship between ϕ_s and q for other purposes, and have neglected the contribution of the gradient of conduction electrons to the charge density, but again there is no simple way to resolve which expression is more useful. An obvious difference between the two calculations though is the fact that ϕ_s does have an explicit dependence on temperature as shown in equation (18), whereas the dependence is only implicit in the calculation neglecting the gradient of conduction electrons. One can also get an expression for a space charge layer from the preceding

calculation if one assumes that effectively the charge at the surface all came from a depth d in the sample. Using Gauss' law to get $\Sigma q_i = (N_d^+ - N_a^-)d$, one then substitutes back into equation (18) which gives

$$d = \left[\frac{2e\phi_s}{e(N_d^+ - N_a^-)} - \frac{2en_B KT}{e^2(N_d^+ - N_a^-)^2} \right]^{\frac{1}{2}} \quad (21)$$

This gives the effective space charge depth in terms of the sample parameters, but a quantitative number is impossible without precise numerical values for these parameters.

It is obvious from the ideas presented in this chapter that detailed calculations of potential barriers may be very elegant and yet not lend themselves to easy experimental verification. On the other hand, the simple definition of an effective acceptor density as given in equation (7) leads to a modification of the compensated semiconductor equation which shows promise of being useful to predict qualitative and possibly quantitative information about equilibrium carrier densities and about transient carrier densities observed in kinetic changes between equilibrium states. For these purposes equation (5) which determines the equilibrium number of carriers is assumed to take on the following form

$$n = \beta N_c \frac{N_d - N_a^*}{N_a} \exp [(E_d - E_c)/KT] \quad (22)$$

The possibilities for experimental checks are considered in the next chapter.

CHAPTER III

CURRENT DECAY TRANSIENTS AND PHOTOCONDUCTIVITY

In this chapter the results obtained in Chapter II will be examined as a function of time. This will lead to certain functional relationships between conductivity and time which can be experimentally verified for the SnO_2 samples of interest thus supporting the general model. Secondly, a general review of non-equilibrium processes (photoconductivity) will be made and some of the particular processes to be studied will be discussed.

Dark Current Transients

In this discussion it will be assumed, as stated before, that equation (22)

$$n = \beta N_c \frac{N_d - N_a^*}{N_a^*} \exp \left[\frac{(E_d - E_c)}{KT} \right] \quad (22)$$

correctly describes the equilibrium number of carriers in the samples. The other assumption* is that the additional chemisorbed oxygen density due to a sudden pressure change which increases the number of oxygens available for chemisorption on the experimental specimens is a logarithmic function of time, obeying the Elovich dependence

* Suggestion by J. L. Rutledge, Physics Department, Oklahoma State University.

$$q(t) \propto \ln[(t+t')/t'] \quad (23)$$

where t is time and t' a constant

This type of dependence has been observed in a variety of systems by a large number of people and discussed theoretically by almost as many. Explanations based on such different mechanisms as bimolecular site-site interaction during adsorption,¹⁴ generation of sites by the act of adsorption^{15, 16}, two step processes of adsorption¹⁷, etc., have been used and all predict the Elovich type dependence between q and t . This myriad of different theoretical approaches all leading to the same result is summed up by Low¹⁸ in his review article by the statement "the use of a particular chemisorption mechanism is almost a matter of personal preference until much more experiment and theoretical work has been done and an adequate model emerges"! Therefore, no attempt to distinguish between these theoretical approaches will be made at this time. The point of interest is how this adsorption process effects equation (22).

One can now using assumption (23) rewrite equation (7) as a function of time

$$N_a(t) = N_a^* + xq(t) \quad (24)$$

where x is ratio of the surface area to which q is being added, to the bulk volume. Using equation (24) and assuming a proportionality constant A in assumption (23) one can now rewrite equation (22) in the form

$$n(t) = c' \left[\frac{N_d - N_a^* + xA \ln [(t + t')/t']}{N_a^* + xA \ln [(t + t')/t']} \right] \quad (25)$$

or

$$n(t) = c' \left[\frac{N_d}{N_a^* + x \ln [(t + t')/t']} - 1 \right] \quad (26)$$

where $C' = \beta N_c \exp [(E_d - E_c)/KT]$. Two considerations are important here: The magnitude and rapidity of changes must be small enough so that the system can be treated as passing through a continuous series of equilibrium states and the same donor level (energy E_d) must control the conductivity during the portion of the change studied. One can now write, remembering i equals a constant times n at a fixed temperature, the two general expressions to be investigated.

$$i(t) = C \frac{N_d - (N_a^* + xA \ln [(t + t')/t'])}{N_a^* + xA \ln [(t + t')/t']} \quad (27)$$

$$i(t) = C \left[\frac{N_d}{N_a^* + xA \ln [(t + t')/t']} - 1 \right]. \quad (28)$$

The problem now is to find different reasonable approximations to simplify one or the other of the above equations.

The first approximation is found when $N_a^* \gg xA \ln [(t + t')/t']$ or the number of acceptors evaluated at $t = 0$ is much greater than the additional chemisorption acceptors and when $(N_d - N_a^*)/N_a^*$ is small, i.e. $N_d \approx N_a^*$. Note this is a good approximation when $(E_c - E_d) < (E_c - E_f)$ at $t = 0$, i.e. the Fermi level is well below the principle donor level before additional acceptors are added. When these

conditions are imposed on equation (27) one gets an equation in the form

$$i(t) \approx C \frac{N_d - N_a^* - xA \ln [(t + t')/t']}{N_a^*} \quad (29)$$

or simplifying and remembering the definition of C one gets

$$i(t) = i_o - \frac{xCA}{N_a^*} \ln \left(\frac{t + t'}{t'} \right). \quad (30)$$

This has the form of an Elovich equation and one can now check this result directly as will be shown later.

The second approximation is found when $N_d \gg N_a^* + xA \ln [(t + t')/t']$ or the number of donors is much greater than the number of acceptors at $t = 0$. This approximation will then be valid until there is a significant number of surface acceptors added to the system. When these conditions are imposed on equation (28) one gets an equation in the form

$$i(t) = C \frac{N_d}{N_a^* + xA \ln [(t + t')/t']} \quad (31)$$

or inverting and simplifying one gets.

$$\frac{1}{i(t)} = \frac{N_a^*}{CN_d} + \frac{xA}{CN_d} \ln \left(\frac{t + t'}{t'} \right) \quad (32)$$

Again, as in equation (30), this has a form which can be checked directly.

Effect Of Light On Electrical Conductivity

The general photoconductivity process involves simply an increase in the conductivity of a material by photon irradiation. In terms of the basic concepts of solid state theory, this would involve the mobilizing of carriers either by (1) creating a hole-electron pair through the excitation of a valence band electron into the conduction band or by (2) creating one free carrier through the excitation of a bound carrier into its respective free band. The nonequilibrium situation which results from these processes is relieved by recombination, i.e., by the carriers returning to their ground states (pair annihilation) and giving up their excess energy as radiation or to the lattice in the form of phonons.

Actually the steady-state photoconductivity process, in one respect, is just as simple as the above description implies. That is, it involves only the balancing of the rate of carrier mobilization by irradiation with the rate of recombination. These rates, however, are extremely complex in their relation to the physical characteristics of a given material. Consequently, a photoconductor can--and does--show a baffling variety of behavior depending on its impurity content, structural defects and surface parameters. Other than the fact that radiation usually increases the conductivity of a solid, the data does not fall into an easily understandable pattern. The photocurrent may raise as a fractional power of the radiation intensity; it may rise linearly or in some cases it may even rise at a greater power than the first with respect to the intensity. The photocurrent may increase, decrease, or it may remain fairly constant as a function of temperature. Sometimes the addition of a second source of radiation may even

cause a decrease in the photocurrent. Therefore, it is not surprising that a mechanistic understanding of photoconductivity processes is somewhat limited.

What has been developed is a framework of different experiments which hopefully identify significant parameters and act as a guide to their exploration. The experiments that will be used for investigation in this work will now be discussed in greater detail.

Photocurrent Transients

Photocurrent decay transients fall into two classes: those following an illumination time which causes complete or near complete saturation and those following a very short illumination time. Both cases must be treated using non-equilibrium statistics since both involve hole-electron pair production by greater than bandgap energy photons (see discussion later in this chapter), but hopefully the second case will reduce to a non-equilibrium process that can be approximately treated by equation (27). This distinction will be loosely made in terms of what happens to the holes after they are produced. In the first case the sample is irradiated until essentially a steady-state value of photoconductivity is reached. At this point there are some holes trapped in all acceptor levels and the conductivity is composed of carriers of both types. When the light is turned off the recombination process and ensuing conductivity decay will be very complex involving motion of quasi-Fermi levels and demarcation levels.¹⁹ Therefore experimental data was taken for this case essentially only to determine the difference in these decays for vacuum and air ambient. The appearance on an Elovich dependence will only be taken to mean the

process is surface controlled. That is, if there is a one-to-one correspondence between the change in the total number of conduction electrons and the change in the total number of chemisorbed oxygen, then since i is proportional to n and q is proportional to $\ln [(t + t')/t']$ (see condition (23) and following discussion), i will be proportional to $\ln [(t + t')/t']$.

In the second case the sample is irradiated for only a short time and the assumption is made that all holes produced by this process go directly to the surface thus mobilizing trapped electrons. Therefore at the time the light is turned off there is only one carrier (electrons) and all of the bulk acceptor levels are completely ionized. Several authors^{12,13} have used this condition and others to predict an Elovich equation. Their analyses and the possibility of treating this process simply with equation (27) will be discussed.

Melnick¹² worked out a theoretical treatment of photoconductivity decay in which the rate-limiting process was electron transfer over a surface barrier. His assumptions were that all the holes go to the surface and do not enter in the conduction process and that the rate of penetration of electrons and therefore the rate of adsorption (one-to-one correspondence between conduction electrons and chemisorbed oxygen) is given by $dn/dt \sim dq/dt \sim \exp(-E/KT)$ where E is the height of the surface barrier. He then calculated the height of the surface barrier neglecting the concentration gradient of electrons (see Chapter II), which gave the result that E was proportional to q^2 . E was then expanded in a Taylor series about some point q_0 and by neglecting terms in $(\Delta q/q_0)^2$ he arrived at the result that E was proportional to Δq . Putting this all together does give the correct Elovich equation in the

differential form but the simple assumption of $dn/dt \sim \exp(-E/KT)$ is suspect. Medved¹³ put this assumption on firmer ground by using a more reasonable starting point and assuming that the number of electrons $\text{cm}^{-2} \text{sec}^{-1}$ penetrating the barrier could be found using the Richardson-Dushman equation for thermionic emission. Unfortunately this leads to the introduction of a pre-exponential n factor and hence to the conclusion that the Elovich dependence should only hold for the first 10% of the decay, i.e. for $\Delta n/n_0 < 0.1$.

Due to the fact that these two theoretical approaches have serious limitations, i.e. the first has a shaky assumption and the second limits the period over which the Elovich dependence should be noted when in reality it is observed for 70 to 80% of the decay, a mechanistic analysis will not be made. Instead for these short time illuminations one might assume that the equations previously obtained for dark current decays hold. Therefore these decays will be analyzed using equation (27) leading to some interesting results.

Photoelectronic Measurements

The photoelectronic measurements made in this study were of thermally stimulated currents, continuous thermal quenching, and spectral response. They were intended to serve mainly as additional tools for correlating surface and bulk parameters.

Since thermally stimulated currents (TSC) received more attention than the other two measurements, it seems appropriate to give an outline of the experimental technique employed and a more complete phenomenological explanation of the results.

(a) The sample was taken to a low temperature in the dark (in

this case -180°C).

- (b) At this temperature it was excited with intrinsic radiation for a period of time after which the photocurrent was allowed to decay in the dark.
- (c) The sample was heated and the current in the sample recorded as a function of temperature.
- (d) The data was plotted as i_{TSC} versus temperature where i_{TSC} is the current recorded minus the actual dark current.

The resulting data was usually composed of one or more current peaks. Physically, the process can be envisioned as follows: when the sample is illuminated with intrinsic radiation and then allowed to decay a non-equilibrium density of carriers is trapped in one or more discrete energy levels because at the low temperature carriers cannot be thermally excited back into the conduction process. As the temperature is increased this non-equilibrium density is relieved by thermal excitation into the conduction band thus creating a mobile carrier density in excess of the equilibrium value.

Several methods of correlating the activation energy of these traps to the observed peaks have been used, but the simplest and the one used in this work was to assume that at the TSC peak the steady-state Fermi level coincides in energy with the trapping state (first suggested by Bube). If one makes this assumption then the expression for the activation energy becomes

$$E_k = KT_m \ln [\mu N_c e / \sigma(T_m)] \quad (33)$$

where T_m and $\sigma(T_m)$ are respectively the temperature and conductivity at the TSC peak and the other symbols have the same meaning as

previously defined. Other TSC measurements were made in which all procedures were the same except that excitation was initiated during the cooling process. They are identified as EWC-TSC measurements in later discussion. A recent comprehensive mathematical treatment of TSC phenomena in general is provided by Dressel and Bube.²⁰

Continuous thermal quenching (CTQ) measurements are simple determinations of saturation photocurrent versus temperature. In these measurements a region of enhanced photoconductivity may be found due to the presence of sensitizing centers. These centers as discussed by Houston²¹ have previously been associated with compensated acceptors, a good example being given in the work by Bube²² on CdSe:Cu. Recent work by Dussel and Bube²³, however, has suggested that this is not the only mechanism available for thermal quenching. This led Houston and Kohnke⁷ to re-examine their earlier work on SnO₂ single crystals with additional optical quenching data and to conclude that this effect was due to electron trapping states. It will be assumed that this is the mechanism for the quenching effect observed in the present work because of the similarity of the data to that obtained on single crystals.

A limited amount of spectral response data was obtained using the technique to be outlined in the next chapter.

CHAPTER IV

SAMPLES, APPARATUS AND EXPERIMENTAL PROCEDURES

Samples

The samples used in this investigation were rectangular specimens of polycrystalline stannic oxide cut from sintered pellets. The pellets were prepared as described in reference 24 and were of two compositions: "pure", those using only reagent grade SnO_2 powder and "doped", those using SnO_2 powder and 0.7% ZnO powder by weight in the original mixture. The results of the relative density (measured density divided by theoretical density) versus firing temperature at a fixed firing time are shown in Figure 3. The actual specimens used in the electrical measurements were cut from the centers of these pellets and were several millimeters on a side.

A short study was made of the surface grain size of the different pellets using a metallograph and it was found that for the "pure" SnO_2 specimens the surface grain size diameter was about 1μ for samples fired to 1175°C for 4 hours--this was about the size of the starting powder--and increased to about 5μ for samples fired to 1460°C for 4 hours. The above numbers were taken from photographs, but this technique was not suitable for obtaining an estimate of the surface grain size of the dense "doped" samples. Later, however, after etching the dense samples in HI it was found that those fired to 1460°C for 4 hours

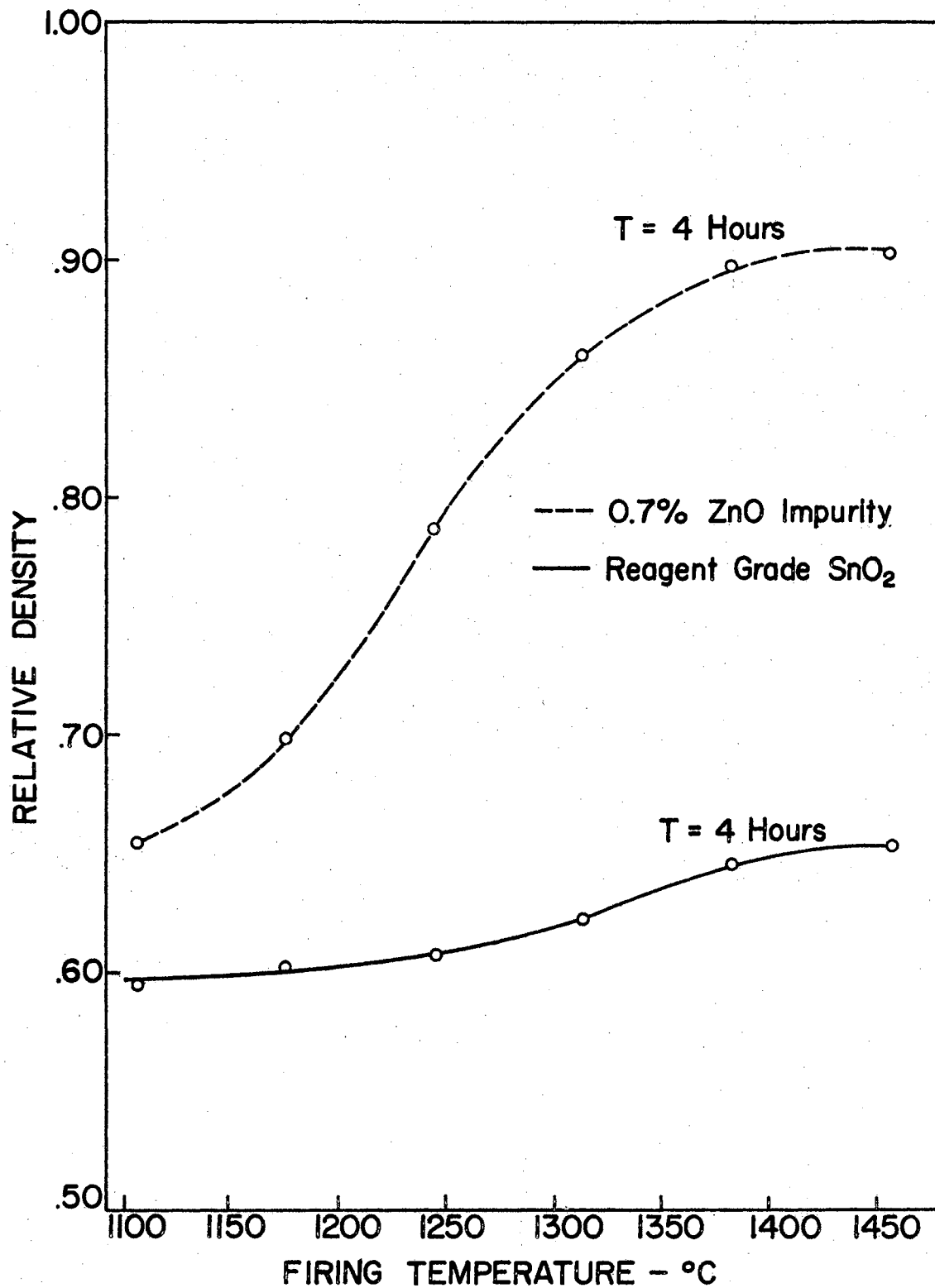


Figure 3. Relative Density as a Function of Firing Temperature at a Fixed Firing Time

had an average surface grain diameter of 4.5μ , in good agreement with that of the "pure" samples. In all cases the surface when examined under a microscope was extremely uniform in texture and after the samples were boiled in aqua regia as they were before each set of data were taken they were a flawless white color.

To obtain specimens, the pellets were mounted in optical wax or Duco Cement on a glass slide and were then cut using a carborundum saw. The physical dimensions were measured carefully using a micrometer and, as mentioned above, the cut pieces were then boiled in aqua regia to remove any surface impurities. To insure that no aqua regia was left on the sample they were washed, boiled, and rewashed in distilled water and then dried thoroughly before attaching electrical contacts. The electrical contacts were silver paint* on the dense samples and pressed tin foil on the less dense samples since the silver paint tended to be absorbed into porous samples through capillary action. These contacts were ohmic in the range 0 to +100 volts as shown in Figure 4 and periodically throughout a measurement the leads were reversed to check for polarization with consistently negative results.

Apparatus

The apparatus consisted of four main parts: the cryostat-sample holder, the gas handling system, the optical system, and the electrical measurements heater system. Since the same gas handling system was used throughout, it will be discussed first. Figure 5 is a block

* Dupont Silver Preparation, electronic grade #4817:

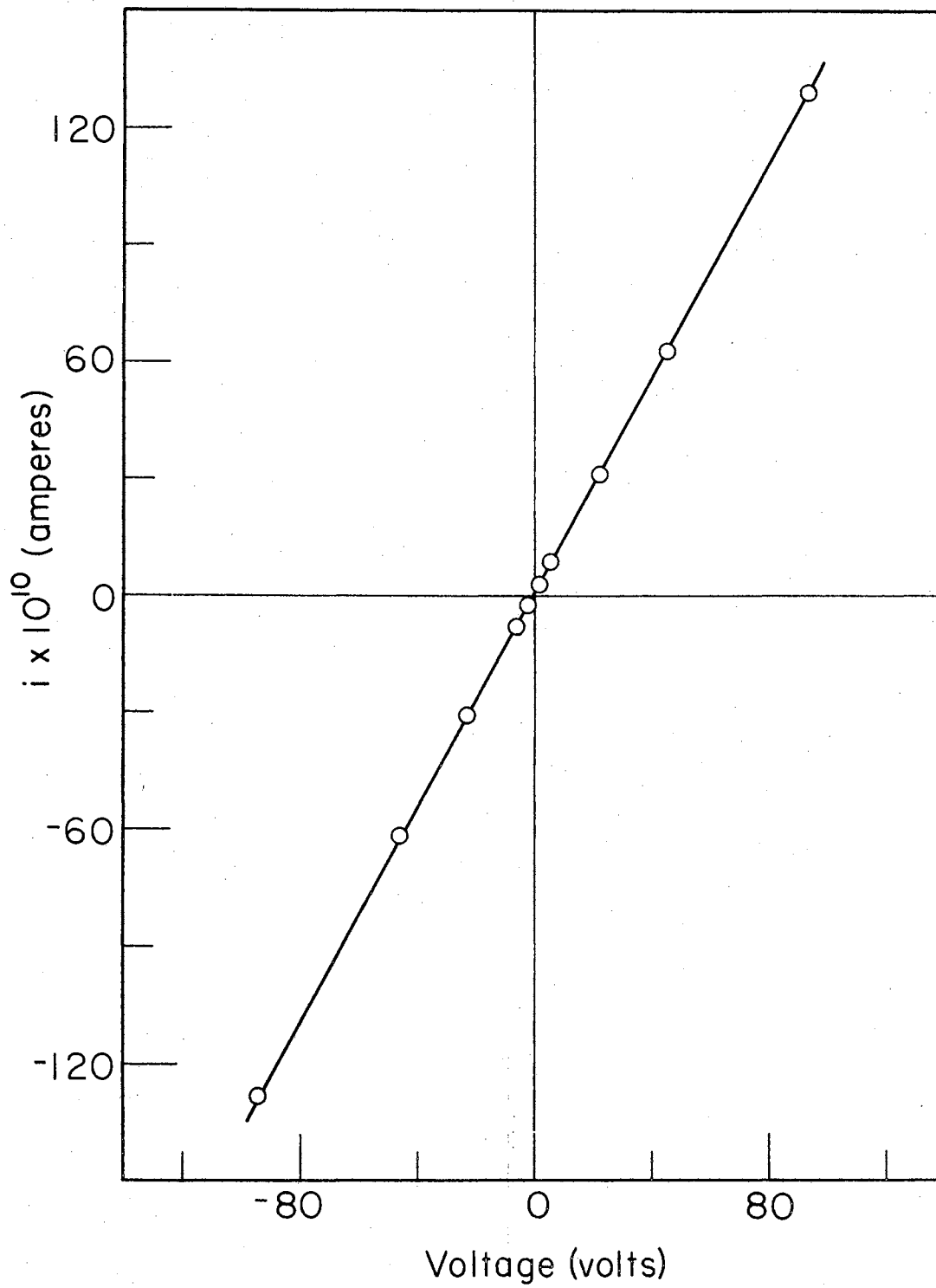


Figure 4. Dark Current as a Function of Sample Voltage

diagram of the basic parts of the gas handling system. This system is quite versatile in that one can use different types of gas, can control and monitor the gas pressure from 1 atmosphere to $\sim 10^{-5}$ torr, and if desirable, pump the gas past the sample at a rate controlled by the opening in the vacuum valve. Two drying traps were employed to insure complete extraction of water from the entering gas and teflon stopcocks were used to eliminate vacuum grease on the inlet side of cryostat sample holder. The placement of the two thermocouple gages and the ionization gage in the system made possible a knowledge of pressures at various points and after a little practice one could satisfactorily control ambient conditions with this system.

The same electrical measurements heater system was also used throughout the measurements. A simplified electrical circuit is shown in Figure 6 which does not include the shielding and the points at which the circuit contained break points. These points and the types of connectors used at these points will be described later. The power dissipated by the heater was measured by the ammeter and voltmeter in the heater circuit and the variable resistors were used to control the circuit current. Using 25 volts the amount of power dissipated by the heater could be varied from 0-35 watts. The voltage developed in the thermocouple was placed on the horizontal scale of the X-Y recorder and with the output from the electrometer on the vertical scale, one could obtain plots of sample current versus thermocouple voltage directly on the recorder tracings. Or, using the X-Y recorder as a time-base instrument, one could obtain directly tracings of sample current versus time at constant temperature.

For the optical measurements a source of narrow band radiation was

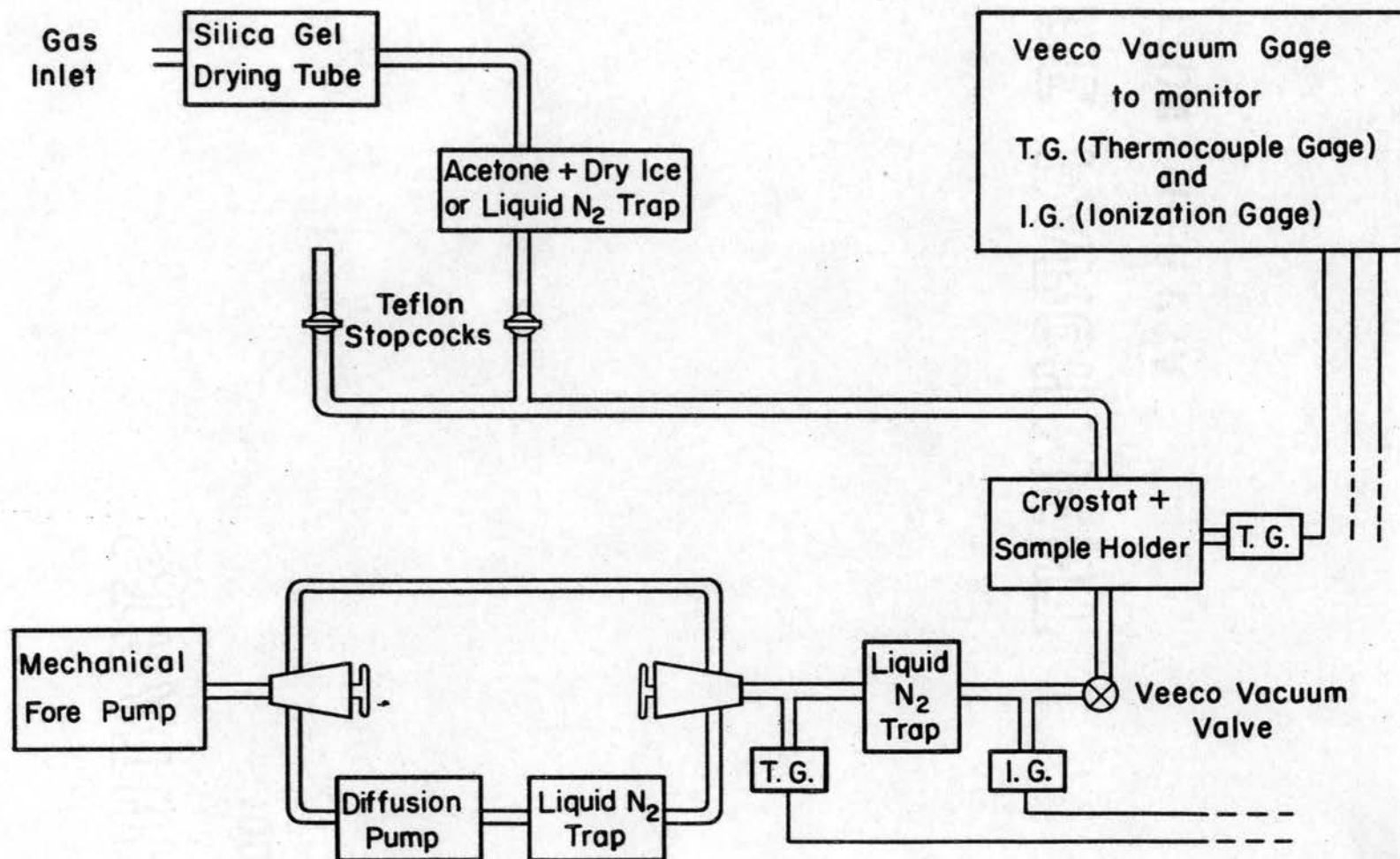


Figure 5. Gas Handling System

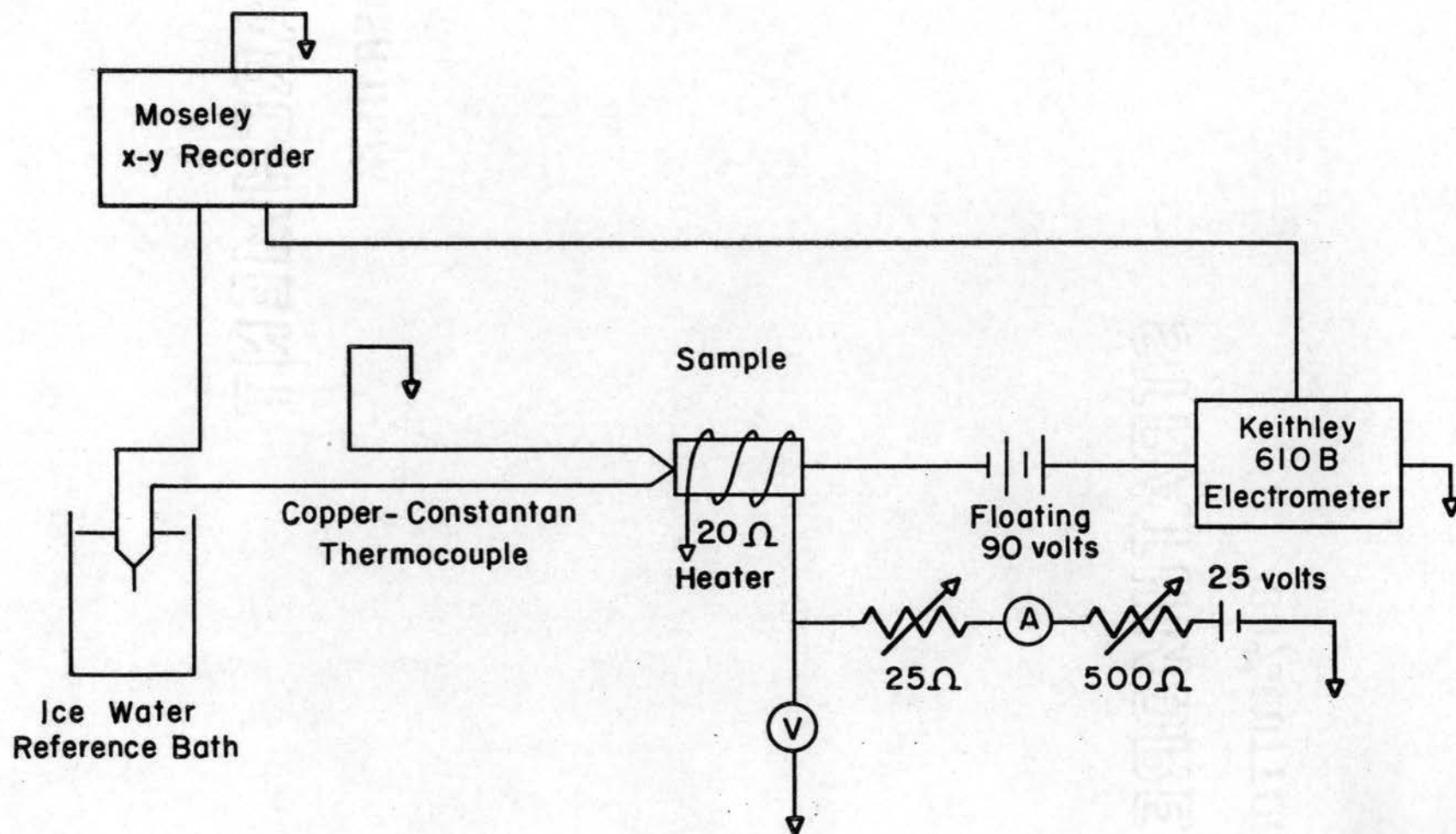


Figure 6. Electrical Measurements - Heater System

needed. This was provided by a simple filter optical system as shown in Figure 7 or by use of a Bausch and Lomb 500 mm grating monochromator which had a range of 200 to 700 μ (millimicrons). The monochromator was used either with a mercury arc lamp for high intensity or with a deuterium lamp when a continuous spectral distribution was required.* The output dispersion curve for the deuterium lamp is shown in Figure 8.

There were two types of cryostat sample holder systems used in the measurements. The first type which was a modification of suggestions by Houston²⁰ is shown in Figure 9. This cryostat consisted of two parts--one a metal vacuum chamber with optical port, gas ports, and a thermocouple gage port and the other a glass dewar with the sample heater chamber and guard tube attached--which were sealed using an "O" ring and spring clamps. All joints on the vacuum chamber were soldered except the optical port in which the quartz was sealed with Apiezon W vacuum wax. The glass dewar was sealed to the sample heater chamber with 60/40 tin lead solder which proved inadequate since repeated thermal cycling caused the joint to crack. To help remedy this situation a copper clamp was then soldered over this joint. Unfortunately, this only lengthened the time between cracks and it is now planned that any new dewars be made entirely of stainless steel so that all joints can be welded. Also in the bottom of the sample heater chamber were soldered heater lead vacuum feed-throughs and a Conax miniature transducer gland, which acted as the vacuum feed-through for the

*The deuterium lamp was a Model D-102 distributed by the George W. Gates Company, Inc.

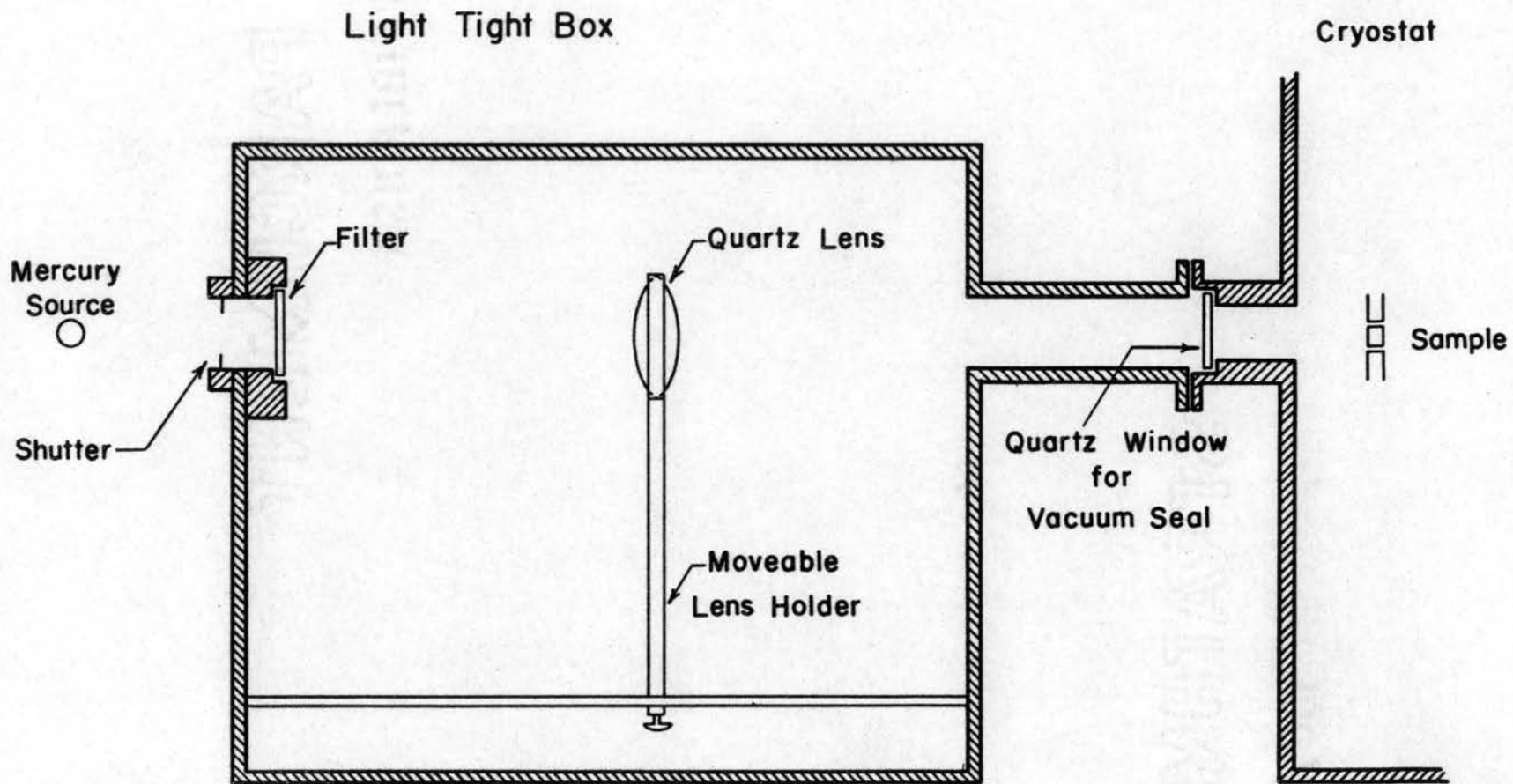


Figure 7. Simple Optical System

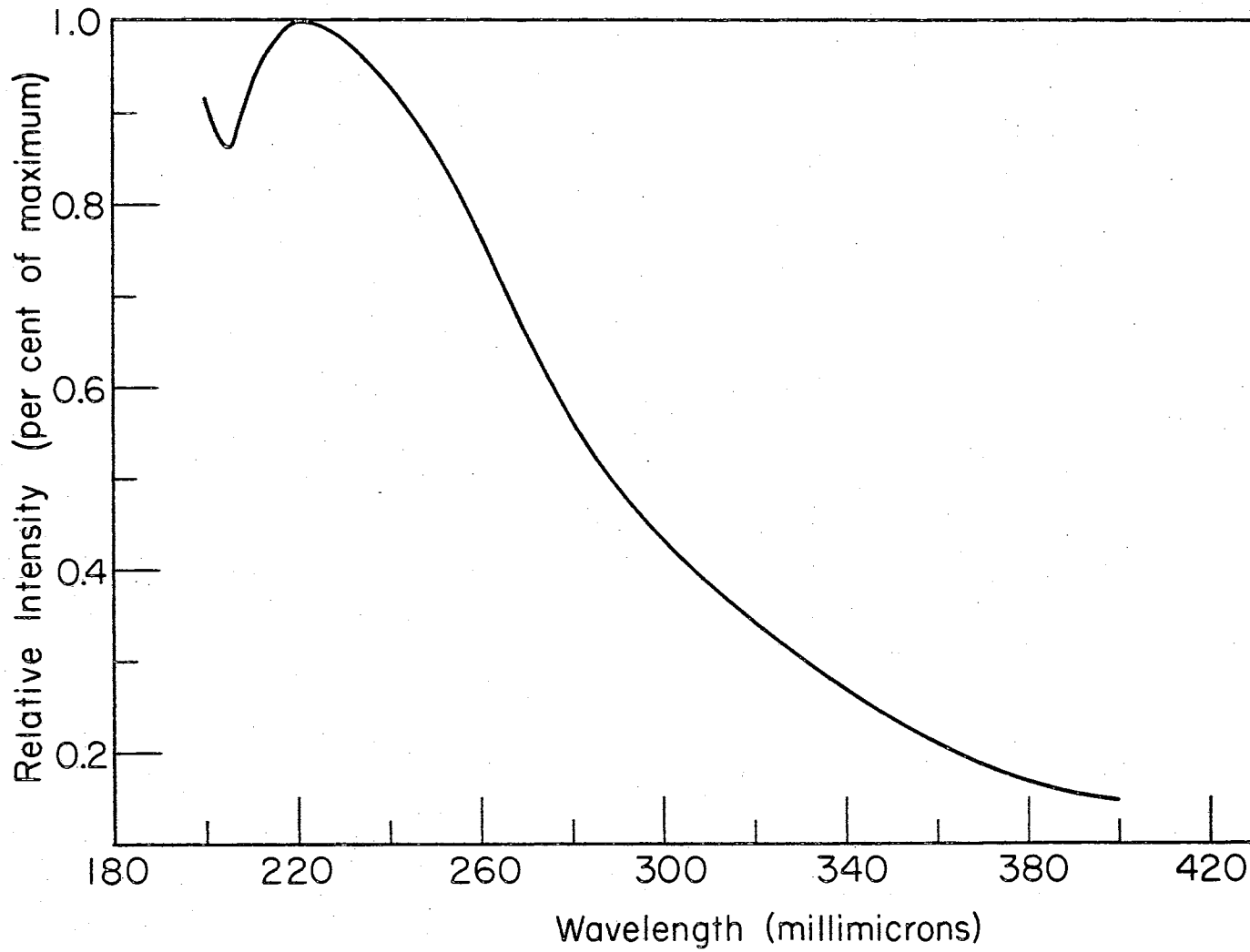


Figure 8. Output Dispersion Curve for the Deuterium Lamp

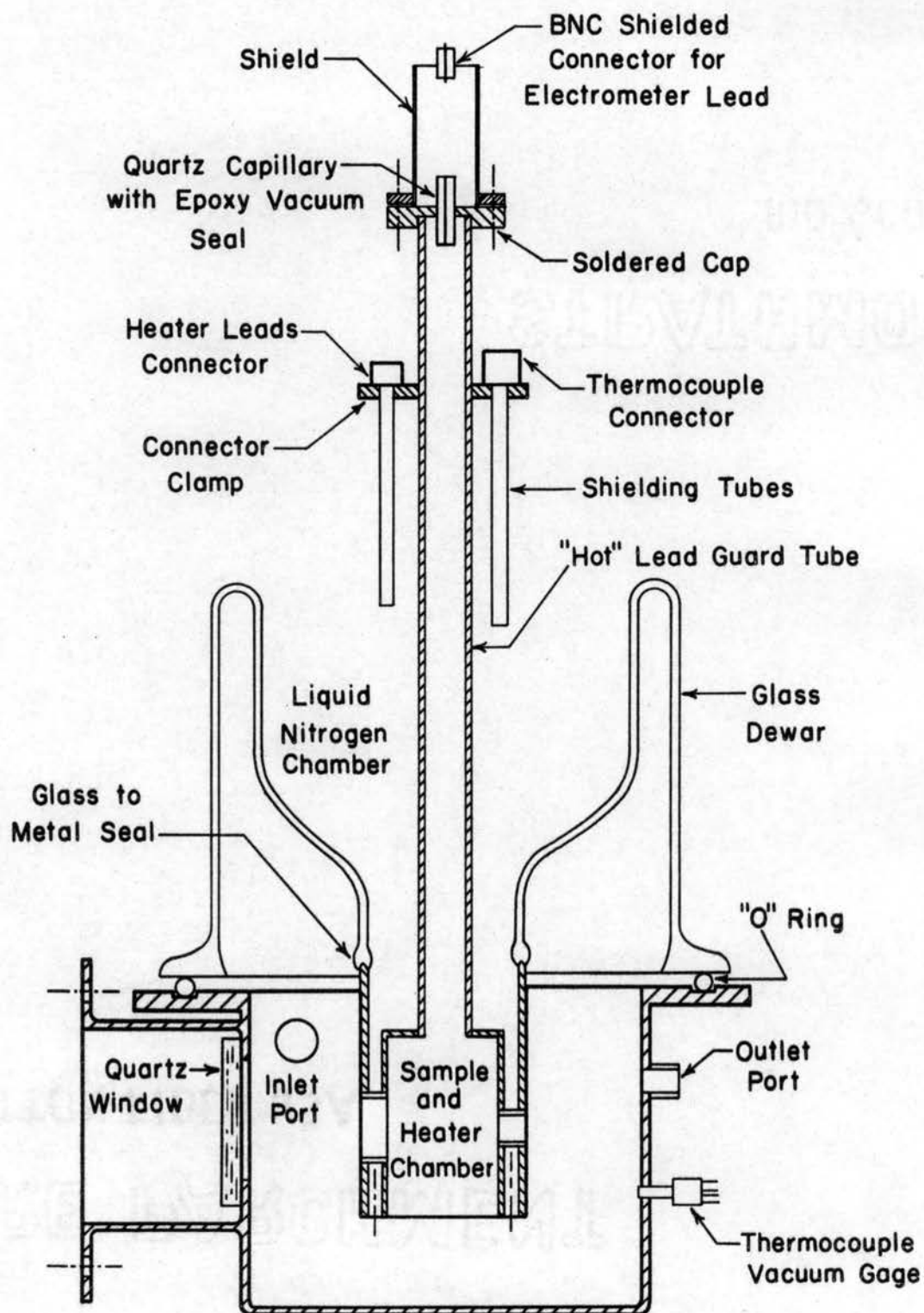


Figure 9. Cryostat Sample Holder System

thermocouple wires. This was done so that these leads from the sample holder would be run through the liquid N_2 to the external circuit, thus reducing heat leaks. The guard tube was soldered into the top of the sample heater chamber and is shown in Figure 10.

The tube consisted of two glass-to-metal seals back to back soldered to two copper tubes with a glass capillary inside held in place by teflon inserts. The purpose of the two glass-to-metal seals was to eliminate the thermal path from the liquid N_2 to the lead connectors. A cap with a machined hole to fit a quartz capillary was soldered to the tube while the vacuum seals for the quartz capillary and hot lead wire were made with epoxy. This not only gave an excellent vacuum seal but by using the quartz capillary there was essentially an infinite resistance between the hot lead and ground (the cap) at this feed-through. At the other end of the glass capillary a glass-to-metal seal was placed such that a copper electrode could be attached to make contact with the electrode on the sample holder as shown in Figure 11. The guard tube was constructed in the above manner for the same reason the heater and thermocouple leads were run through liquid N_2 , that is, to reduce thermal leaks to the sample when it was at low temperatures. The hot lead could not be run directly through liquid N_2 as the others were because of the high resistance of the samples to be measured. The consequent necessity of reducing electrical leakage to an absolute minimum was also a problem in building the sample holder and necessary precautions were taken as shown in Figure 11.

The sample was made out of a copper tube surrounding a heater and spring housing--the copper tube was heated and slipped over the housing while expanded--with teflon and quartz for electrical insulation.

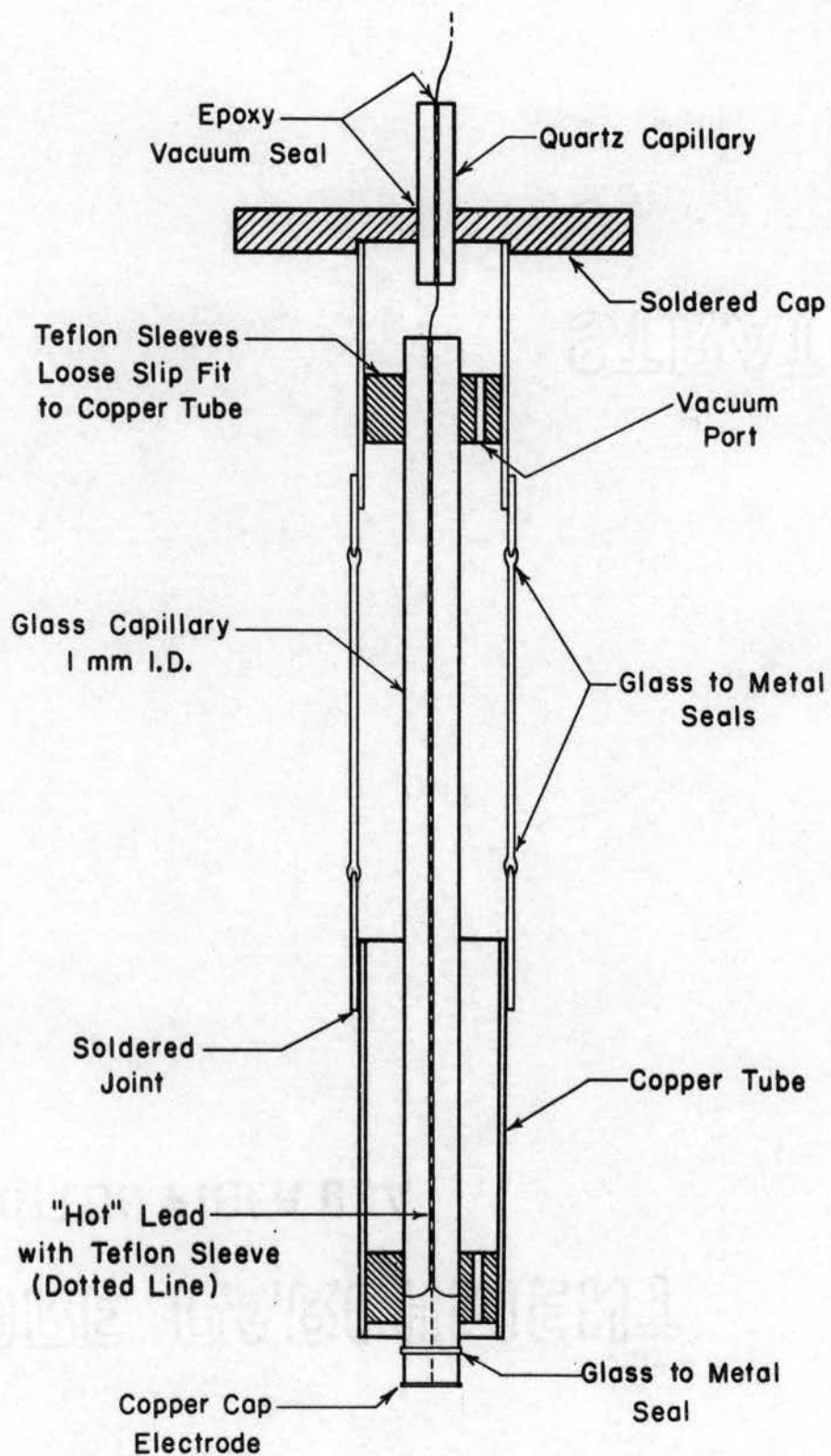


Figure 10. Guard Tube

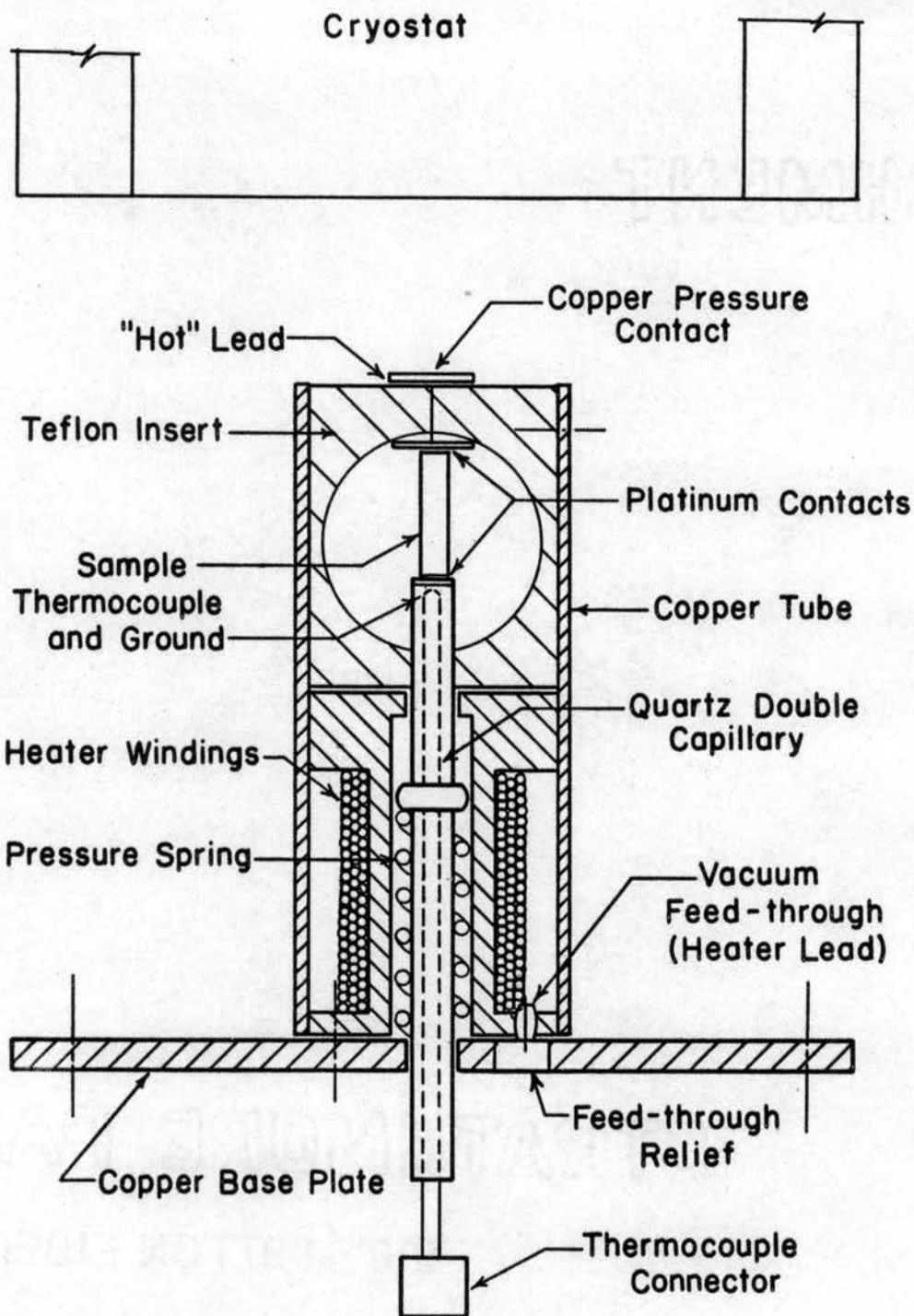


Figure 11. Sample Holder

Pressure contacts were made to the sample as shown and several sizes of samples could be accommodated by changing the length of the pressure spring. The heater was made of asbestos-covered number 28 gage nichrome wire and was grounded to the copper housing. Temperature measurements were made at the lower contact and the copper thermocouple wire was also used as the sample ground. The copper base plate which attached to the cryostat could either be put in direct thermal contact or shielded from the heater housing by use of teflon inserts for the connecting screws. The overall design provided very low electrical leakage and excellent control of the sample temperature. The only problem was that the copper base plate could not be coupled and decoupled from the liquid N_2 thereby forming a variable thermal contact during the course of an experiment. It is suggested for future work that a screw mechanism using a vacuum bellows be constructed so that the base plate can be lowered and raised at will thereby providing a variable heat leak to the liquid N_2 .

The other type of system was a glass system patterned after the one used by Houston and using the same sample holder as he did. This system is adequately described in reference 20. It was constructed so that it could be hooked directly to the Bausch and Lomb monochromator thereby simplifying the photoconductivity measurements. But, although it simplified these measurements, it limited the pressures and temperatures at which they could be taken. A much better cryostat and sample holder system could be built using the existing metal system as a pattern (Figures 9, 10 and 11) and incorporating suggestions made in the discussion of this system.

Measuring Techniques

The bulk of the data was taken using the system shown in Figures 6 and 9 and falls into two main classes. These are conductivity versus temperature in a particular ambient and conductivity decay transients in a particular ambient. In both of these cases radiation may have been introduced during or before the measurement. Whether this was done will become clear in the context of the individual experiments. Most of the experimental data required continuous monitoring of the conductivity as a function of temperature or time and this functional relationship was obtained by plotting the two variables on the Mosely X-Y recorder. The conductivity was plotted using the output of the Keithley electrometer and the temperature could be obtained using the plotted output of the thermocouple. For time measurements the recorder was converted to a time-base instrument and conductivity plotted as above. The data were then analyzed from these tracings.

Dark conductivity as a function of temperature was taken after different "fixing" procedures (see Chapter I) by varying the temperature with the heater around the sample. This was done at various temperatures when the temperature was increasing or decreasing as will be shown later. Dark conductivity decay transients were taken by stabilizing the conductivity in a particular vacuum condition and then quickly letting dry air into the system. The photoconductivity decay transients were taken in the same ambient as that in which the sample was illuminated and again conductivity was plotted versus time on the recorder.

Thermally stimulated current measurements (TSC) were made in the

dark after a low temperature irradiation. The procedure consisted of taking the sample to a low temperature (liquid N_2) in the dark and irradiating for several seconds to several minutes. After a time sufficient for the decay of most of the resulting photoconductivity, the sample and the current in the sample circuit was recorded as a function of thermocouple voltage. Usual heating rates were of the order of $0.3 \text{ }^\circ\text{C sec}^{-1}$. The data were then corrected by subtracting the dark current at every temperature.

In the case of continuous thermal quenching (CTQ), the sample was taken to a low temperature and irradiated as described above, but the light was left on until saturation was reached--usually about 20 minutes. The sample was then slowly heated by letting the temperature drift up without turning the heater on, and the light was left on during the rise. Again, the current in the sample circuit was recorded as a function of thermocouple voltage and the data corrected for the dark current. For both TSC and CTQ measurements, irradiation was accomplished by either of two intrinsic wavelengths, 2536 or 3131\AA .

The only experiments in which the X-Y recorder was not used were those for determining the spectral response. Ideally, spectral response data would be taken as saturation photocurrent versus wavelength at a fixed temperature. However, since the samples do not saturate for long periods of time, a compromise was necessary and the current was recorded after several minutes at each wavelength. In order to approximate the true spectral response the data were corrected for the output dispersion curve of the deuterium lamp.

CHAPTER V

RESULTS

Introductory Remarks

The purpose of the present chapter is to systematically present the results of the experimental measurements previously discussed. It should be pointed out here that the data chosen for presentation, although restricted to a few samples, are representative of the behavior of all samples of the particular type reported. The specimens are subdivided into two classifications--dense or porous for comparative purposes.

Results are described for the four broad categories: (1) equilibrium dark current measurements, (2) dark current decay measurements, (3) photodecay measurements, and (4) selected photoelectronic measurements. This last category included observations of spectral response, thermal quenching (CTQ), normal thermally stimulated currents (TSC), and thermally stimulated currents after an excitation while cooling (EWC-TSC). A basic parameter of interest in all of these measurements was the ambient gas pressure.

Equilibrium Dark Conductivity

The first kind of measurements taken were dark conductivity versus temperature after various fixing procedures (see Chapter I). Data

reported were taken on two types of samples, Zn-doped polycrystalline specimens which had a density of 6.40 gm/cc (hereafter referred to as the dense samples) and Zn-doped polycrystalline specimens which had a density of 4.65 gm/cc (hereafter referred to as the porous samples). All conversions between measured currents and calculated conductivities were accomplished using gross values for the geometrical parameters length and cross-sectional area.

Figure 12 shows results obtained on the dense samples. Before explaining the different curves it should be noted that parts of this data were taken on two different dense specimens in both sample holders discussed in Chapter IV and one curve (curve A) represents data obtained independently* on a third sample in an apparatus designed primarily for thermoelectric power measurements at low pressures and high temperatures. This illustrates that these effects are not only real but are reproducible from sample to sample. The fixing procedure for the different curves is given below.

- A - Sample fixed at 10^{-6} torr, 100°C for 10 minutes and measurements made while temperature decreased;
- B - Sample fixed at 2×10^{-1} torr, 94°C for 14 hours and measurements made while temperature increased;
- C - Sample fixed at 3×10^{-1} torr, 110°C for 80 hours and measurements made while temperature increased;
- D - Sample fixed at 1 Atmosphere Dry Air, 24°C for 12 hours and measurements made while temperature decreased;

*Measurements by James L. Rutledge, Physics Department, Oklahoma State University.

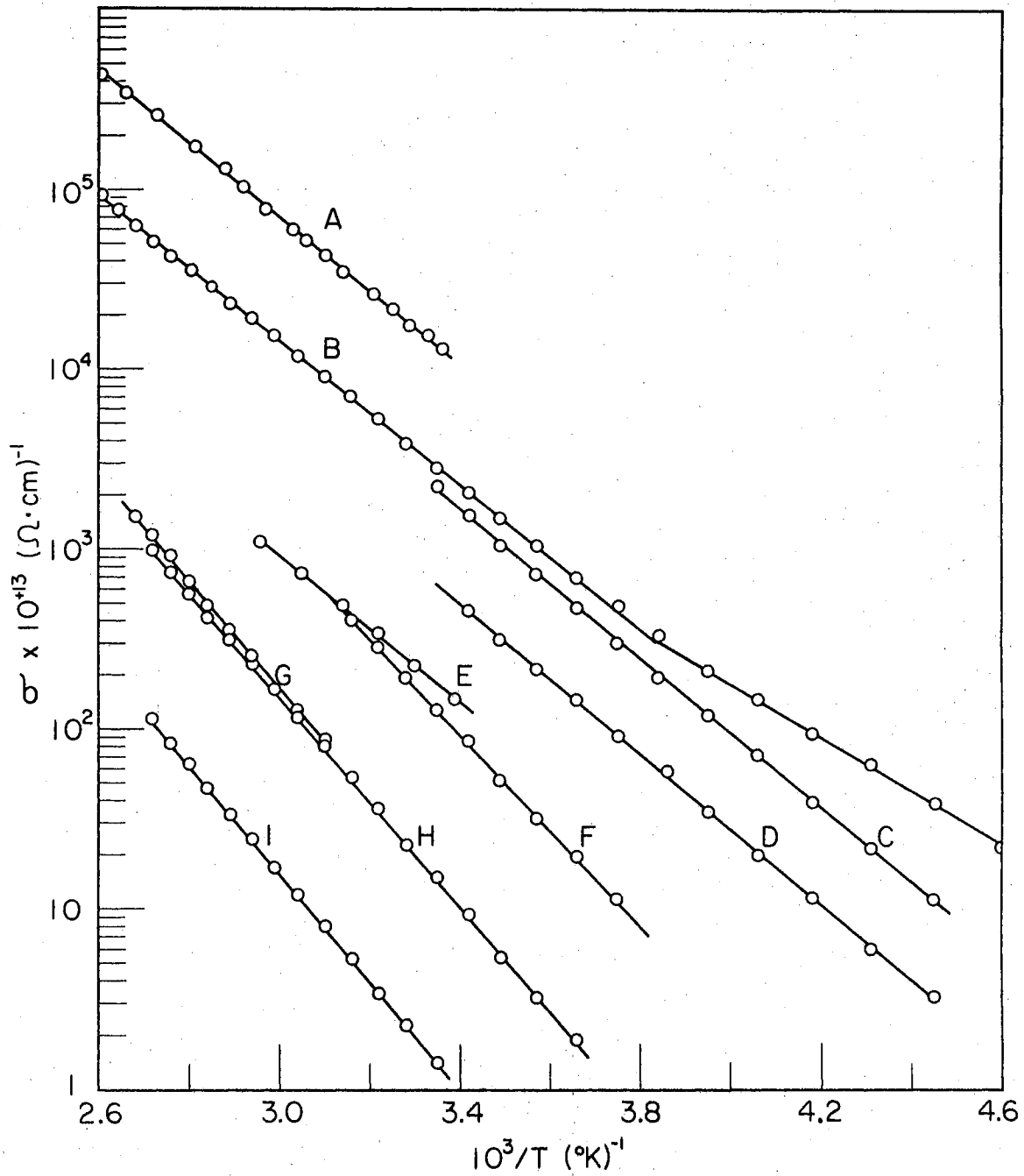


Figure 12. Dark Conductivity as a Function of Temperature for a Dense Sample After Various Fixing Procedures

- E - Sample fixed at 1 Atmosphere Dry Air, 24°C for 40 hours and measurements made while temperature increased;
- F - Sample fixed at 1 Atmosphere Dry Air, 24°C for 67 hours and measurements made while temperature increased;
- G - Sample fixed at 1 Atmosphere Dry Air, 137°C for 15 hours and measurements made while temperature decreased;
- H - Sample fixed at 1 Atmosphere Dry Air, 50°C for 67 hours and measurements made while temperature increased;
- I - Sample fixed at 1 Atmosphere Dry Air, 105°C for 66 hours and measurements made while temperature increased.

Figure 13 shows data taken on the porous sample with the fixing procedures for the different curves given below.

- A - Sample fixed at 5×10^{-4} torr, 112°C for 6 hours and measurements made while temperature decreased;
- B - Sample fixed at 1×10^{-2} torr, 90°C for 13 hours and measurements made while temperature decreased;
- C - Sample fixed at 8×10^{-1} torr, 56°C for 9 hours and measurements made while temperature decreased;
- D - Sample fixed at 1 Atmosphere Dry Air, 24°C for 10 hours and measurements made while temperature increased;
- E - Sample fixed at 1 Atmosphere Dry Air, 103°C for 21 hours and measurements made while temperature decreased.

In order to demonstrate the exponential character of the conductivity data, measurements were made from -88°C to +72°C. The results for this temperature range are presented in Figure 14 (curve D in Figure 13 also represents some of this data) and show the predicted linear behavior of $\ln \sigma$ versus T^{-1} for 5 orders of magnitude. The

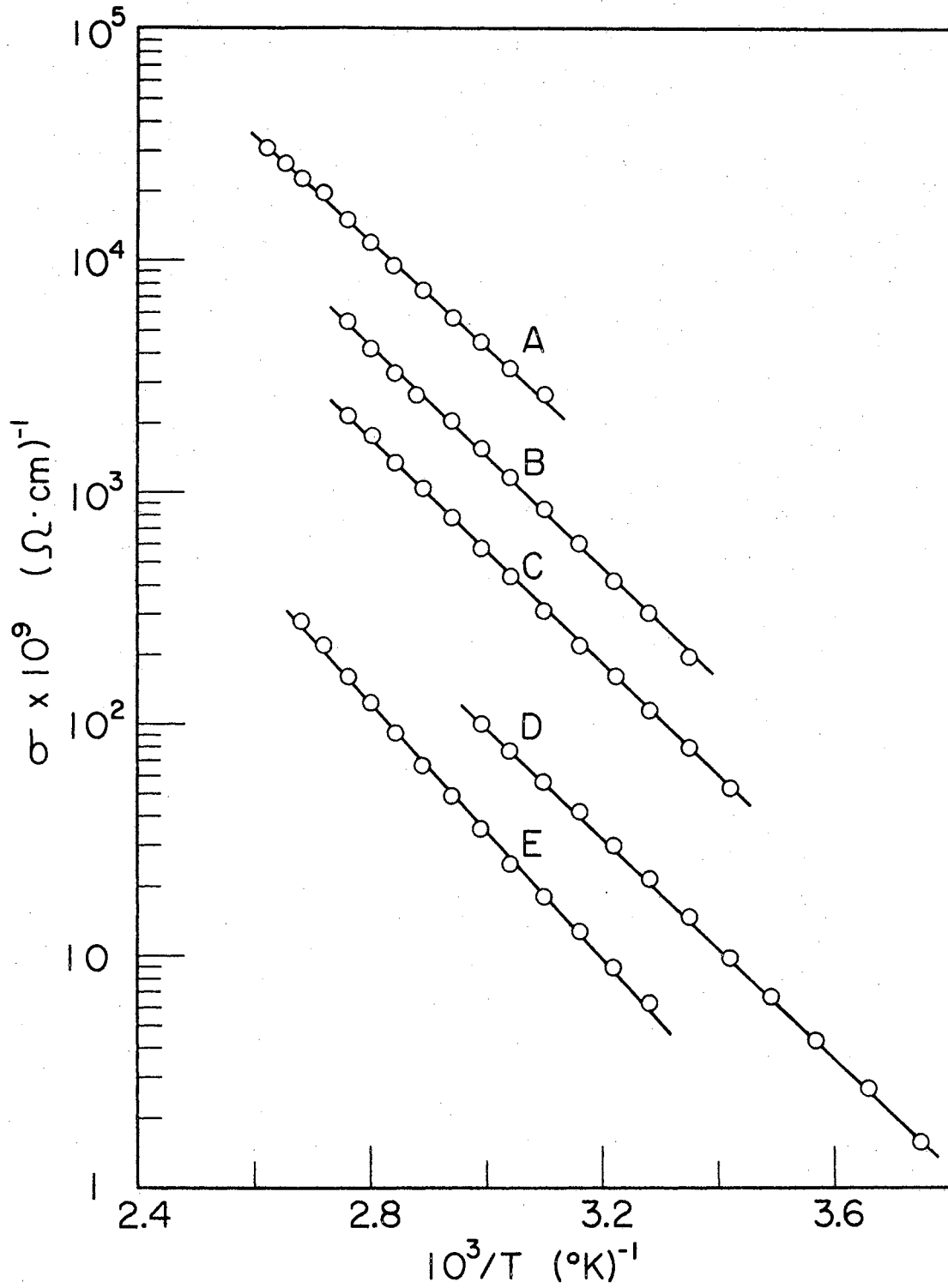


Figure 13. Dark Conductivity as a Function of Temperature for a Porous Sample After Various Fixing Procedures

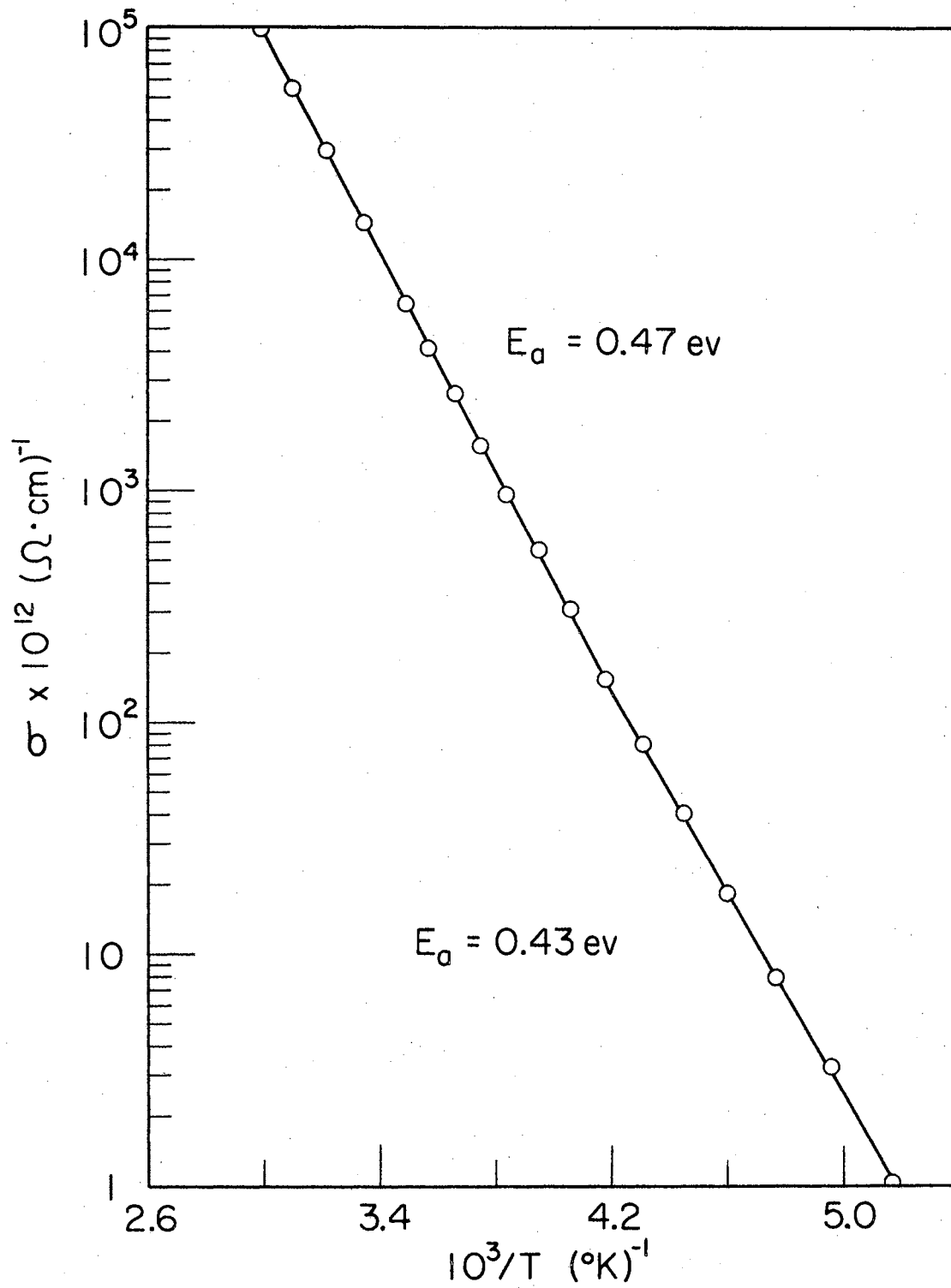


Figure 14. Dark Conductivity as a Function of Temperature for a Porous Sample

activation energies E_a calculated from the slopes of these curves and any other calculations or comments pertaining to Figures 12 and 13 will be given in the next chapter.

Dark Current Decays

In order to better understand the mechanism responsible for the different room temperature current levels observed following different fixing procedures shown in Figures 12 and 13, measurements were made of the current change following a rapid ambient change at this temperature. These measurements were made from several different initial values of current. Figure 15 shows the current decay of a dense sample which was fixed to an initial current level of 5.76×10^{-9} amperes and Figure 16 shows the decay of the same sample fixed to an initial value of 2.82×10^{-10} amperes. Although the decay is much slower in the second case, both decays have a characteristic i versus $\log(t + t')$ functional dependence.

The same type of measurement was made on a porous sample and the results are shown in Figure 17. Notice that the curves for all three figures show the functional dependence predicted by equation (30).

Photocurrent Decays

The photocurrent decay measurements are divided into two classes: those following a long excitation to saturation, and those following a very short excitation. In each class a definite difference between decays in air and vacuum was found. Only dense specimens were studied because the higher dark current level of the porous samples limited their relative response. Figure 18 shows the relative difference of

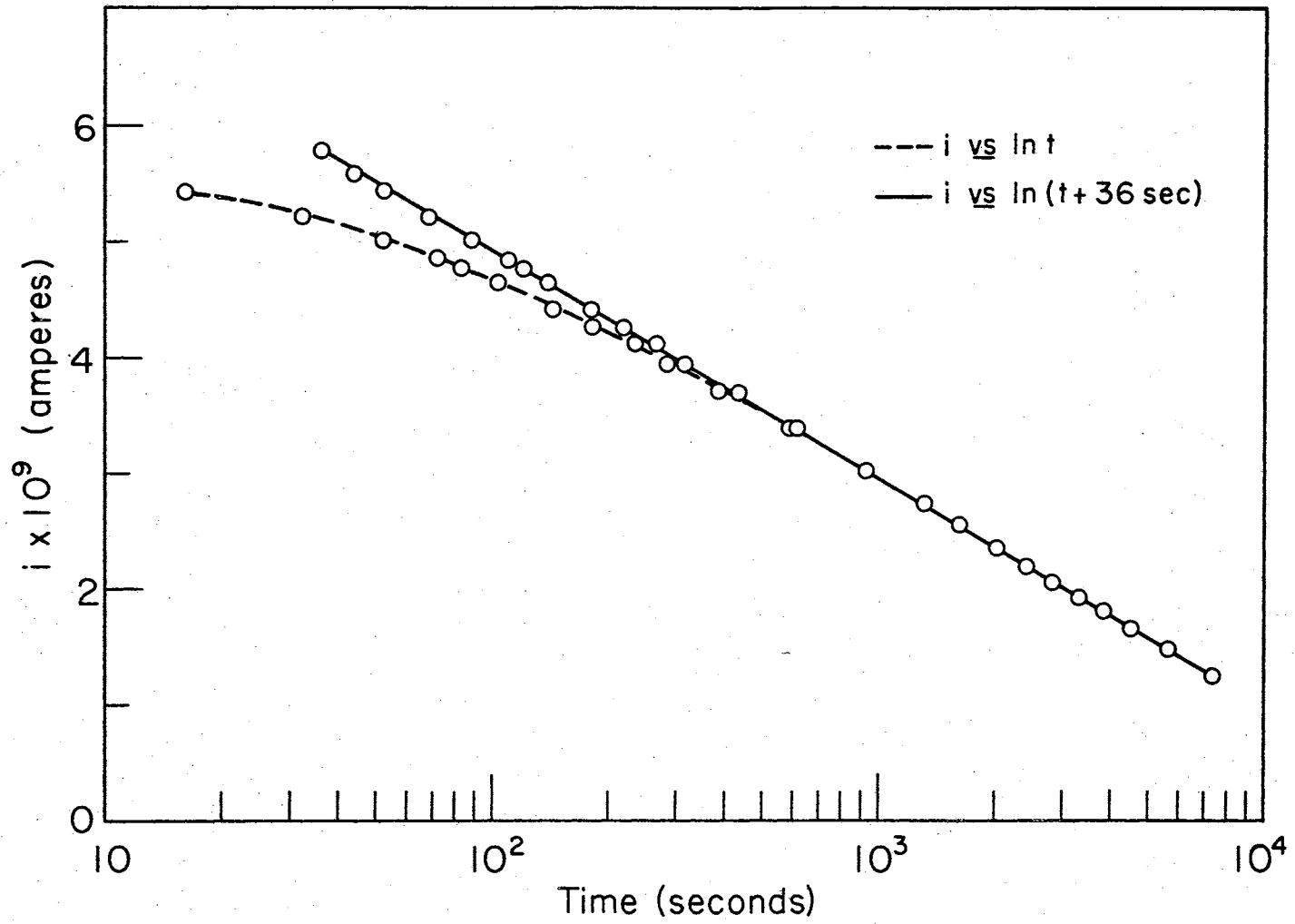


Figure 15. Dark Current Decay of a Dense Sample

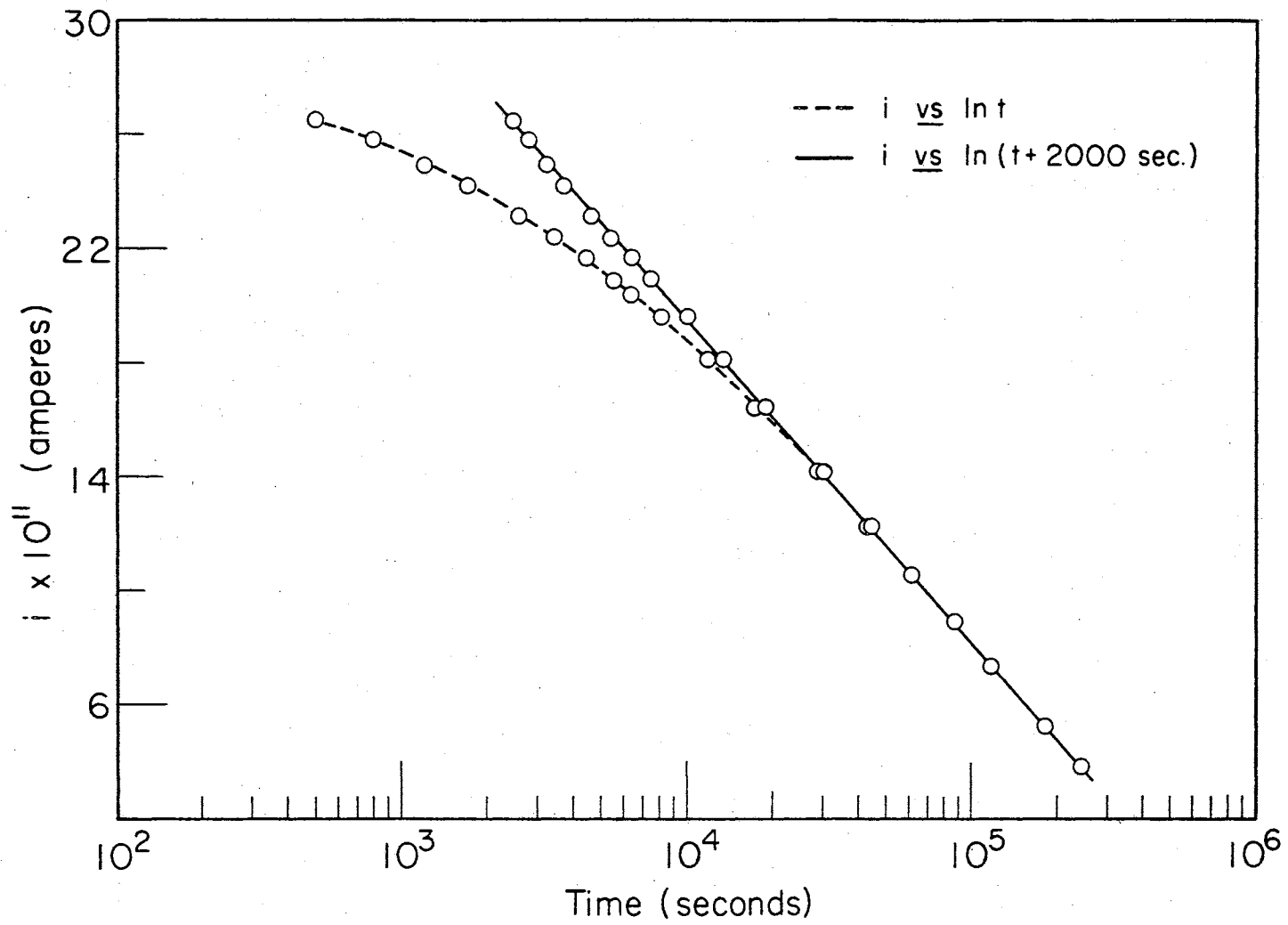


Figure 16. Dark Current Decay of a Dense Sample

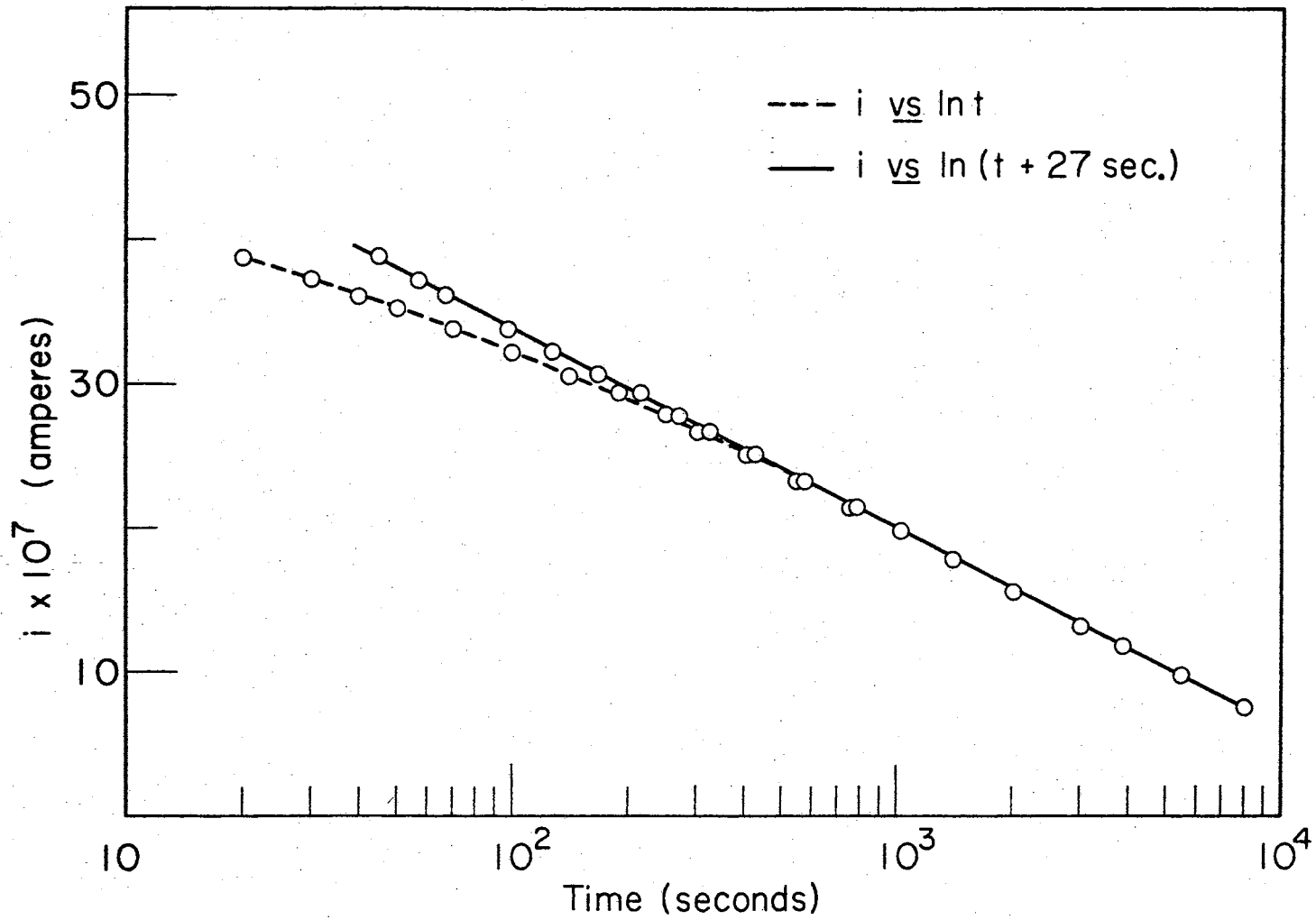


Figure 17. Dark Current Decay of a Porous Sample

decay following an excitation by 3131\AA radiation for 150 seconds.

Notice that is a difference both in the peak photocurrent reached and the speed of the decay. The next several figures represent investigation of the decay.

In Figure 19 one sees a photo-decay in air at 20°C following a 5 hour excitation using 2536\AA radiation. Notice the two straight line dependences of i versus $\log t$ and the breakover between them. Again in Figure 20 which is a photo-decay in air at 60°C following an 18 hour excitation using 2536\AA radiation one sees a similar functional dependence and breakover. But, in Figure 21 which is a photo-decay at a pressure of 7×10^{-2} torr following a 5 hour excitation using 2536\AA radiation one does not see the above functional dependence. Nor does one in Figure 22 which is a photo-decay at a pressure of 1×10^{-2} torr following a 5 hour excitation using 3131\AA radiation.

In Figure 23 two curves of photo-rise and photo-decay in air at 24°C are shown for a short irradiation of 16 sec. The difference in the two is the intensity of the 2536\AA radiation used. One can now replot this decay data to give a linear plot on a $1/i$ versus $\ln(t + t')$ scale as is done in Figure 24. It is immediately noticed that these data for short illumination do not follow the same functional behavior as the saturation data.

Photoelectronic Measurements

A measurement was made of the spectral response of a dense sample as shown in Figure 25. Data were taken at -140°C and corrected for the output dispersion of the deuterium lamp shown in Figure 8. Notice measurements were taken both in vacuum and air and since the

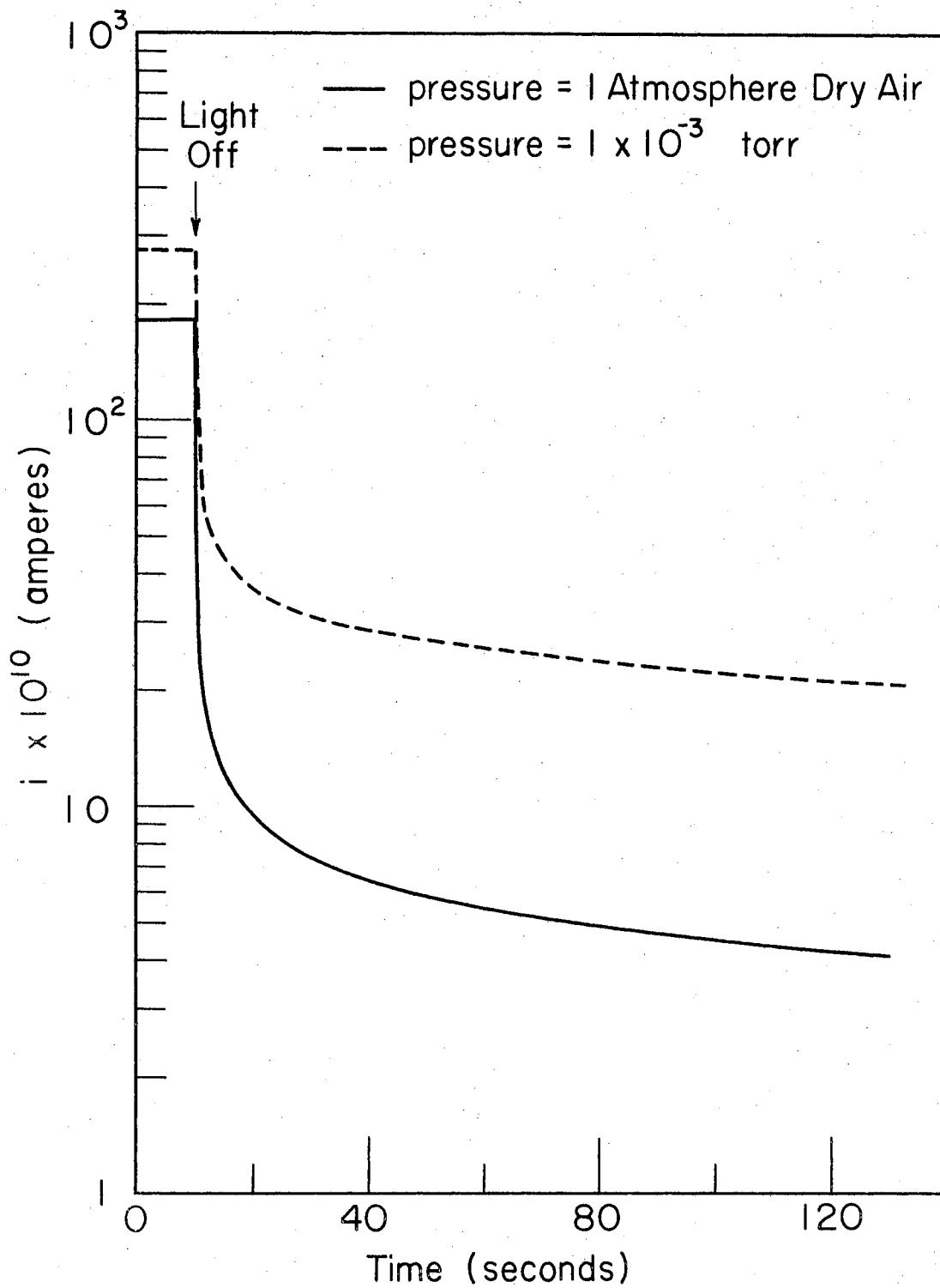


Figure 18. Photocurrent Decay of a Dense Sample in Different Ambients (3131\AA)

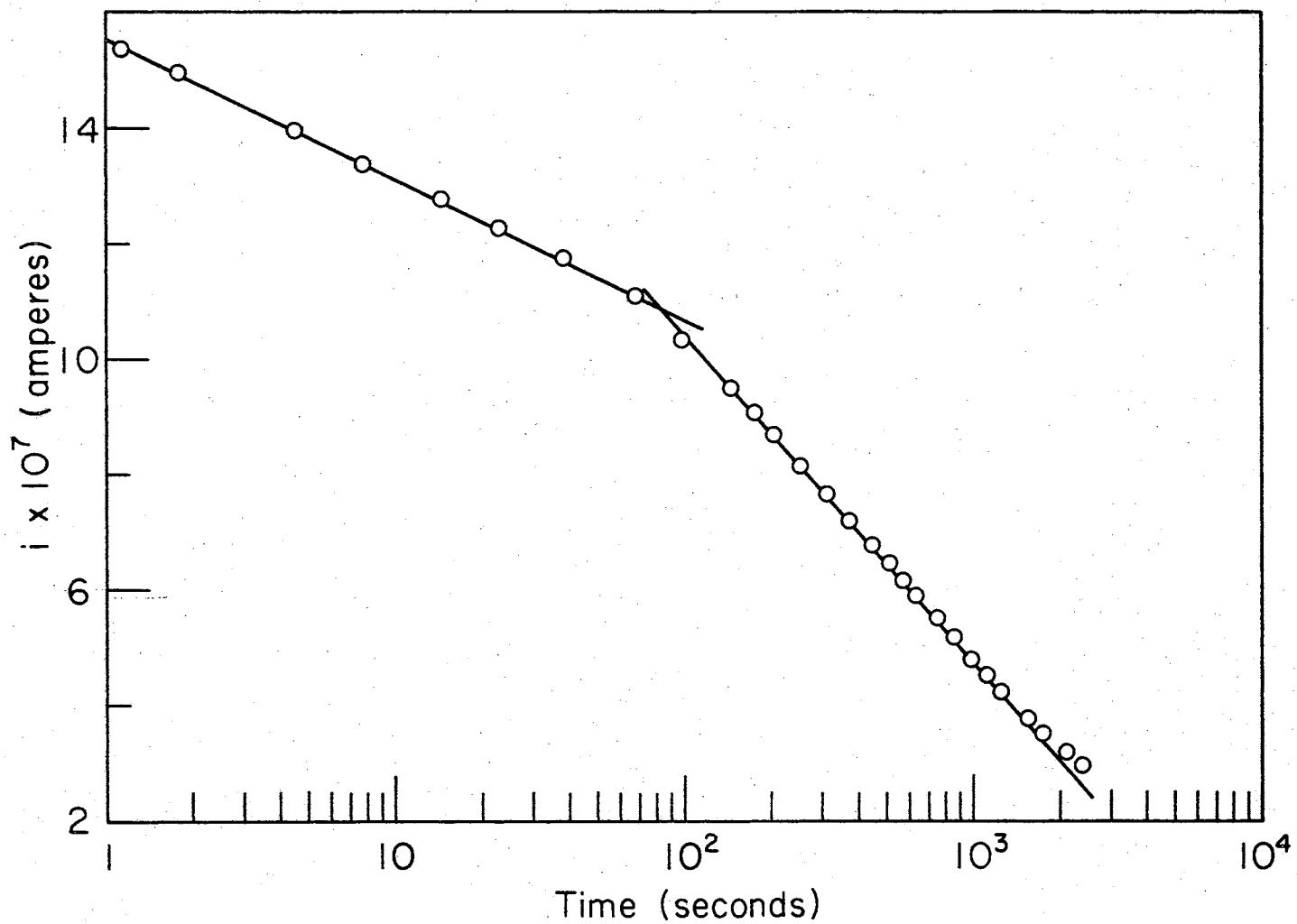


Figure 19. Photocurrent Decay of a Dense Sample in Air at 24°C (2536\AA)

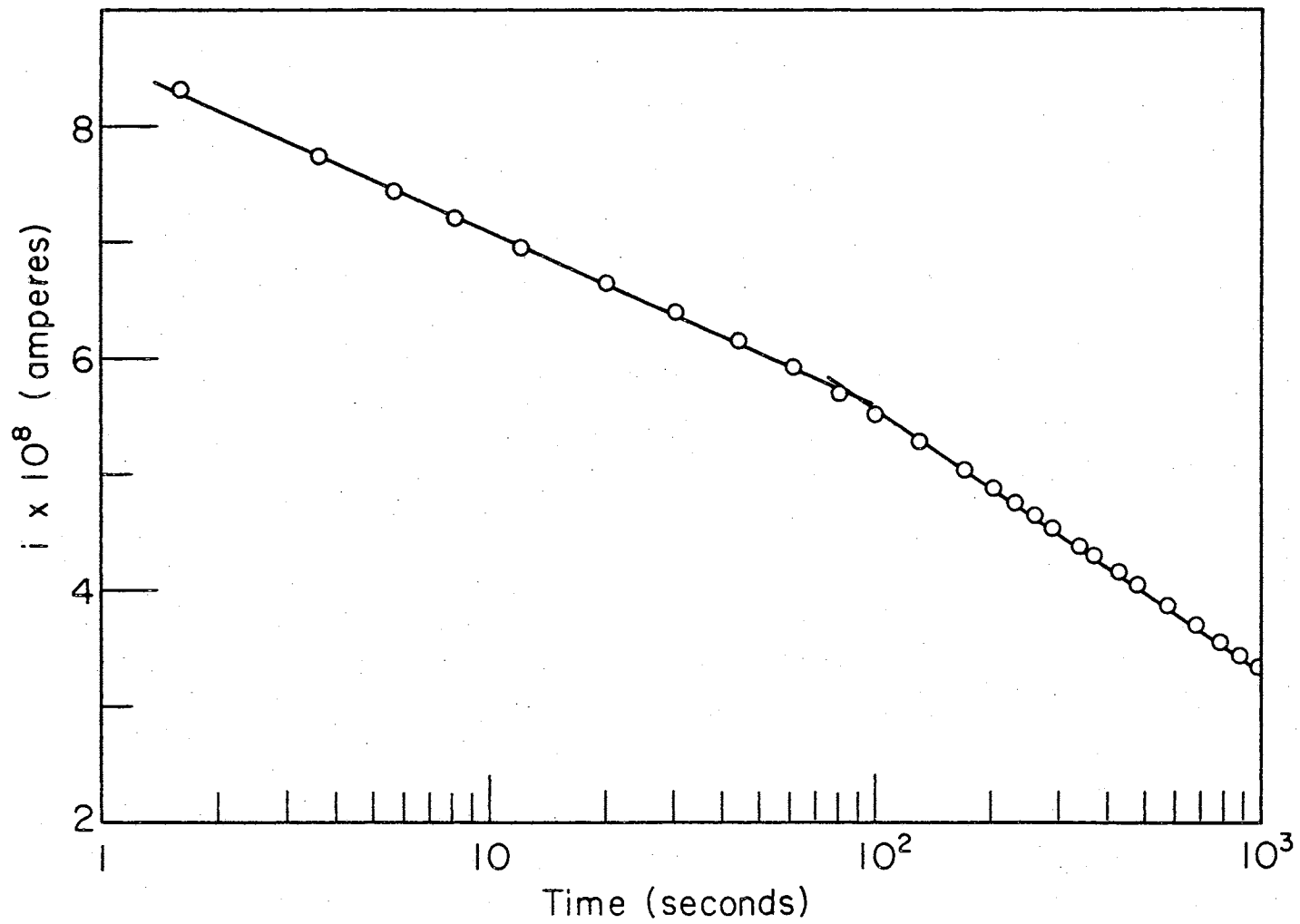


Figure 20. Photocurrent Decay of a Dense Sample in Air at 60°C (2536\AA)

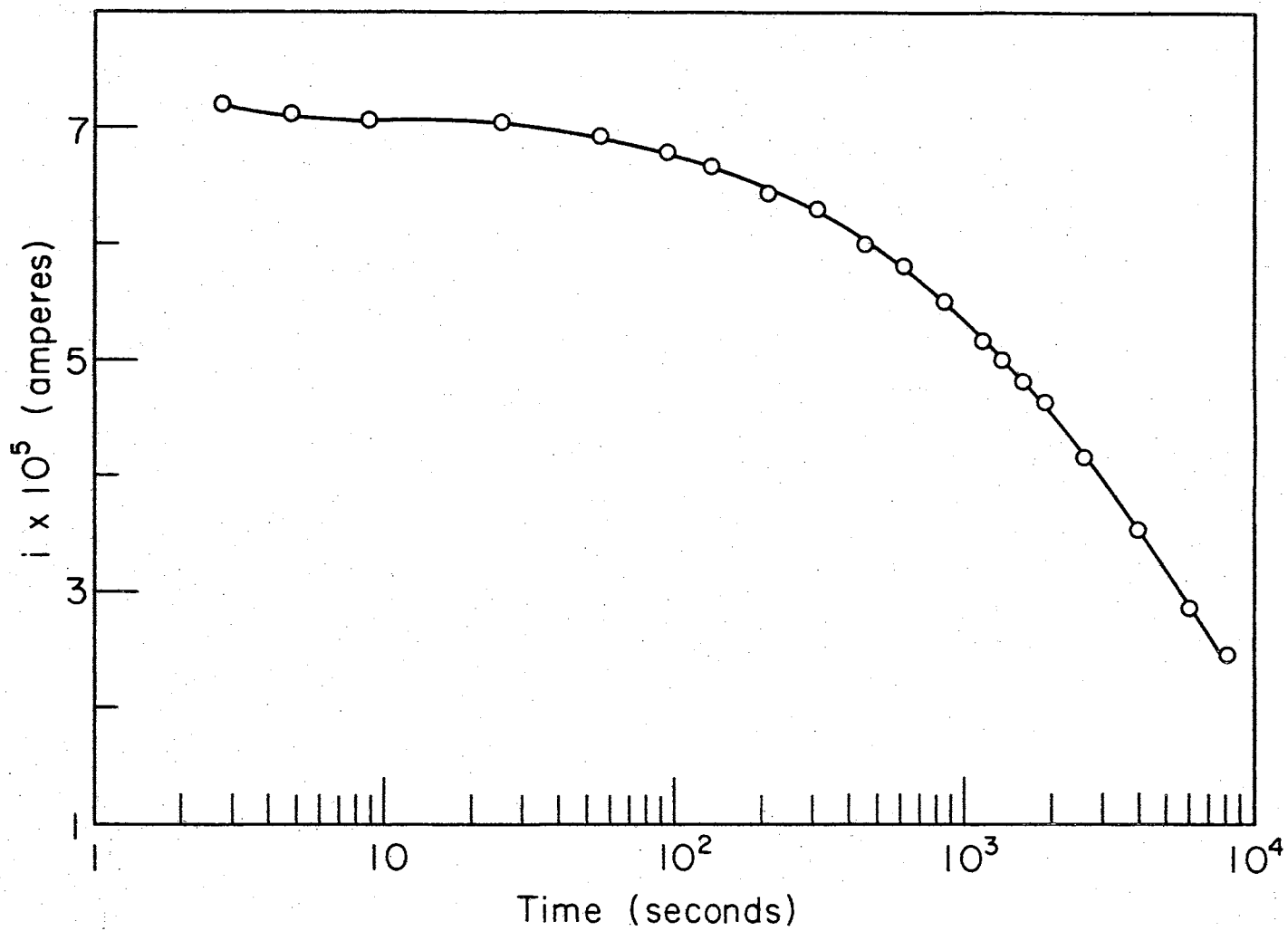


Figure 21. Photocurrent Decay of a Dense Sample in Vacuum (2536\AA)

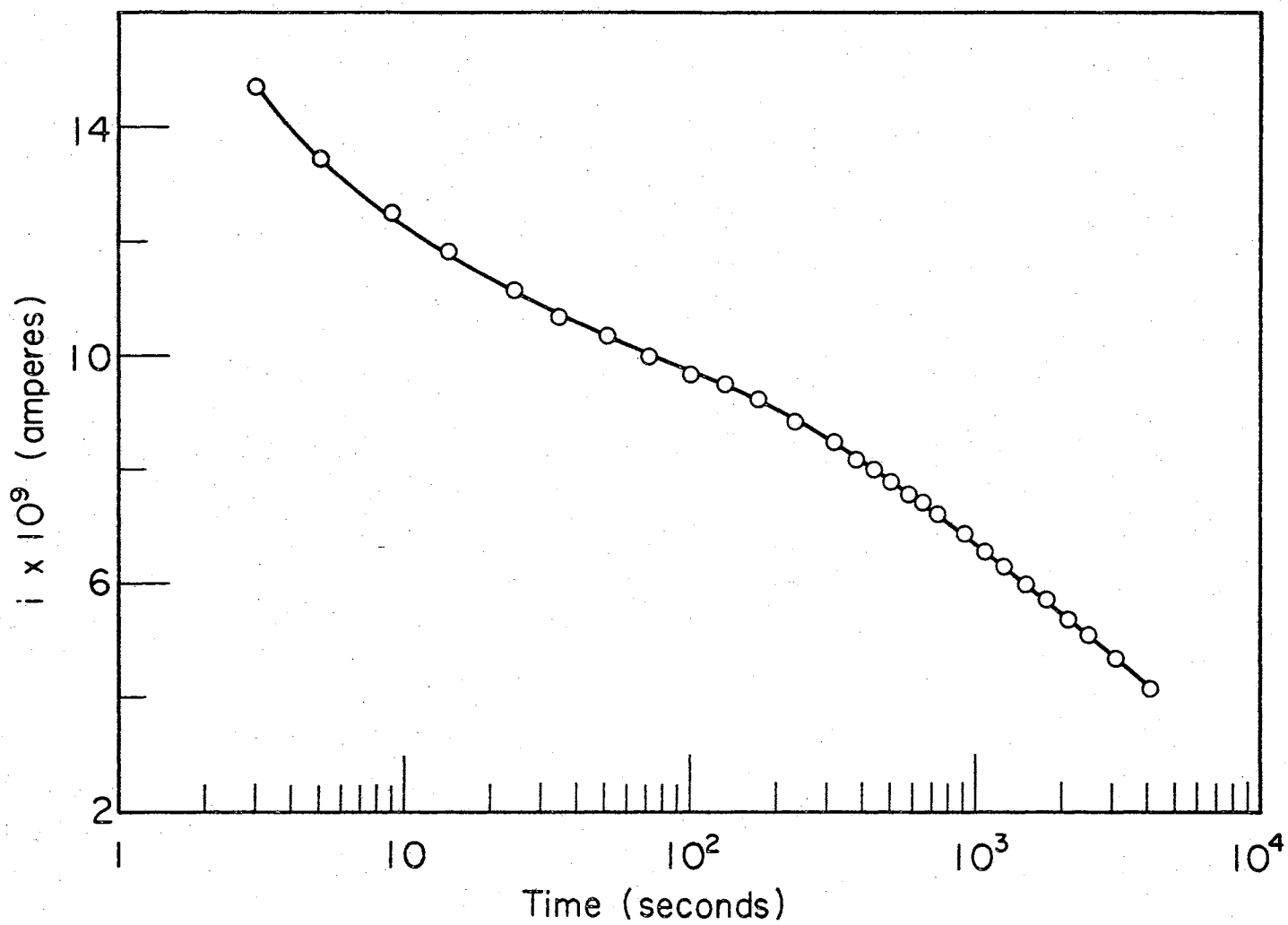


Figure 22. Photocurrent Decay of a Dense Sample in Vacuum (3131\AA)

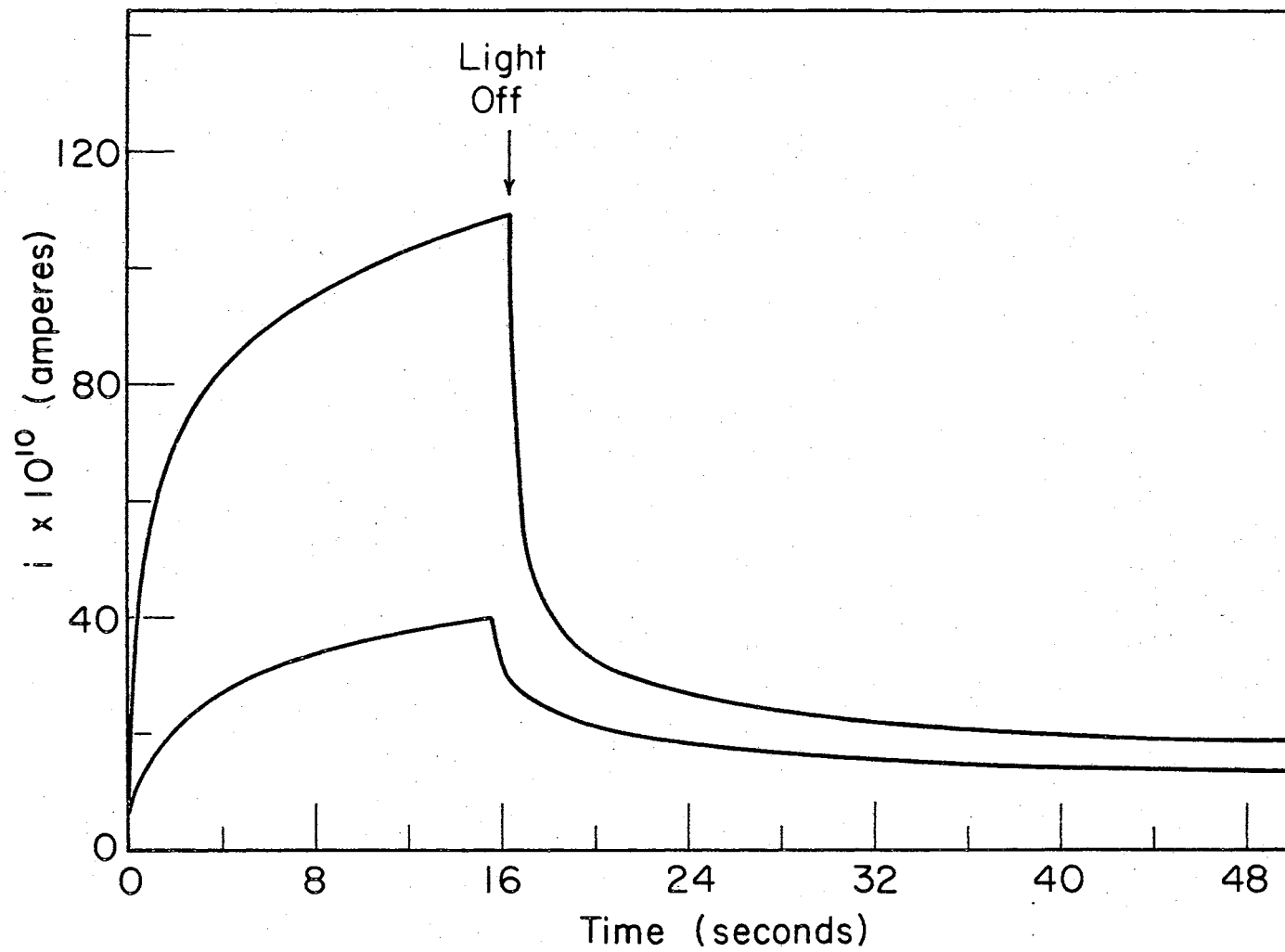


Figure 23. Photocurrent Rise and Decay of a Dense Sample in Air (2536Å)

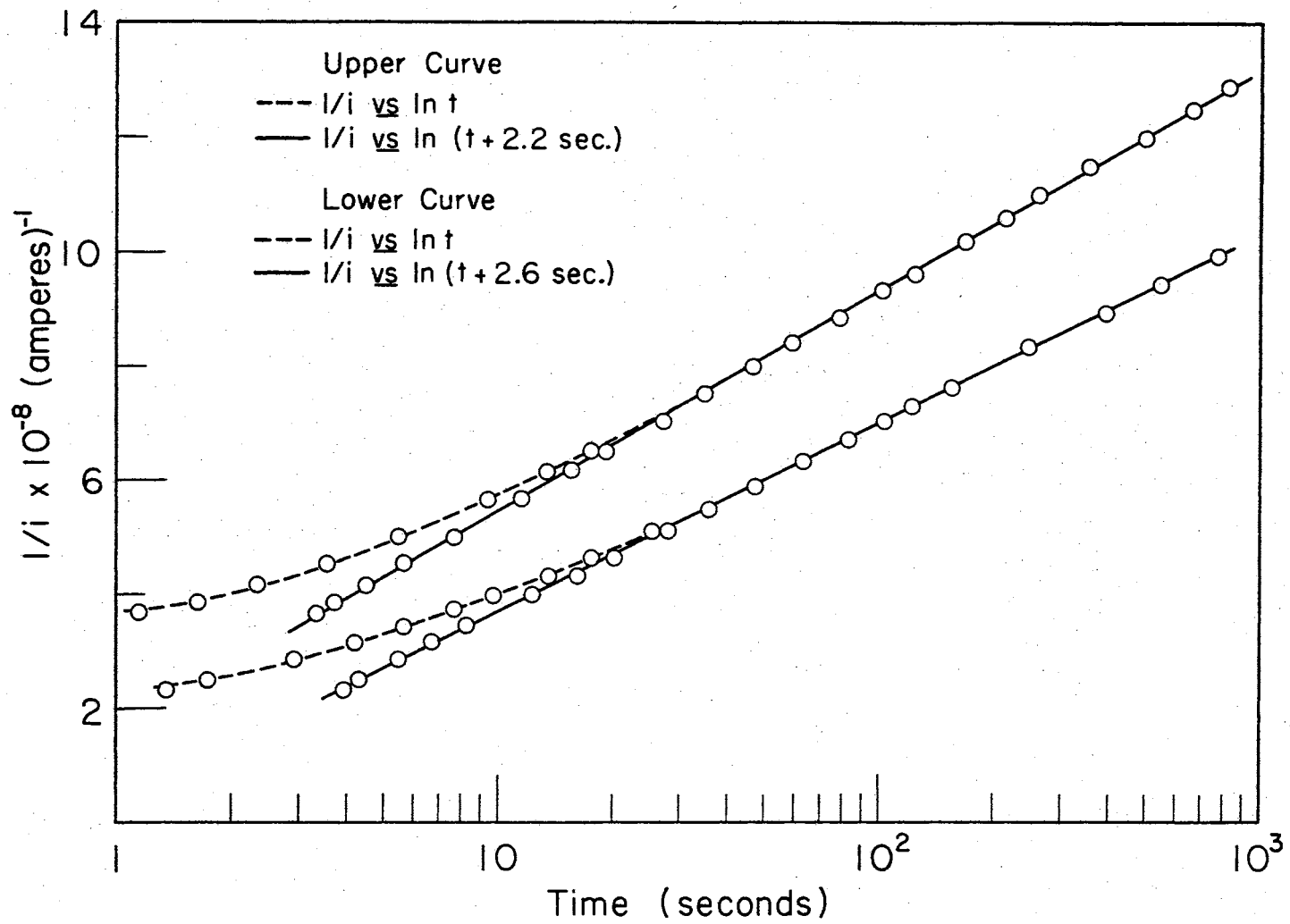


Figure 24. Photocurrent Decay of a Dense Sample in Air from Two Different Current Values (2536\AA)

photo-response was enhanced in a vacuum they were normalized to the peak value.

The thermal quenching data was also taken both in vacuum and air. Figure 26 shows thermal quenching of a dense sample using 3131Å radiation and Figure 27 using 2536Å. Notice the slight variation of the low temperature quenching peak in both cases (peak at -82°C in vacuum and -79.5°C in air) and the greater difference between the magnitudes of the vacuum and air peaks using the 2536Å radiation relative to that observed with 3131Å radiation. In Figure 28, which is thermal quenching for a porous sample using 3131Å radiation, one sees a further separation of the low temperature peaks (peak at -88°C in vacuum and -72°C in air) and some additional structure in the vacuum. Higher dark conductivity precluded measurements above -30°C .

In the TSC data there is also a definite difference between the vacuum and air results. Figure 29 shows the TSC data for a dense sample irradiated with 3131Å radiation for 60 seconds at the low temperature and Figure 30 shows results for the same sample irradiated with 2536Å radiation under the same conditions. Notice there is enhancement of the higher temperature peaks in vacuum with respect to those in air in both Figures but this is more pronounced in Figure 30 (2536Å). Again in Figure 31 which was taken on a porous sample irradiated with 3131Å radiation for 600 seconds at the low temperature one sees definite enhancement of the high temperature peak in vacuum. In all the TSC or EWC-TSC data the activation energies shown were calculated using the simple quasi-Fermi level calculation which is represented in equation (33). There were no energies calculated for the lower temperature peaks because although there is a true TSC peak there,

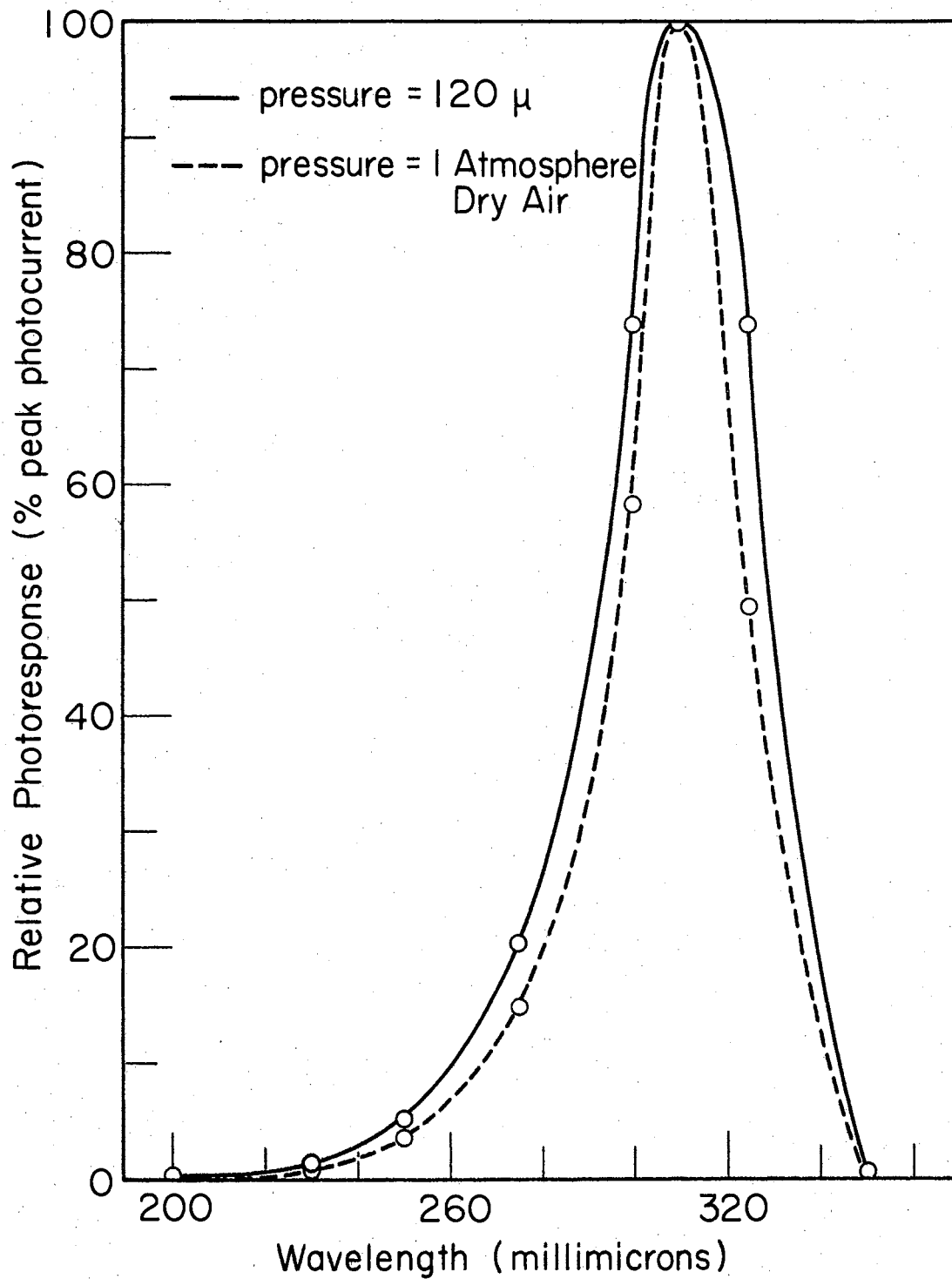


Figure 25. Spectral Response of a Dense Sample in Different Ambients

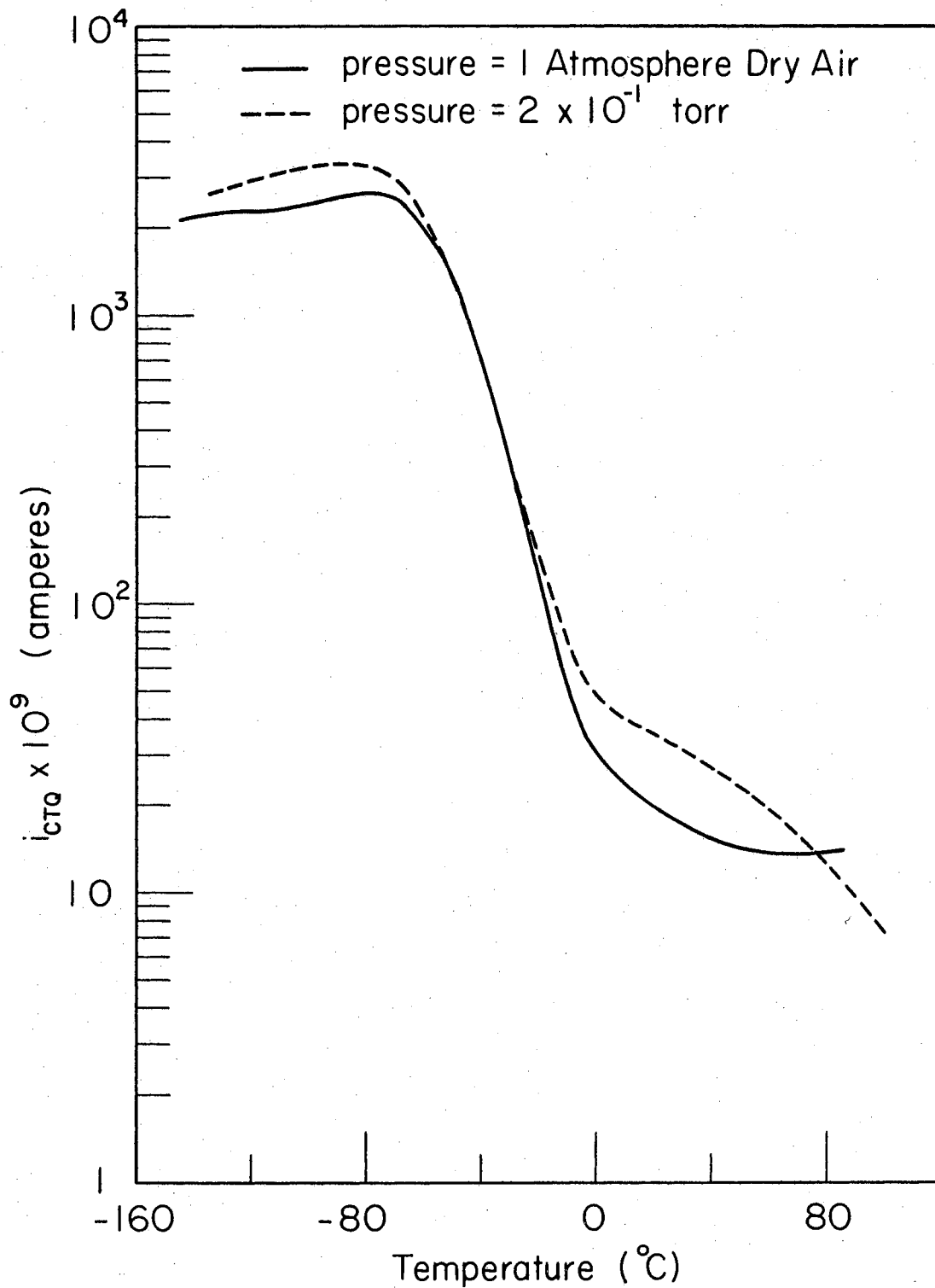


Figure 26. Continuous Thermal Quenching for a Dense Sample in Different Ambients (3131A)

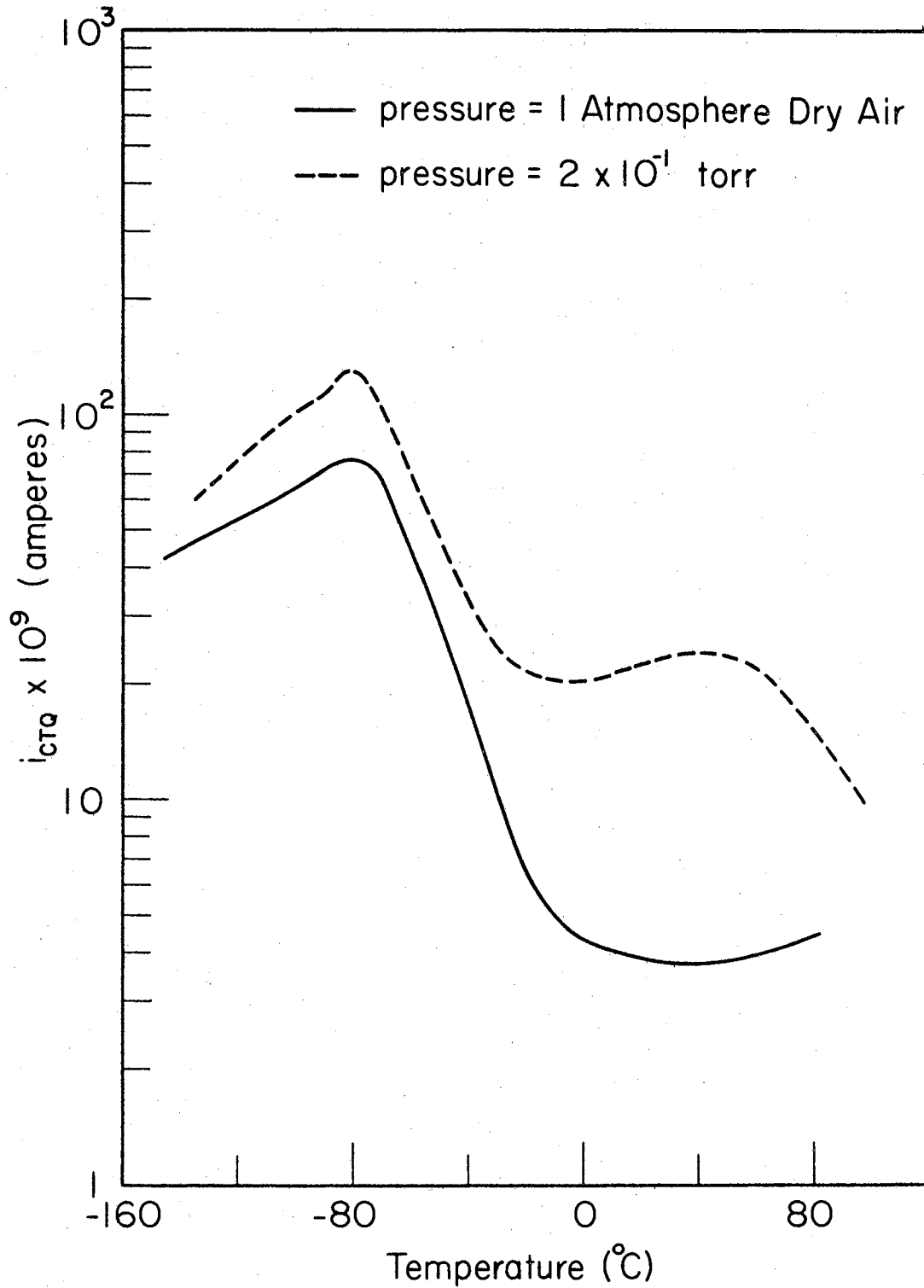


Figure 27. Continuous Thermal Quenching for a Dense Sample in Different Ambients (2536\AA)

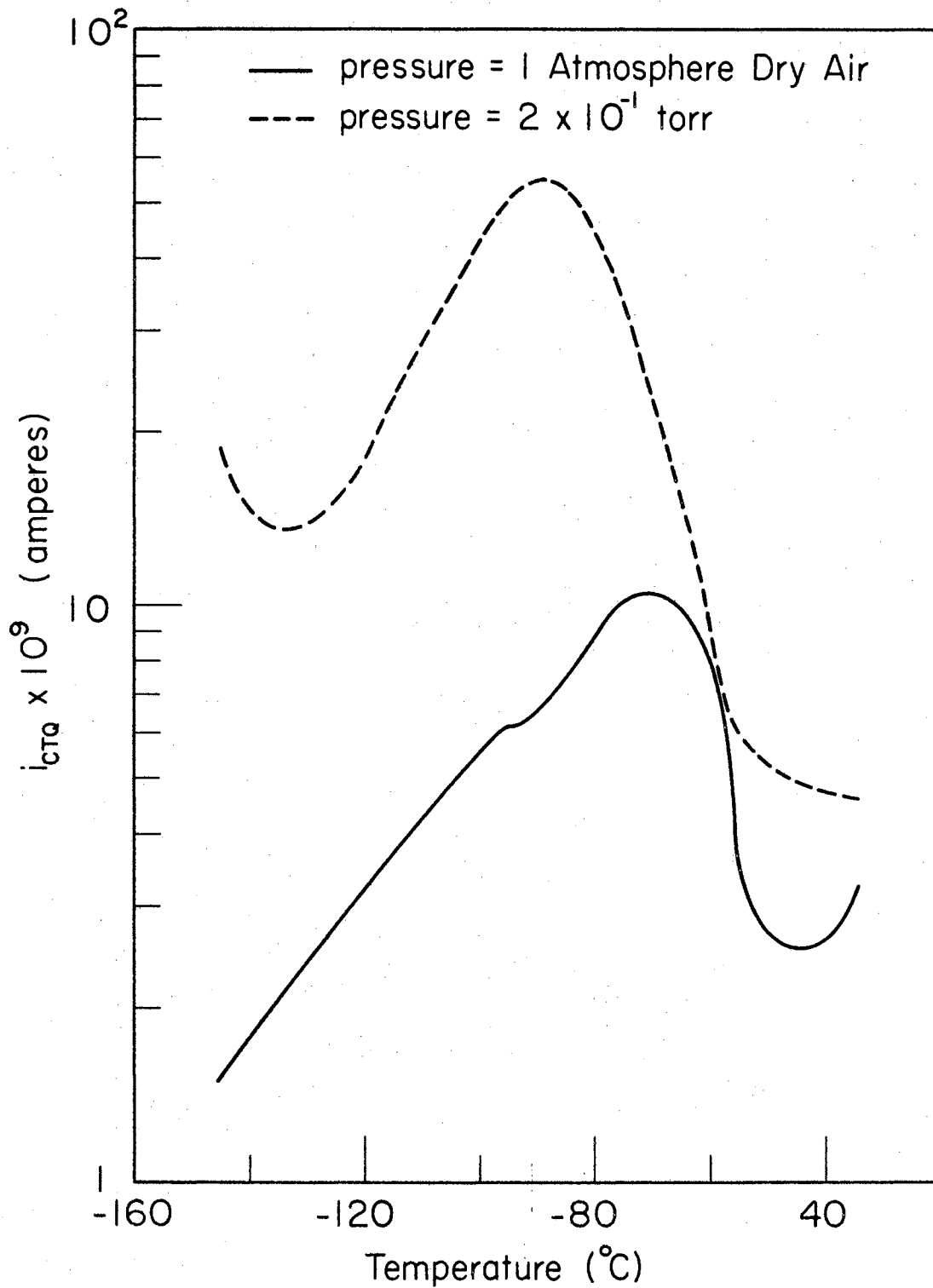


Figure 28. Continuous Thermal Quenching for a Porous Sample in Different Ambients (3131\AA)

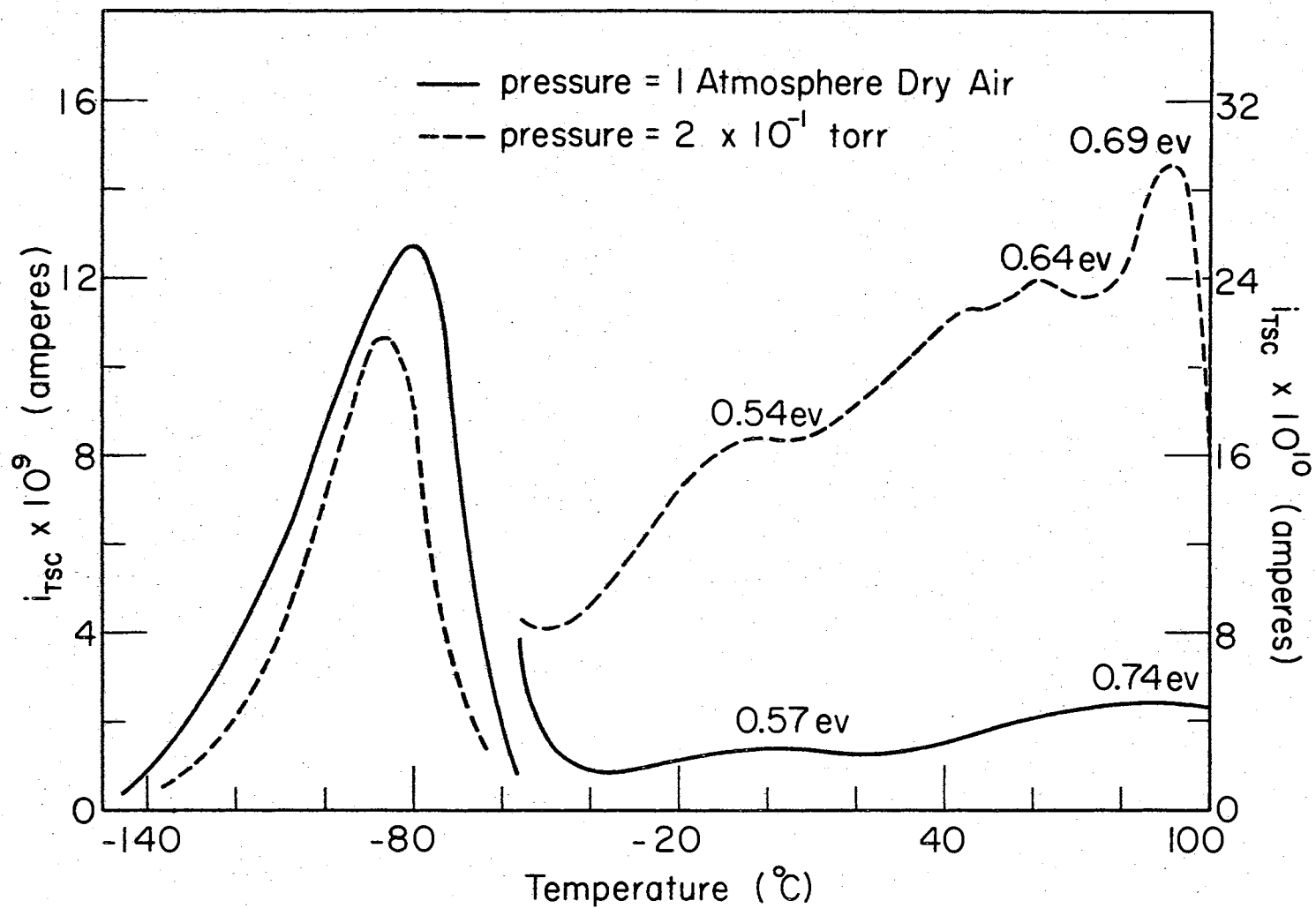


Figure 29. Thermally Stimulated Currents of a Dense Sample in Different Ambients (3131A)

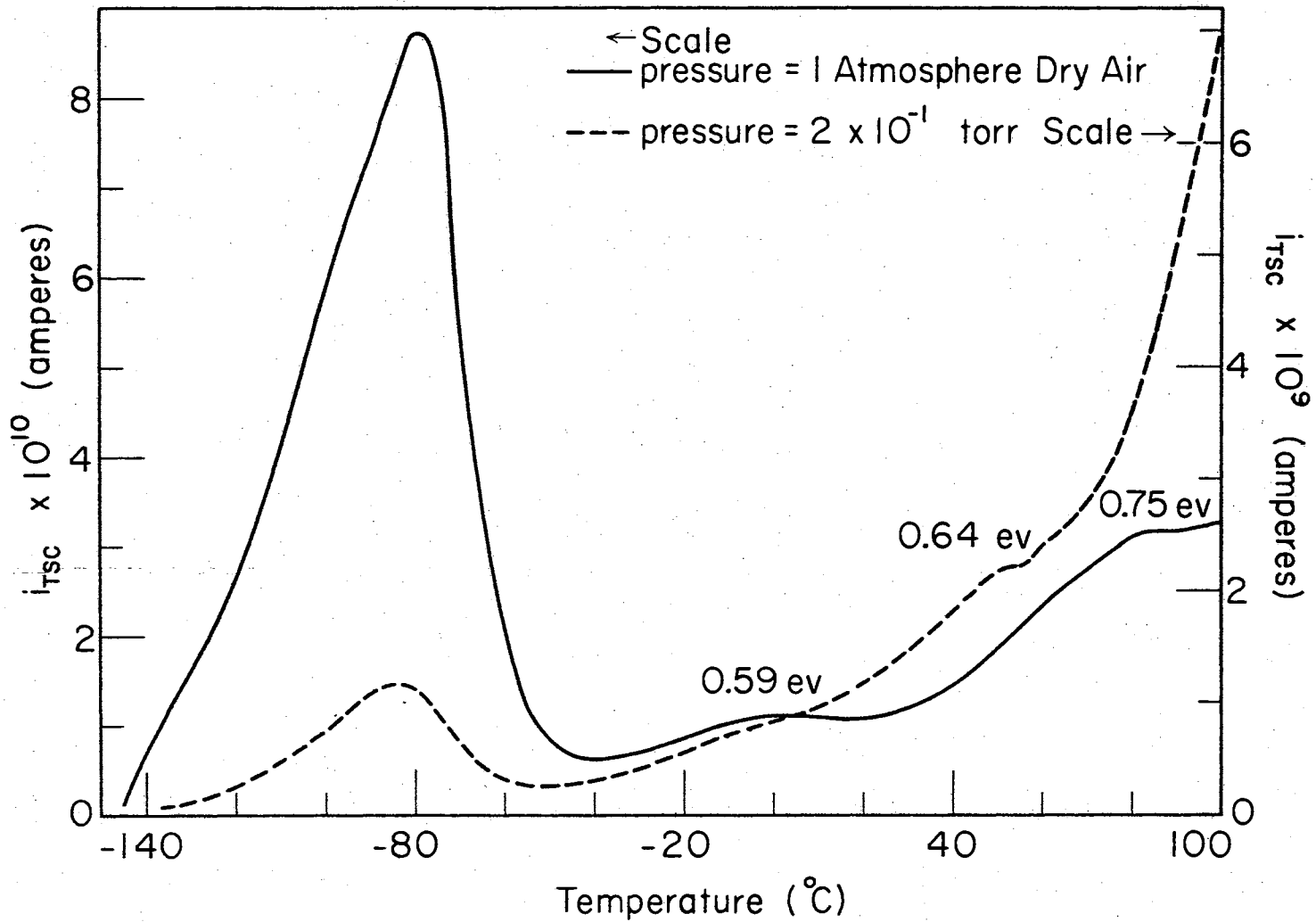


Figure 30. Thermally Stimulated Currents of a Dense Sample in Different Ambients (2536\AA)

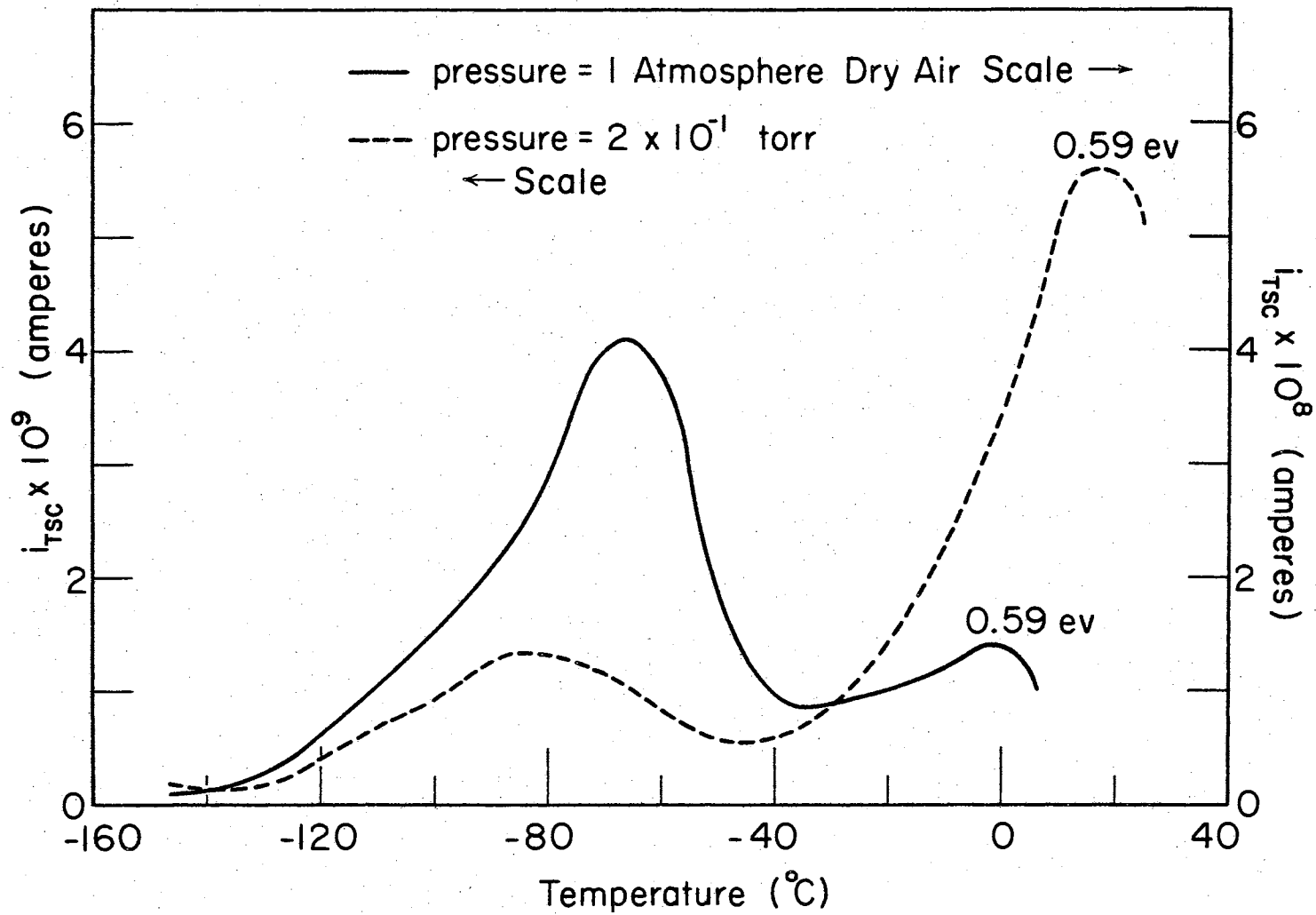


Figure 31. Thermally Stimulated Currents of a Porous Sample in Different Ambients (3131A)

the position is determined by the strong lifetime change represented by Figures 27, 28, and 29. More will be said about this later,

The EWC-TSC data again show a definite pressure dependence for the higher temperature peaks. Figure 32 compares the EWC-TSC data for 3131Å excitation in air with ordinary TSC data taken the same way and Figure 33 gives a similar comparison for 2536Å excitation at a pressure of 2×10^{-1} torr. Both sets of data were taken on a dense sample. There is a slight enhancement in the temperature peaks in Figure 32 which might be expected due to the longer excitation period, but upon comparing this EWC-TSC to another TSC taken following a 10 minute excitation one is convinced that at least part of the high temperature enhancement is real. In Figure 33 one sees a very large enhancement of the high temperature peak under EWC-TSC. Figure 34 represents comparative data for EWC-TSC and ordinary TSC measurements made on a porous sample at a pressure of 2×10^{-1} torr using 3131Å radiation. Notice that the EWC-TSC high temperature peak is 22 times larger than the corresponding TSC peak.

This completes the results obtained in the present study. An attempt will be made in the next chapter to correlate these observations using the general model proposed in Chapter I.

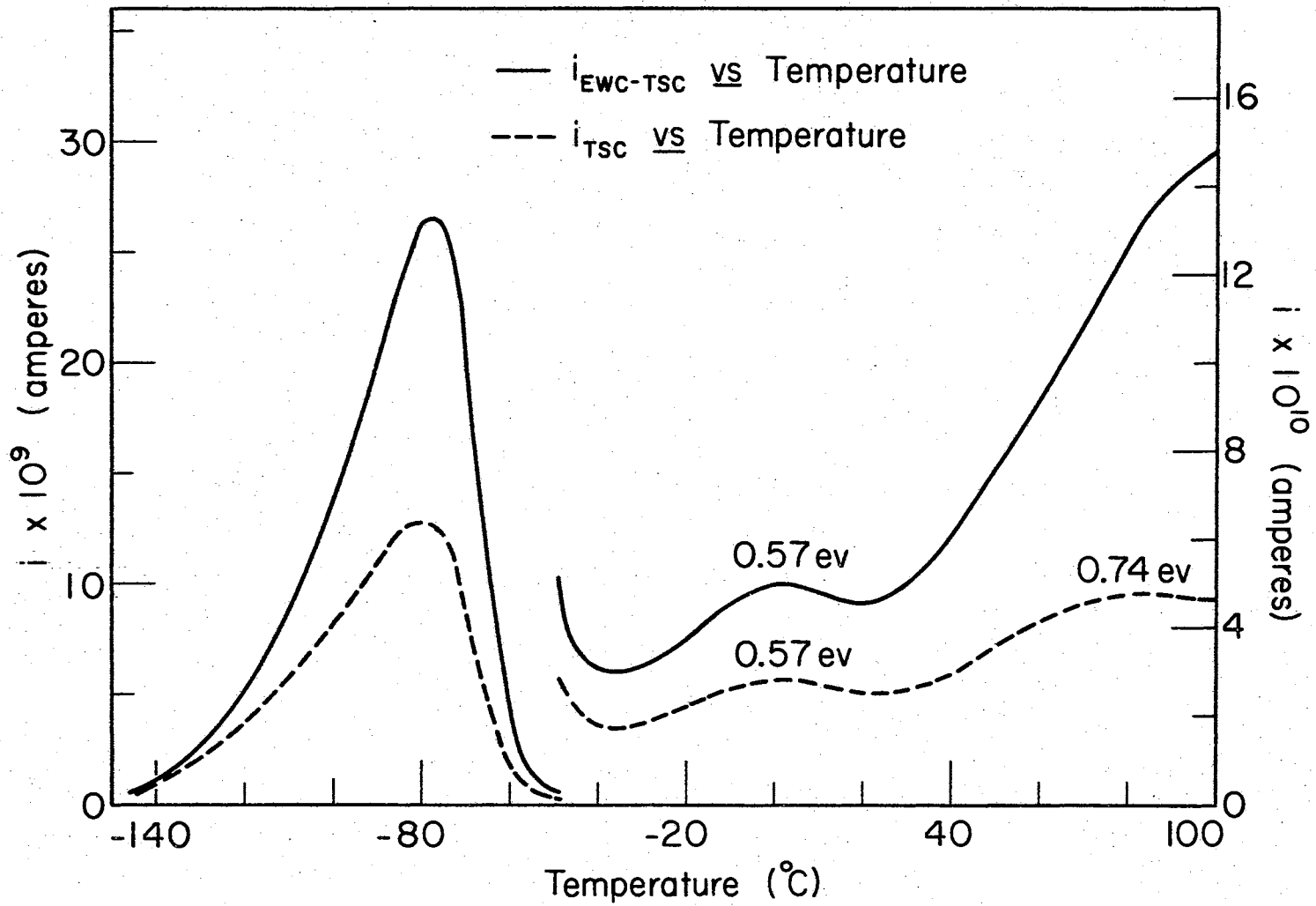


Figure 32. Comparison of Thermally Stimulated Currents of a Dense Sample in Air Following Different Pre-measurement Treatment (3131\AA)

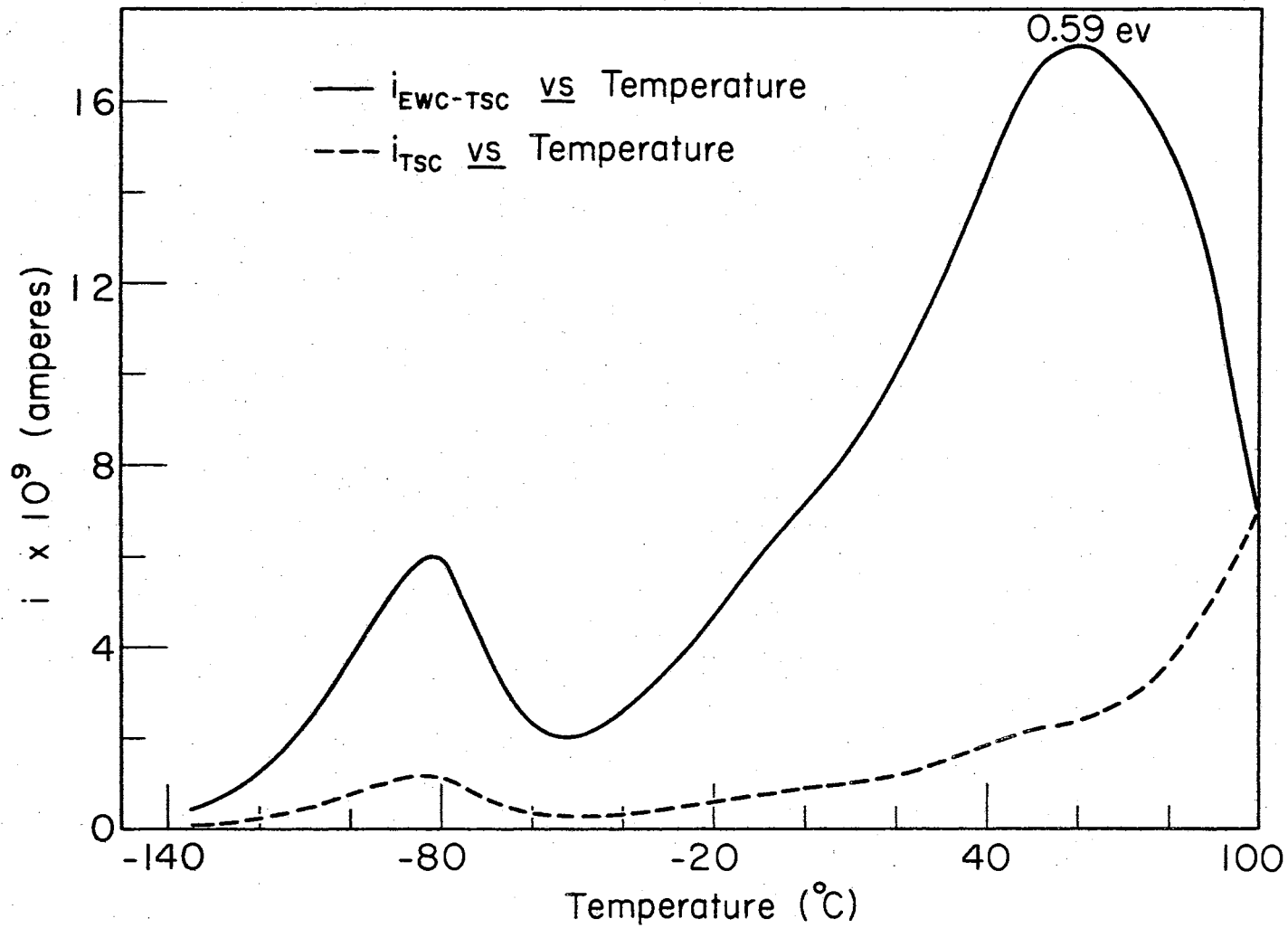


Figure 33. Comparison of Thermally Stimulated Currents of a Dense Sample in Vacuum Following Different Pre-measurement Treatment (2536Å)

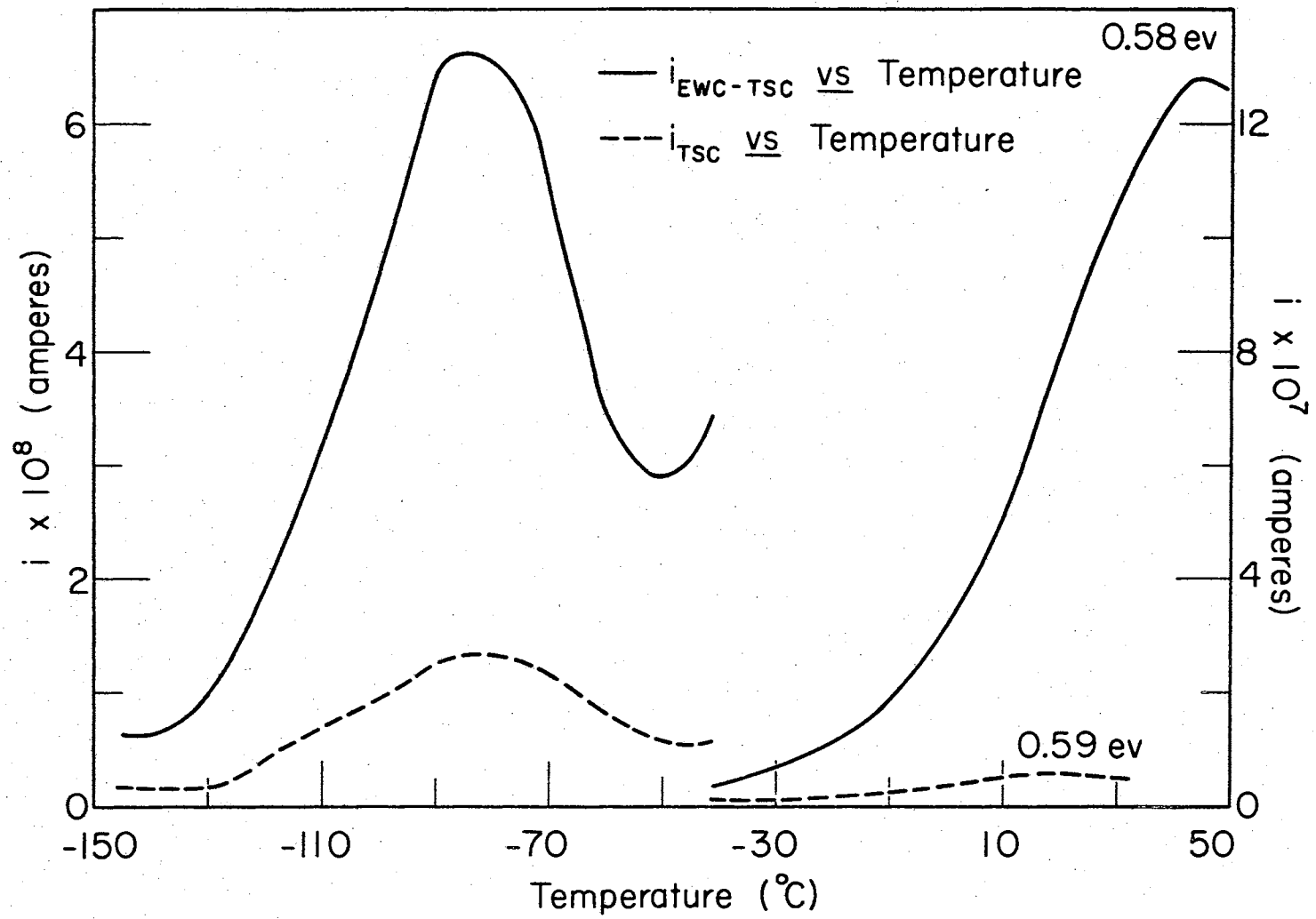


Figure 34. Comparison of Thermally Stimulated Currents of a Porous Sample in Vacuum Following Different Pre-measurement Treatment (3131A)

CHAPTER VI

DISCUSSION AND CONCLUSIONS

Summary of Results

Before a discussion is given of the data presented in Chapter V, a restatement of the general model will be made and a summary of the results presented. The general model invoked for the material to explain the experimental data is that these samples are compensated n-type insulators with surface acceptor states arising from the presence of chemisorbed oxygen. To substantiate this model, the important information one seeks in these data is the dependence of electrical conductivity effects on oxygen pressure.

In the dark conductivity data one sees this dependence in the equilibrium and the current decay data. Figures 12 and 13 show the monotonic variation of the dark conductivity level with fixing procedure for both dense and porous samples. Figures 15, 16, and 17 show the current decay between two equilibrium values when oxygen is quickly added to the system. These decays fit behavior predicted using modifications of equations pertinent to compensated semi-conductors.

In the photo-decay data one again sees a definite ambient pressure dependence. Figure 18 shows this dependence of the data for the two cases of decay in air and decay in vacuum. In Figures 19 and 20 one sees the definite functional behavior that can be ascribed to decays from photocurrent saturation in air whereas Figures 21 and 22 which are

decays in vacuum do not follow this behavior. Figures 23 and 24 show the decay in air following a short excitation and the functional dependence this decay follows. Although it is not the same as decay from saturation it too can be treated using the proposed modification of compensated semi-conductor statistics.

With photoelectronic measurements the ambient pressure dependence is again strikingly exhibited. In the spectral response, Figure 25, there is a definite difference in the shape of the curves in air and vacuum and from the uncorrected data it can be seen that the peak at 310 $m\mu$ is almost twice as large in a vacuum. Figures 26, 27, and 28 demonstrate the dependence of the quenching data on ambient pressure both in the magnitude and structure of the peak photocurrent. In all the TSC data whether normal TSC or EWC-TSC, Figures 29 through 34, one sees changes in magnitude and position of peaks due to a change in ambient pressure.

Summarizing then, all of the data presented show some type of ambient pressure dependence. An attempt to explain this dependence in terms of the general model will now be made after a brief discussion of the surface adsorption process.

Surface Adsorption Process

To attempt an understanding of the surface adsorption process and the species involved, one needs first to investigate the physical configuration of the surface upon which adsorption sites are formed. The as-grown physical surface of SnO_2 single crystals is the {110} plane²⁶ which is the plane of maximum density. Since there is crystal growth of the individual grains during the sintering process of the

polycrystalline samples, it is here assumed that this is the favored crystalline surface plane at all free surfaces. If one assumes complete electron transfer to form discrete ions then one can draw a pictorial representation of the $\{110\}$ plane in SnO_2 using Pauling ionic radii for O^{2-} and Sn^{4+} as is done in Figure 35. In this figure the solid balls represent the tins (smaller) and oxygens in the basal $\{110\}$ plane and the solid balls with 0 in the center represent the extra oxygens needed to furnish 2 oxygens for each tin. The points marked A and B are the centers of possible sites for a chemisorbed species. The dashed ball whose center is marked A occupies a lattice site (if it were in the bulk) and is therefore tightly bound and the points marked B are centers for chemisorbed species more loosely bound.

Although no detailed calculations can be made using just the pictorial representation of Figure 35 without knowledge of the chemisorbate species involved, one does definitely see the 2 inequivalent sites available for chemisorption. These sites are different not only energetically but also in size. A discussion will be made of the possibilities for the actual chemisorbed species in terms of energetics and size later after the determination of the chemisorbate.

The data reported in Chapter V always showed a difference when taken in air or vacuum. The problem then is to determine which component of the air, oxygen or nitrogen, is responsible for these changes. Other authors^{27,28} who have noted this effect have attributed it to oxygen. In order to check this, a measurement was made to see what the effect of pure N_2 was on the electrical conductivity. A sample was fixed at a pressure of 2.5×10^{-2} torr at 96°C for 40 hours and then was subjected to reasonably pure N_2 . After 40 minutes the dark

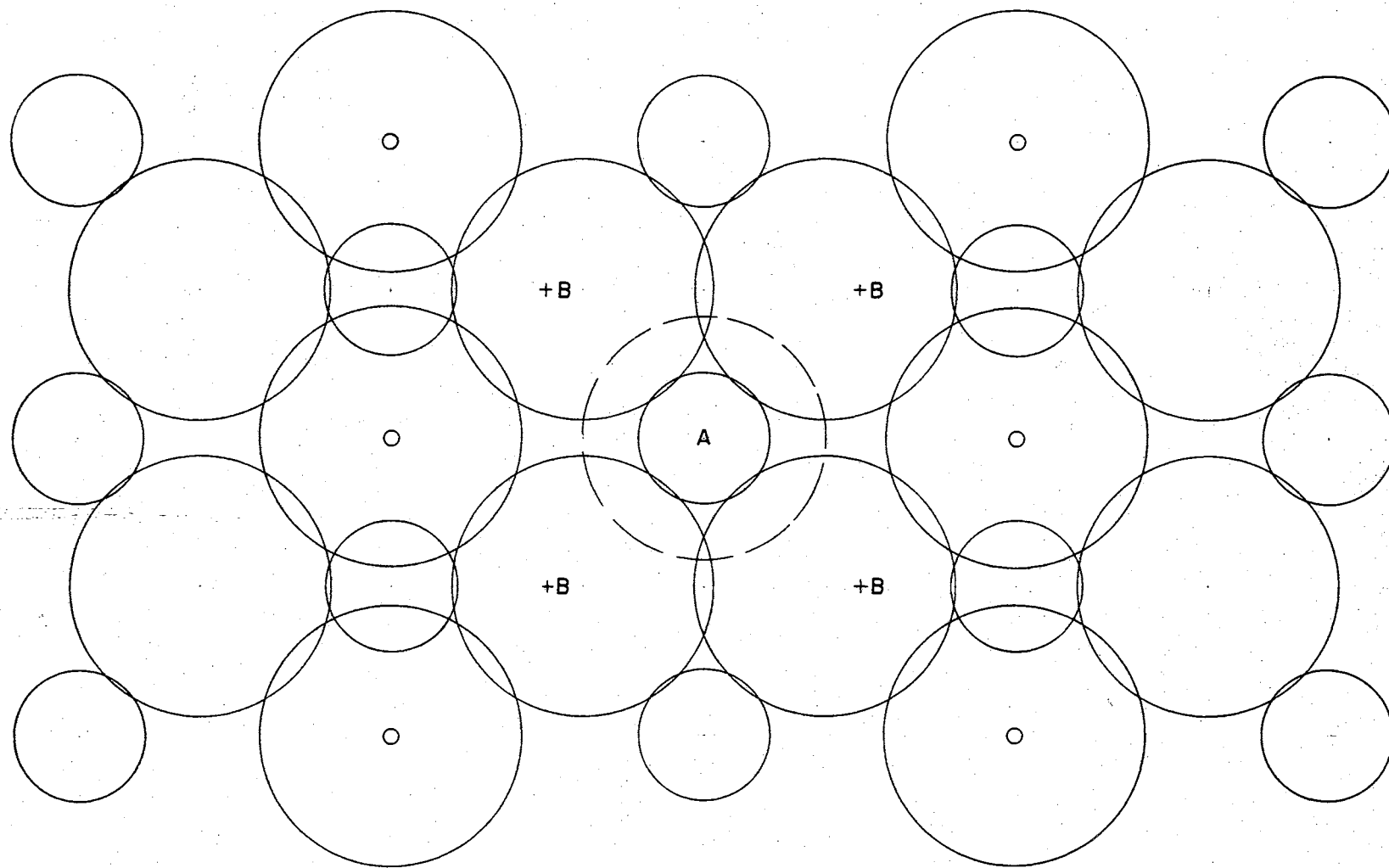


Figure 35. Pictorial Representation of SnO_2 Surface

conductivity had decreased from 7.7×10^{-8} amperes to 5.4×10^{-8} amperes and then remained essentially constant. A similar experiment in which air was added to the system after fixing the sample for 48 hours at 2×10^{-2} torr at 86°C produced a decrease in current by a factor of 6 in 5 minutes and of one order of magnitude in 24 minutes. In another experiment when air was let in at 115°C the current decreased by one order of magnitude in 5 minutes and decreased 3 orders of magnitude in 6 hours.

Another experiment was done in which photo-rise and photo-decay were done in N_2 , air, and vacuum. The sample was illuminated with 3131\AA radiation for 150 seconds and the results are shown in Table I.

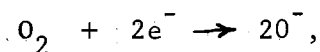
TABLE I
RESULTS OF PHOTO-MEASUREMENTS IN DIFFERENT AMBIENTS

Ambient	Peak Photo-current (Amps)	Current level after 50 seconds (Amps)	Current level after 1000 seconds (Amps)
3×10^{-1} torr	4.25×10^{-8}	4.75×10^{-9}	1.96×10^{-9}
N_2	4.25×10^{-8}	4.75×10^{-9}	1.74×10^{-9}
Air	1.77×10^{-8}	7.00×10^{-10}	5.5×10^{-11}

Notice that the vacuum and N_2 data are nearly identical with the air data being markedly different. It was therefore concluded that the effect of N_2 on the sample was essentially the same as any inert gas or vacuum. The slight difference in the data, the somewhat faster decay and the slight dark current decay, is probably due to the presence of a small amount of oxygen in the N_2 . All effects are therefore ascribed

to the oxygen and this identifies it as the chemisorbate in this work.

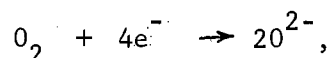
The question still arises, though, as to what is the actual chemisorbed species. There are three logical species O^- , O^{2-} , and O_2^- which will be considered. Since all of the species must evolve from the physically adsorbed O_2 molecule, one might first look at the energetics involved in these reactions. In order to compare these calculations, they will be made assuming the end product to be two chemisorbed ions. The first reaction would have the overall form



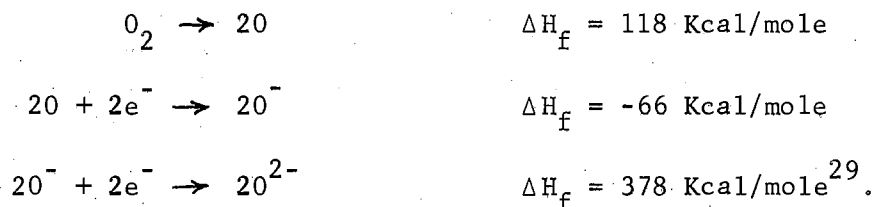
but the step-wise process would be as follows:



Therefore the reaction would be endothermic by the amount of 52 Kcal/mole. The second reaction would have the overall form



but the step-wise process would be as follows:



Therefore the reaction would be endothermic by the amount of 430 Kcal/mole. The third reaction is simply a one step process:



The relative sizes of the end products are as follows: radius of $O^- = 0.75\text{\AA}$ (Note that since there is no information available for the discrete ion, this number is found by dividing the radius of O_2^{2-} in BaO_2 or H_2O_2 in half), radius of $O^{2-} = 1.4\text{\AA}$, and radius of $O_2^- = 1.28\text{\AA}$.

It can be seen from the above data that energetically O_2^- is preferred over either of the other two species. Taking into additional consideration the fact that this reaction only involves one step and only needs one site and that the spaces available on the surface (see Figure 35) can easily accommodate O_2^- makes it the logical choice from the above reasoning. It should be pointed out, however, that this calculation has assumed that the end products O^{2-} , O^- , and O_2^- interact equally with the surface thus limiting its validity. Although the true nature of this interaction is not known at this time, it is felt that O_2^- is the most probable species.

Equilibrium Dark Conductivity

The term polycrystalline body or ceramic brings to mind several preconceived ideas of the physical structure of this type specimen. Therefore before discussing the data presented, there will be a short review of the problems involved in making conductivity measurements on polycrystalline samples. This will aid in defining the assumptions made to reduce the data.

The common picture of a polycrystalline body is that it is simply made up of a large number of tiny crystals randomly fused together and this is essentially correct. Using this as a model one can see that throughout the bulk of the sample there will be boundaries between these crystals (grain boundaries) and some regions where these crystals may

only touch at a few places (necks). In the porous samples both of these configurations exist and the complex question of how conduction through a neck region effects the overall conductivity of the sample is particularly important. For example, the oxygen effect is now spread through the macroscopic bulk of the sample and may present situations not covered in Chapter II. In the dense samples though, the basic problem is that of grain boundaries since the samples apparently have little or no porosity accessible to oxygen in the macroscopic bulk. Any porosity it has is probably trapped inside a grain. This result is deduced from the leveling off of the density as a function of temperature (Figure 3) and the measured densities. The density of a grown single crystal is 7.02 gm/cc, the density of a natural single crystal is 6.62 gm/cc, and the density of the dense polycrystalline samples is 6.41 gm/cc.

The assumption is made then that the dense samples act like bulk single crystals and can be treated as such using gross geometrical parameters for conductivity calculations. This assumption is reinforced further by the statement "The effect of grain boundaries in polycrystalline materials is related to the mean-free path of the ions or electrons between collisions. This is the order of inter-atomic distances for ionic conduction and is usually less than 100 to 150 Å for electronic conductivity. This means that except for very thin films or extremely fine-grained samples (less than 0.1 Micron) the effects of boundary scattering are small compared to the lattice scattering."³¹ made by Kingery. In the case of the porous samples gross geometrical parameters for conductivity calculations will be used simply because no significantly better way to treat the problem is known at this time.

Figure 12 shows the results of dark conductivity versus temperature for the dense samples. The pattern of the results is clear. A significant reduction in specimen conductivity level can be brought about either by increasing the treatment pressure at fixed treatment temperature or by increasing the treatment temperature at fixed pressure. At the lowest conductivity levels, a higher activation energy is also observed. No systematic investigation was made of treatment time effects but they are not considered of central importance to the model to be presented here.

There now remains the problem of identifying an appropriate mechanism which can provide several orders of magnitude difference in room temperature conductivity for a specimen fixed under varied conditions. Measurements were carried out in a light-tight sample holder, eliminating possible photo-effects. The maximum temperature used in the fixing process was of the order of 100°C , making it implausible that any bulk changes were occurring in the specimen. Dismissing these possibilities and reviewing the demonstrated importance of the ambient gas pressure suggests that a surface phenomenon such as oxygen chemisorption may account for the results. However, it must still be shown that enough electrons could be immobilized on the surface by an increase in chemisorbed oxygen density to cause significant conductivity changes.

Remembering that the samples are being treated as compensated semiconductors, i.e. the equilibrium number of carriers is determined by equation (22), one can now make calculations using the data shown in Figure 12. Values of donor activation energies can be obtained from the slopes of the curves and estimates of the "compensation factor"

$\beta(N_d - N_a^*)/N_a^*$ can be made using the conductivities as previously described in Chapter II. This was done, choosing reasonable room temperature values of $10 \text{ cm}^2/\text{volt}\cdot\text{sec}$ for the electron mobility³² and 0.2 electron masses for the density-of-states effective mass.³³ Results for a few of the curves in Figure 12 are given Table II.

TABLE II
ACTIVATION ENERGIES AND COMPENSATION FACTORS
CALCULATED FROM CURVES OF FIGURE 12.

Curve	Activation Energy E_a (eV)	Room Temperature Compensation Factor $\beta \left(\frac{N_d - N_a^*}{N_a^*} \right)$
A	0.41	3×10^{-3}
C	0.41	5×10^{-4}
E	0.41	4×10^{-5}
H	0.58	4×10^{-3}
I	0.60	4×10^{-4}

Recognizing that the compensation factors listed in Table II may be compared only for curves having the same activation energy, one readily sees that the high degree of compensation (indicated by the small compensation factor) can account for the marked changes in room temperature conductivity level that result from minor variations in fixing procedure.

Consider, for example, Curves H and I. Assuming that the donor level spin degeneracy factor $\beta = 1/2$ and the principal donor level density N_d remains constant, an increase of 0.7% in the effective bulk density of acceptor states N_a^* (defined as total acceptor density less

the density of depleted donor states lying above the principal donor level) could provide the observed change in compensation factor. However, even such a small change in bulk properties as this seems highly unlikely under a fixing temperature change from 50° to about 100°C.

A more plausible source of additional compensation is provided by the previously suggested mechanism whereby only a minor fractional increase in the surface density of chemisorbed oxygen would be accompanied by the transfer of enough additional electrons to the surface to explain the observed decrease in conductivity level. To illustrate the point, a choice of 10^{15} cm^{-3} for N_a^* and 10^2 cm^{-1} for the true surface-to-bulk ratio would require less than a one-part-in-ten-thousand increase (e.g., one percent in a one percent monolayer coverage) in chemisorption density to account for the difference between Curves H and I. Similar considerations are applicable to the Curves A, C and E. The difference in the activation energies for the two sets of curves indicates that it is possible for surface compensation to increase to such a degree that an active donor level can be depleted and a lower-lying one brought into play.

To extend this idea, data were taken on the porous samples as shown in Figure 13. Again one sees the same pattern of results as shown in Figure 12. But, if one compares the results of the calculated Fermi level--assuming the same mobility and effective mass as before--to the measured activation energy one sees a close correlation implying a compensation factor of approximately one. This is done in Table III.

TABLE III
 ACTIVATION ENERGIES AND CALCULATED FERMI
 LEVELS FROM CURVES IN FIGURE 13.

Curve No.	Number of Carriers at $T = 289^{\circ}\text{K}$ (cm^{-3})	E_a from Curve (ev)	E_f at $T = 289^{\circ}\text{K}$ (ev)
A	2.37×10^{11}	0.44	0.40
B	6.9×10^{10}	0.48	0.43
C	2.56×10^{10}	0.48	0.46
D	4.9×10^9	0.47	0.50
E	1.12×10^9	0.55	0.54

This seems contradictory since one would think that, considering the earlier dense sample results and the high surface-to-bulk ratio exhibited by these porous specimens, that they should be even more highly compensated. A clue to this problem is found in the difference in conductivity between curve E of Figure 13 and curve I of Figure 12. They were fixed in essentially the same manner but the dense sample had a conductivity 4 orders of magnitude lower. Therefore it was decided that since the sample had been only lightly fired there might be a high concentration of Zn ions left in the sample to act as donors. A check using X-ray fluorescence* did indeed show a difference by a factor of 10 in the Zn ion concentration of a sample having a density of 5.98 gm/cc as opposed to one having a density of 6.38 gm/cc, the more dense containing the least Zn.

It is therefore suggested that the reason for this correlation

*Courtesy of Continental Oil Company, Ponca City, Oklahoma.

between E_a and E_f can be ascribed to either or both of the following mechanisms. Although there may be compensation by the chemisorbed oxygens to such an extent that the principal donor level can change, these levels have a high density due to the large Zn concentration and essentially "pin" the Fermi level. Or, because of the inherent geometric problems of making conductivity calculations on porous samples as previously described, these results are misleading. It has not yet been satisfactorily shown which of or if the above reasons apply to the measurements.

Current Decays

In order to substantiate further the assumption that the decrease in current level is due to additional chemisorption, measurements were made of the kinetic changes between equilibrium dark conductivity points and of kinetic changes following photo-excitation of the sample, i.e. photo-decay. The dark current decays are shown in Figures 15, 16, and 17 and the photo-decays in Figures 18 through 24.

In Figures 15, 16, and 17 one sees the Elovich-type relationship between sample current and time predicted by equation (30). Reviewing briefly, this equation was derived using the equation for compensated semiconductor statistics and the assumption that any additional chemisorption of oxygen followed an Elovich dependence (See Chapter III). One can now calculate i_0 from the curves and compare this with the measured initial current to check the validity of extrapolating equation (30) to the static condition at $t = 0$. The results are shown in Table IV.

TABLE IV
COMPARISON OF INITIAL CURRENT VALUES

Figure Number	Calculated i_0 using Eq. (30) (Amps)	Measured initial current (Amps)
15	5.78×10^{-9}	5.76×10^{-9}
16	2.73×10^{-10}	2.82×10^{-10}
17	4.25×10^{-6}	4.86×10^{-6}

The excellent agreement between the measured and calculated initial currents implies that equation (30) is valid from the static condition at $t = 0$. Since the general equation based on equilibrium statistics worked in this non-equilibrium case, one now looks for other non-equilibrium situations in which it might apply. Therefore a series of measurements was made of photo-decay under various conditions.

The first measurements were photo-decays from a saturation value of photocurrent. Because of the complexity of the problem one is hesitant to treat this situation as a perturbation to the equilibrium as was done in the dark current decays. However, if there is a one-to-one correspondence between adsorbed oxygen and conduction electrons lost during the decay process, one would expect the measurements to again follow an Elovich equation (see discussion of these points in Chapter III). This type of relationship between sample current and time is observed when the decay is taken in air, Figures 19 and 20, but not in vacuum, Figures 21 and 22. The fact that there is an Elovich-type relationship when the decay is in air and none when the decay is in

vacuum seems consistent with the general model. Also evident in both Figures 19 and 20 is a breakover or change in speed of the decay at approximately 100 seconds after the light was turned off. This type of behavior has been noted before for ordinary adsorption kinetics^{34,35} on other systems and was regarded to be indicative of a changeover from one kind of site to another at a certain stage of the adsorption.¹⁴ One is immediately tempted to apply the same reasoning to the case in point in view of the two inequivalent surface adsorption sites discussed earlier in this chapter.

The second group of measurements explored photo-decays following a very short excitation as shown in Figure 23. Because of the possibility of only having one carrier (see discussion in Chapter III), it seems reasonable this situation may be treated in the same fashion as the dark current decays, i.e. as a perturbation of the equilibrium case. Before doing this, one must consider the action of light on the conduction mechanism of the sample. When intrinsic light is shone on the sample it creates hole-electron pairs near the surface. The holes are assumed to immediately go to the surface because of the large concentration of negative charge there thus leaving only electrons, at least for the first part of the process, as the conduction species. But, as bound surface electrons are freed, most of them are immediately trapped by the large concentration of ionized donors. Therefore even though the current increases, this increase is not indicative of the number of freed electrons if one uses an equilibrium mobility. Instead one must use a "drift mobility"^{*}. Estimating this and then calculating

* A good discussion of this is found in reference 19, page 68.

a quasi-Fermi level for the peak photocurrent, one finds that it is well above the principal donor level. Therefore if these decays can be treated as a perturbation of the equilibrium case, the assumption discussed in Chapter III leading to equation (32) should apply for the kinetic behavior. This relationship is obeyed in Figure 24.

In retrospect, the photo-decays have fallen into two classes: those that could not be treated as a perturbation to the equilibrium case and those that could. In the first class there is a definite difference in the photo-decay as a function of oxygen pressure. Current decays in air have behavior indicative of electron immobilization by chemisorbed oxygen whereas in vacuum they do not. In the second class a functional dependence not seen in any other decays and specifically predicted by use of the equilibrium statistics modification was found. This behavior not only complements the general model but shows success in simply treating certain non-equilibrium processes as a perturbation to the equilibrium case.

Photoelectronic Measurements

Measurements of the optical absorption coefficient in SnO_2 single crystals have been made by two different groups^{36,37} and their results agree reasonably well. Magnitudes for the wavelength range of interest are of the order of $10^3 - 10^5 \text{ cm}^{-1}$ with higher values observed for $E \perp C$ than $E \parallel C$. Consequently, it can be assumed that practically all of the light is absorbed within 10^{-3} cm from the grain surfaces with the 3131\AA light having the maximum penetration depth.

In Figure 25 one sees data for spectral response of a dense sample done in vacuum and air. The peak maximum is at 3100\AA which corresponds

to an energy of 4ev and is in excellent agreement with the absorption data^{36,37} and spectral response on single crystals.⁷ The raw data shows a difference of almost a factor of 2 for the magnitude of the peaks (i at 3100Å in vacuum = 2.1×10^{-7} amperes and i at 3100Å in air = 1.2×10^{-7} amperes). This difference in the peak photocurrent may be explained in the following way. The effect of oxygen on the surface during illumination is to provide a fast recombination site. This follows from the fact that oxygen immobilizes electrons on the surface. In other words, when hole-electron pairs are produced near the surface by light, electrons will be trapped if there are physically adsorbed oxygens nearby. These electrons will then recombine with holes and the process will be repeated. If there are no physically adsorbed oxygens on the surface then recombination must take place in the bulk by a slower process. Therefore the photo-rise levels off at a lower value of current (greater number of recombination sites) in air than in vacuum as observed, and the photo-decay is faster in air (see Figure 18).

The spectral response maximum, then does occur at an energy value which is in agreement with other published data on SnO₂ single crystals and shows a predictable ambient dependence. This ambient dependence is seen even more dramatically in CTQ and TSC data.

In Figures 26 and 27 one sees continuous thermal quenching for a dense sample and in Figure 28 for a porous sample. As mentioned in Chapter III the levels responsible for the quenching effect are probably electron trapping states so one looks at the data for differences which might cast light on their origin.

The thermal quenching effect is highly dependent in magnitude and

structure on both the ambient conditions and the surface-to-bulk ratio of the sample. The magnitude differences observed are consistent with the fact that CTQ values are a qualitative measure of electron lifetimes, i.e. they are inversely dependent upon electron recombination rates. Consequently, it is to be expected that CTQ will be larger (recombination diminished) for vacuum measurements. The structure of the curves has not yet been explained, however, it seems plausible at this time to say that electron trapping states responsible for the quenching effects either are, or are greatly affected by the chemisorbed oxygen states.

In Figures 29 and 30 one sees the thermally stimulated currents for a dense sample and in Figure 31 for a porous sample. Three significant differences are noted:

- (1) difference in the magnitude of the curves in different ambients,
- (2) difference in structure of the curves in different ambients, and
- (3) difference in the relative magnitudes of the low and high temperature peaks for a given curve.

These differences will only be discussed for the high temperature peaks as there is still some problem as to what the low temperature peaks mean. Since they closely coincide in position with the comparable thermal quenching peaks regardless of magnitude, their position is probably less indicative of the activation energy than of a lifetime change. Judging from the width of the peaks there is no one discrete level causing this behavior. A similar situation was observed in CdS³⁸ where further analysis revealed a quasi-continuous distribution

of levels giving rise to such a peak. Furthermore, the heights of the peaks are also a function of the time following removal of illumination time at the low temperature since there are phonons at this temperature with enough energy to partially empty shallow traps. Until these peaks receive further investigation by other methods no more will be said about them.

The high temperature peaks do behave in a consistent way. In both figures representing data on a dense sample the high temperature peaks taken in vacuum were not only higher in magnitude but showed additional structure. This same type of behavior, i.e. higher current values and additional structure, was previously noted by Houston after vacuum fixing on single crystals (Figure 38 of reference 21). But, as he pointed out, the origin of this behavior cannot be attributed to one single factor without lifetime data. Figures 30 and 31 show that when the hole-electron pairs are created nearer the surface (Figure 30) or when there is a large surface-to-bulk ratio (Figure 31), the higher temperature peak becomes dominant. Again this data is not capable of differentiating between increased density of traps or increased lifetime but the effect is certainly surface dependent. In summary, then, the thermally stimulated currents are definitely dependent on ambient conditions and, although no calculations other than quasi-Fermi level trapping energies were made from these data, there is qualitative substantiation of the general model.

The thermally stimulated currents taken after excitation with cooling (EWC-TSC) introduced an additional effect over and above the usual ambient dependence of the physical measurement. This was the large enhancement of particular peaks by the action of excitation with

cooling in vacuum. Figure 32 shows the comparison of a TSC and EWC-TSC in air for a dense sample. Looking at the curves one sees a slight increase of all peaks but nothing like the increase seen in the vacuum data on a dense sample (Figure 33) or on a porous sample (Figure 34). Bube has observed similar behavior in CdS crystals³⁸ and has attributed it to the presence of traps with a repulsive barrier requiring activated filling. While the differences between comparable TSC and EWS-TSC curves are again ambient dependent, further work is necessary to elucidate the mechanism involved.

Summary

In the preceding discussion there have been a number of specific arguments pertaining to the general model proposed in Chapter I. Reviewing, this model was that Zn-doped polycrystalline SnO_2 samples are compensated n-type insulators with surface acceptor states arising from the presence of chemisorbed oxygen. Therefore specimen electrical properties should be dependent on the density of this chemisorbed oxygen. One now attempts a succinct evaluation of the important data presented in terms of this model.

The first problem after observing there was an ambient dependence of the electrical properties was identifying the chemisorbate responsible. This was shown to be oxygen as predicted and several arguments were made for O_2^- as the actual species. Geometrical considerations involving the physical surface identified 2 inequivalent adsorption sites the presence of which was made plausible by interpretation of photo-decay measurements.

Now that the chemisorbate was known, the problem was what effect

it had on bulk electrical properties. This problem was attacked by using equilibrium semiconductor statistics and modifying the bulk density of acceptors to include surface acceptors associated with the presence of the chemisorbate. By doing this one was able to explain the changes in equilibrium dark current in terms of small changes in this effective acceptor density. The approach was then extended to non-equilibrium processes by including in the effective acceptor density an Elovich time dependence term suggested by commonly observed gas adsorption kinetics. By doing this and making certain reasonable approximations, two particular functional dependences for current versus time were predicted for two different sets of initial conditions of the sample. One set was valid for dark current decays following a rapid ambient change and the other for photo-decays following short illuminations. The observed decays did follow the predicted functional dependences.

A series of exploratory photoelectric measurements proved compatible with the general model providing qualitative substantiation for it. In addition they indicated several fruitful areas for further investigation.

Suggestions for Further Study

Throughout the bulk of this report a number of suggestions for further study have been given along with reasons why the information they would provide would prove helpful. In the following outline these are listed and supplemented by additions which are intended as a guide to future work.

- I. Dark current transients
 1. Measure temperature dependence of t' in equation (30).
 2. Measure temperature dependence of A in equation (30).
 3. Correlate effect of different initial currents at a fixed temperature on t' and A.
 4. Look at the effect of different ambient gases on the transient behavior.
- II. Photocurrent transients
 1. Correlate time of illumination with type of current decay at fixed temperature and light level.
 2. Measure temperature dependence of current decay at fixed light level and illumination time.
 3. Look at the effect of different gases on the current decay.
- III. CTQ
 1. Measure CTQ as a function of light level (see reference 7).
 2. Look at effect of different gases on CTQ.
- IV. TSC and EWS-TSC
 1. Investigate methods to reduce dark current levels.
 2. Determine which peaks are indicative of discrete trapping levels.
 3. Resolve the individual peaks using method of decayed TSC.
- V. Miscellaneous
 1. Investigate identification of chemisorbed species (ESR and mass spectrometry).
 2. Investigate correlation between Zn ion concentration and conductivity magnitude (X-ray fluorescence).

3. Investigate effects of ions other than Zn on sintering properties of SnO_2 .
4. Investigate correlations between ultrasonic attenuation and sintering kinetics.

BIBLIOGRAPHY

1. Subbarao, E. C., Sutter, P. H. and Hrizo, J., J. Am. Ceram. Soc., 48, 443 (1965).
2. Kingery, W. D., Introduction to Ceramics, John Wiley and Sons, New York (1960).
3. Kunkle, H. F. and Kohnke, E. E., J. Appl. Phys., 36, 3961 (1965).
4. Marley, T. A. and Mac Avoy, T. C., J. Appl. Phys., 32, 2504 (1961).
5. Harvill, M. L. and Roy, R., Am. Ceramic Soc. Bull., 44, 297 (1965).
6. Rutledge, J. L., Proc. Okla. Acad. Sci., 46, 137 (1966).
7. Houston, J. E. and Kohnke, E. E., J. Appl. Phys., 36, 3961 (1965).
8. Hurt, J. E. and Kohnke, E. E., Relationship Between Photoconductivity and Chemisorption Kinetics for Stannic Oxide Crystals, Tech. Report #2, Contract #Nonr.-2595(01) (1963).
9. Roy R., Unpublished Lecture Notes of Summer Institute "Inorganic Materials Preparation and Characterization", Pennsylvania State University (1965).
10. Blakemore, J. S., Semiconductor Statistics, Pergamon Press, New York (1963).
11. Lee, V. and Mason, D. R., J. Appl. Phys., 34, 2660 (1963).
12. Melnick, D. A., J. Chem. Phys., 26, 1136 (1957).
13. Medved, D. B., J. Phys. Chem. Solids, 20, 255 (1961).
14. Taylor, H. A. and Thon, N. J., J. Am. Chem. Soc., 74, 4169 (1952).
15. Vol'kenshtein, F. F., Zhur. Fiz. Khim., 23, 917 (1949).
16. Landsberg, P. T., J. Chem. Phys., 23, 1079 (1955).
17. Meller, A., Monatsh. Chem., 87, 491 (1956).
18. Low, M. J. D., Chem. Revs., 60, 267 (1960).

19. Bube, R. H., Photoconductivity in Solids, John Wiley and Sons, New York (1960).
20. Dussell, G. A. and Bube, R. H., *Phy. Rev.*, 155, 764 (1967).
21. Houston, J. E., Photoelectronic Analysis of Imperfections in Grown Stannic Oxide Crystals, Tech. Report #4, Fe. 1965, Contract #Nonr-2595(01).
22. Bube, R. H., *J. Phy. Chem. Solids*, 1, 234 (1957).
23. Dussell, G. A. and Bube, R. H., *J. Appl. Phys.*, 37, 13 (1966).
24. Houston, J. E. and Kohnke, E. E., *J. Appl. Phys.*, 37, 3083 (1966).
25. Matthews, H. E. and Kohnke, E. E. A Preliminary Study of Certain Electrical Properties of Stannic Oxide Ceramics, NASA Contractor Report CR-376, Jan. (1966).
26. Koffyberg, F. P., *J. Appl. Phys.*, 36, 844 (1965).
27. Bube, R. H., *J. Electrochem. Soc.*, 113, 793 (1966).
28. Mark, P., *J. Phys. Chem. Solids*, 26, 959 (1965).
29. Harvey, K. B. and Porter, G. B., Introduction to Inorganic Physical Chemistry, Addison-Wesley Publishing Co., Reading, Mass. (1963).
30. Pack, J. L. and Phelps, A. V., *J. Chem. Phy.*, 44, 1870 (1966).
31. Page 682 of Reference 2.
32. Loch, L. D., *J. Electrochem. Soc.*, 110, 1081 (1963).
33. Marley, J. A. and Dockerly, R. C., *Phys. Rev.*, 140, 304 (1965).
34. Sickman, D. V. and Taylor, H. S., *J. Am. Chem. Soc.*, 54, 602 (1932).
35. Liang, S. C. and Taylor, H. S., *J. Am. Chem. Soc.*, 69, 1306 (1947).
36. Reddaway, S. F. and Wright, D. A., *Brit. J. Appl. Phys.*, 16, 195 (1965).
37. Summitt, R., Marley, J. A. and Borrelli, N. F., *J. Phys. Chem. Solids*, 25, 1465 (1964).
38. Bube, R. H., Dussell, G. A., Ching-Tac, and Lewis, M. D., *J. Appl. Phys.*, 37, 21 (1966).

VITA

Herman Excell Matthews, Jr.

Candidate for the Degree of

Doctor of Philosophy

Thesis: PHOTOCONDUCTIVITY AND SURFACE EFFECTS IN Zn-DOPED POLYCRYSTAL-
LINE STANNIC OXIDE

Major Field: Physics

Biographical:

Personal Data: Born in Houston, Texas, March 16, 1940, the son
of Herman and Catherine Matthews.

Education: Graduated from Reagan High School in Houston, Texas,
in 1958; received Bachelor of Science degree from Lamar State
College of Technology, Beaumont, Texas, with a major in
Physics, in May, 1962; received the Master of Science degree
from Oklahoma State University, with a major in Physics in May,
1965; completed requirements for the Doctor of Philosophy
degree in July, 1967.